Advanced

Seismic Assessment

Guidelines

By: Paolo Bazzurro[1], C. Allin Cornell[1], Charles Menun[1],
Nicolas Luco[2], Maziar Motahari[1]

September 30, 2004

[1] J. A. Blume Earthquake Engineering Center Department of Civil and Environmental Engineering, Stanford University, Stanford CA
[2] AIR Worldwide Co., 388 Market Street, Suite 610, San Francisco, CA 94111

TABLE OF CONTENTS

Acknowledgements

Format of the Document

This document comprises text in two different forms:

- Guidelines provide the engineer with the basic information needed to apply the methodology presented here. Guidelines are written in normal font.
- *Commentary presents relevant notes useful to the understanding of the guidelines but not strictly necessary to its implementation. The paragraphs with commentary, which are italicized, indented and proceeded by a capital* **C,** *will appear interspersed with the guidelines in this draft.*

Introduction

The objective of this document is to provide guidelines for the assessment of the seismic performance of existing structures that are common in the building inventory of major electric utility such as Pacific Gas and Electric (PG&E), a co-sponsor of the PEER Lifelines Program. Predicting the post-earthquake functionality of such structures is a crucial step in evaluating the likelihood that the PG&E power distribution network will not be able to provide power to customers. As an important by-product, the results of the procedure outlined in this report also provide a rational support to the engineer inspecting the facility after an earthquake on whether to permit the occupancy of a building soon after the occurrence of a damaging earthquake. Currently, the occupancy status of a damaged building is assessed by an engineer from a firm retained for this purpose by PG&E based solely on visual inspection.

The final product is cast in terms of the so-called fragility curves for structural limit states directly related to after-earthquake building occupancy status, namely green, yellow, and red tags. A limit-state fragility curve provides the conditional probability that the specified limit state will be reached or exceeded as a function of the severity of the future ground motion at the site. Besides these three states, this document provides the fragility curves for two additional structural limit states, the onset-of-damage and the collapse states, which are not directly related to the building functionality status. The onset-of-damage state relates to the beginning of detectable structural damage. The five limit states in increasing order of damage severity are:

- ***Green tag,*** **G:** the building has been inspected and deemed fit for immediate occupancy.
- ***Onset of Damage***, **OD**: FEMA 356 and HAZUS manual define the onset of significant nonlinear behavior (Immediate Occupancy in FEMA 356 and Slight Damage in HAZUS) for different types of structures, such as those in the PG&E building stock. No limitations on post-earthquake access are implied by this limit state.

- *Yellow tag,* **Y:** the building has been inspected and deemed fit for restricted occupancy. The access is limited to specialized personnel only, until detailed engineering evaluation is completed.
- *Red tag,* **R:** the building has been inspected and deemed unsafe. Access is not allowed until completion of detailed engineering evaluation, retrofit or rebuilding.
- *Collapse,* **C:** the building has collapsed or is on the verge of global instability or local collapse.

Hence, the Onset-of-Damage limit state lies within the green-tag state boundaries while the collapse state is, of course, the most severe stage of the red-tag condition. For post-earthquake structure operability only yellow- and red-tag states are relevant.

Coupling the fragility curves for PG&E buildings and similar results for other elements of the PG&E network with probabilistic seismic hazard analysis will permit assessments of the risk of seismically induced outages in the regional distribution system. In the aftermath of a severe earthquake the use of limit state fragility curves along with the observed spectral acceleration values available from instrumentation networks, such as TriNet, will also provide PG&E with a rapid damage estimation tool prior to building visual inspection.

The procedure developed in this project is, of course, of more general applicability. It is also consistent with the broader approach to Performance-Based Earthquake Engineering put forward by the Pacific Earthquake Engineering Center (e.g., Moehle and Deierlein, 2004).

PG&E building inventory

The total PG&E building stock comprises more than a thousand buildings, the majority of which are not deemed critical to the operation of the power distribution network. A subset of about 200 structures, which includes operation buildings and substations, is currently insured against earthquake damage. These guidelines are intended to be applicable to this subset of important buildings, which here will be referred to as the PG&E building inventory. The inventory comprises many different types of structures often of older and mixed construction, sometimes built and subsequently expanded and/or retrofitted in different phases. For the purpose of this document, these buildings can be categorized into the building classes shown in Table1 (PG&E, 2001c).

These guidelines are *structure-independent* and, therefore, can be applied, with few exceptions[1], to all buildings in the PG&E inventory. It is important to note, however, that

---

[1] Because this methodology estimates the dynamic response of buildings from static nonlinear pushover analyses, its application to tall, flexible buildings is not recommended. For this type of structures the accuracy of nonlinear static pushover analysis in assessing the building seismic response is, in general, questionable.

the guidelines in this present form are not *structure-generic*, namely they are not readily applicable to a generic structure belonging to a certain building class. The guidelines are not *structure-generic* because, as will become clear in the next section, *building-specific* results of nonlinear static procedure (NSP) analysis are necessary for their application.

Description	Number
Concrete Tilt-Up Wall Buildings with Wooden Roof Diaphragm	18
Steel Frame Buildings with Concrete Infill Walls (Mill-Type Buildings)	35
Prefabricated Metal Buildings	44
Concrete Shear-Wall Buildings	11
Steel Moment-Resisting Frames (SMRFs)	3
Braced Steel Frame Buildings	29
Steel Frames with Infill Unreinforced Masonry Walls	3
Concrete Block Buildings with Wood/Metal Deck Roof	19
Wood-Frame Buildings	34
Concrete Frames with Infill Unreinforced Masonry Walls	1
Other or Unknown	8
	205

Table 1: Building types in the PG&E inventory. The number of mill-type buildings is approximate.

The successful application of these guidelines to any specific building depends on the correct modeling of structural details that appropriately capture the failure modes observed during damage reconnaissance investigations. Such structural details, in general, are different for different building types. For demonstration purposes only, the procedure presented here will be applied (see the example section) to two specific structures of the PG&E building inventory:

- a steel moment-resisting frame (SMRF) building,
- a tilt-up building.

Additional example applications of these guidelines by practicing engineers can be found in Degenkolb (2004) and Rutherford & Chekene (2004).

Appendix A includes an overview of the additional steps that may be followed to make these guidelines applicable to a generic structure of a specific building class. Appendix A provides the theoretical framework only. No attempt is made to suggest numerical values for the sources of additional uncertainty defined there. Quantifying such uncertainties is a major task that is beyond the scope of this document. Appendix B will provide an overview of the expert elicitation process carried out for acquiring some of the dispersion parameters necessary for the computation of the fragility curves. Finally, Appendix C contains a copy of some references that are directly related to these guidelines. In particular, the reader can find a paper on the methodology devised for these guidelines (Bazzurro, *et al.*, 2004), a paper on the analyses that supported the calibration of the static versus dynamic evaluation of residual displacements in damaged buildings after the mainshock (Luco *et al.,* 2004), and a document on aftershock probabilistic seismic hazard analysis (APSHA) and its use in the context discussed here (Yeo and Cornell*,* 2004).

Procedure

In brief, the methodology presented here uses the knowledge of the nonlinear *static* behavior of a specific building subject to incremental lateral loads to infer its nonlinear *dynamic* response expected for different levels of ground motion severity. Quantitative measures of the implied degradation in building safety will be used to associate each of several post-earthquake *structural damage states* with an appropriate post-earthquake *structural limit state* that may imply some degree of occupancy restrictions (e.g., yellow or red tagging). These restrictions dictate the facility effectiveness in the electrical distribution network in the immediate aftermath of an earthquake and provide valuable information to estimate expected downtime. A unique aspect of this procedure is that the building safety while in a damaged state is measured in terms of its ability to protect occupants from death or injury due to aftershocks that might occur prior to its repair. 2004 experience in Japan with the Honshu earthquakes shows once again that aftershocks may cause ground motions as large or larger than the mainshock values. The mainshock damage may cause either

- decreased global lateral collapse capacity,
- decreased seismic capacity with respect to loss of vertical resistance, locally or more widely, to gravity and live loads.

Finally, the uncertainty inherent in building response and capacity for different ground motion levels due to both record-to-record variability and to uncertainty in structural modeling and evaluation process is used to obtain the desired fragility curves for the five structural limit states identified in the introduction.

It is not the intent of this document to provide the validation of all of the steps. For the interested reader, an overview along with a list of references is included in the commentary.

The procedure has six steps:

- **STEP 1: *Nonlinear Static Procedure (NSP) for the intact building.*** Conduct a conventional nonlinear static procedure (NSP) analysis (also known as static pushover, SPO) of the selected structure (in each orthogonal direction) in the as-is condition using a displacement-controlled approach that includes P-delta effects and strength degradation of structural elements[2]. Increase the deformation until either the structure base shear has significantly dropped (e.g., to 20 or 30% or less) compared to its peak value or until at least one of the structural elements or connections has reached its ultimate capacity to withstand vertical loads even in absence of any future ground shaking. The NSP analysis should also be stopped when the value of global ductility obtained in the analysis becomes unattainable

---

[2] This procedure requires that the applied lateral load be allowed to drop. This can be achieved by including strength degradation at the element level and by limiting at each step of the analysis the incremental displacement at one, or more, key node(s) of the structure.

in reality. Identify important *damage states* along the displacement axis of the NSP curve(s).

- **STEP 2: *NSP for the damaged building.*** For each of the damage states that do not include loss of local vertical capacity (STEP 1), conduct analogous NSP analyses assuming the structure is in that damage condition after the mainshock. These results will be used (STEP 3) to estimate the residual (dynamic) capacity to resist aftershocks and hence the relative life safety threat of the building when in one of these potential states. Omit STEP 3 and go directly to STEP 4 for all the damage states that show at least one element that cannot carry vertical loads.

- **STEP 3: *Inferring dynamic response from static response.*** Convert each of the *intact structure*'s two NSP curves (STEP 1) into estimates of the peak <u>dynamic</u> displacement (and, hence, post-earthquake damage state) expected under a range of potential (mainshock) ground motions, using the SPO2IDA spreadsheet tool provided (Vamvatsikos and Cornell, 2001b). This step computes the incremental dynamic analysis (IDA) curve for the intact structure in each direction. The ordinate of the highest point on the IDA provides the *(dynamic) capacity* of the intact building, which is expressed here in terms of (median) ground motion level necessary to induce either global lateral instability of the structure or local collapse anywhere in the structure. Then, for the *damaged structure* in all damage states (with no local loss of vertical capacity), apply the same tool to each of the corresponding NSP curves (STEP 2) to estimate the residual capacity in terms of the (aftershock) ground motion intensity necessary to cause collapse (either global or local). This residual capacity will depend on the residual displacement offset expected (or measured) after the mainshock. If necessary, compute the residual capacity of the damaged structure in both directions. Note that for the damaged structure the step above provides also the entire IDA, which, however, will *not* be used in this procedure.

- **STEP 4: *Occupancy Status for Damaged Building.*** Categorize each potential *damage state* with no loss of local vertical capacity as one of the following five structural *limit states*: green-tag, onset-of-damage, yellow-tag, red-tag, or collapse. The tagging is based on the corresponding residual capacities identified in STEP 3 and on the (site-specific) mean annual frequency of exceedance of the (aftershock[3]) ground motion values corresponding to such residual capacities. Damage states, if any, for which vertical capacity is lost at least at one structural component are associated with the collapse limit state[4].

---

[3] Two schemes of tagging are presented below one based explicitly on the aftershock hazard and one only implicitly using the original, customary mainshock hazard as a proxy for the aftershock hazard, which is currently less familiar.

[4] Local loss of vertical capacity is potentially life threatening and for this reason this condition is associated here with structural collapse. Note that local loss of vertical capacity does not necessarily implies that the structure has no global lateral capacity left to resist aftershocks.

- **STEP 5:** _**Ground motion level associated with a structural limit state.**_ Using the results of STEPS 3 and 4, identify the four (mainshock) ground motion levels expected to cause the structure to enter the onset-of-damage state, the yellow-tag state, the red-tag state, and the collapse state according to a pre-defined criterion provided in this step. Such ground motion levels are identified by their median values and related dispersion measure.

- **STEP 6:** _**Computation of the fragility curves.**_ Based on the median values and corresponding dispersion measure of the four ground motion levels number provided at STEP 5, plot the fragility curves associated with the onset-of-damage, the yellow-tag, the red-tag, and the collapse states. The fragility curve corresponding to the green-tag state is equal to unity for all levels of ground motion.

Discussion of the Six Steps

STEP 1: *Nonlinear Static Procedure (NSP) curve for the intact building*

The knowledge of the post-elastic behavior of the building subject to incremental lateral seismic loading is the starting point of this procedure. In line with other current Guidelines (e.g., FEMA 273, 1997; FEMA 356, 2000), it is assumed here that the engineer is accustomed to performing nonlinear static procedure (or static pushover) analyses at least for the two main orthogonal directions of the structure. The nonlinear static procedure normally involves the monotonic application of lateral forces (or displacements) to a model of the building until a target deformation is reached. The lateral load is selected to follow a predetermined or adaptive pattern (Kunnath and Balram, 1999; Balram and Kunnath, 2000) that approximately represents the inertial forces at the locations of the significant masses. In this application the pushover analysis should include element strength degradation and should be conducted to failure, namely until either severe lateral force degradation or local loss of vertical capacity of at least one structural component (e.g., beam, column, connection, etc.) are reached. The reader is referred, for example, to Section 3.3 of FEMA-273 for details on how to perform a NSP analysis.

It is important to emphasize that the seismic evaluations performed within the framework of these guidelines should use expected strength values rather than nominal or lower-bound strengths. The intent here is to estimate the realistic response of a structure and not to apply conservative procedure to achieve a "safe" building design.

The NSP curves expressed in terms of base shear versus roof drift (i.e., roof displacement divided by the height of the building) for the two main orthogonal directions of the structure are the main products of the NSP analysis. The engineer identifies on the NSP curves the major inelastic events that occur in the structure (e.g., failure of a significant portion of the roof/wall connection of a tilt-up building, fracture of at least 10% of all top flanges in a steel moment-resisting frame, or local collapse of beam-column connection due to shear failure) along with associated roof drift levels. These major inelastic events sometimes cause significant drops in the base shear or changes in the global stiffness of the building which in turn translate into changes in slope of the NSP curve, as depicted in Figure 1. In other cases their occurrence may only moderately change the global stiffness of the structure and, therefore, may not produce sharp kinks in the pushover curve.
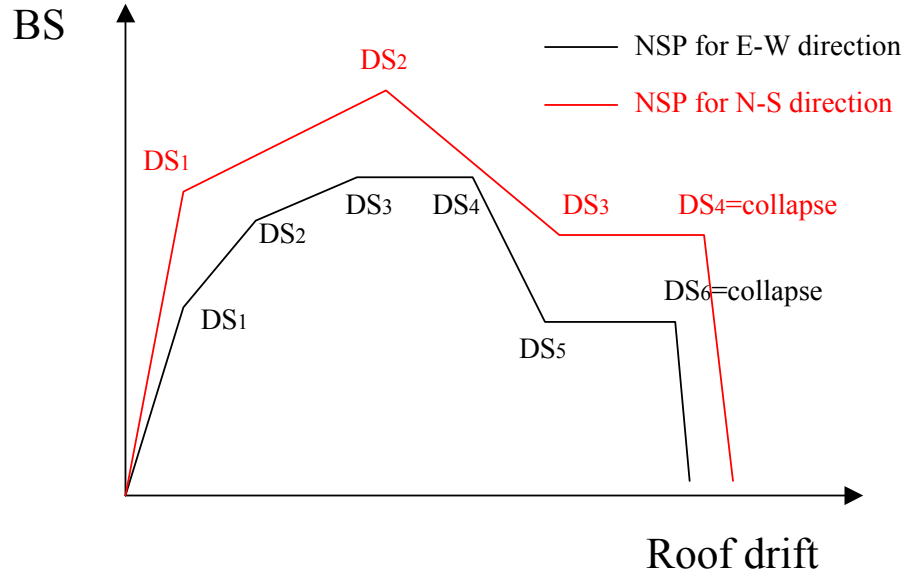
Figure 1: Hypothetical Static Pushover curves for the two orthogonal directions of a building. Legend: BS stands for base shear.

The engineer needs also to assess whether the structural members that are damaged at any stage of the NSP curve are still able to withstand gravity and live loads. As mentioned above, if local loss of vertical capacity at a certain damage state is likely, then there is no need to continue the NSP analysis is stopped. The decision can be based, for example, on whether the ultimate deformation of a ductile element (or connection) or the maximum strength of a brittle member (or connection) have been attained. For example, a steel beam-column connection that reaches a curvature sufficient not only to fracture the flanges but also to pull off the shear tab connection may not physically collapse (due, for example, to membrane effects in the slab) but it cannot be considered suitable for withstanding vertical loads of any significance. Such ultimate strain and strength values are sometimes available from laboratory tests published in the literature. If tests are not available either a detailed finite element analysis of the member (or connection) or simply engineering judgement need to be used. Although it is outside the scope of these guidelines to provide such values, the reader can find useful information in FEMA 273 (1997) for several structural components for steel, reinforced concrete, and masonry constructions; in FEMA 288 (1997), FEMA 289 (1997), and FEMA 355D (2000) for steel beam-column connections; in Pardoen *et al*. (1999) for tilt-up wall-roof-connections; in ATC-11 (1983) and Paulay and Priestley, (1992) for concrete beam-column connections; and in Duffley *et al*. (1994) for shear-wall concrete structures.

These inelastic events are to be associated with specific *damage states*. More formally, the occurrence of the ith major inelastic event (or a set of events at approximately the same deformation level) identifies the ith *damage state*, DS_i. DS_i is therefore defined by a) a roof drift value, Δ_i, and b) a detailed description of the structural damage associated with that event, including whether any element has reached ultimate vertical capacity. The damage description can be valuable to engineers to compare with observable damage during the inspection of a facility before deciding on the possible building occupancy restriction after an earthquake. Each one of these damage states will be later associated

with one (and only one) *structural limit state.* The limit states are defined here in terms of a color tagging condition (Green, Yellow, or Red) or of Onset of Damage or of Collapse as discussed in STEP 4.

Summary of STEP 1: apply NSP techniques to both directions of the intact building and identify major damage states DS_i that the structure could be in after being hit by an earthquake mainshock.

Output of STEP 1: two NSP curves of the two main perpendicular directions of the intact building, a series of structural *damage states* DS_i, a detailed description of the physical damage for all states DS_i, and Δ_i values associated with such states.

> *C: The* **conventional** *NSP inherently assumes that the response of the structure until collapse is dominated by its first mode. A word of caution is given here on the accuracy of such a hypothesis for some of the building types in the PG&E inventory. For example, the most frequent failure mode of tilt-up buildings after the 1994 Northridge earthquake involved the failure of the connections between the roof diaphragm and the concrete walls. For example, for mill-type buildings, the high concrete infill walls are expected to be vulnerable when moving in the out-of-plane direction (e.g., Paulay and Priestley, 1992). This failure mode cannot be correctly captured using conventional NSP analysis unless particular care is taken during modeling and load pattern application.*

> *C: If the building is not symmetrical about a plane orthogonal to the applied lateral loads, in principle the lateral loads should also be applied in both positive and negative directions for the purpose of estimating the residual capacity.*

> *C: 3D Static Pushover analysis is feasible but not common. For the purpose of these guidelines the engineer should repeat the analyses for both directions unless it is evident that one direction is weaker than the other. In such case the analyses should be performed only on the weaker of the two directions. In the illustrative example the analyses are carried out for the E-W direction only.*

> *C: If a structure is located close to a fault it may be affected by forward directivity effects, which cause the ground motion component to be statistically higher in the direction perpendicular to the fault strike. Hence, for a generic structure it may not be appropriate to consider only the weaker building direction because of the statistical difference between the fault parallel and fault normal ground motions. The engineer should exercise his/her judgment to establish if the NSP analysis needs to be performed for one of both orthogonal directions.*

STEP 2: *NSP curves for the damaged building*

The NSP analyses performed at STEP 1 identify a suite of potential *damage states*, DS_i, that the structure may be in after an earthquake. While in that damaged condition the building is vulnerable and could experience more extensive and severe damage in future

events, in particular in aftershocks prior to repair. This life-safety threat drives the tagging of damaged buildings.

To evaluate the post-earthquake residual capacity of the building to withstand future lateral loads, this step of the procedure requires obtaining the NSP curves for the building in every damage state. NSP curves for each damage state are needed for characterizing (STEP 3) the residual lateral capacity left in the structure after different levels of damage that might have been inflicted on it by the mainshock. The residual lateral capacity is the quantity used when assigning a *damage state* to a structural *limit state* (STEP 4) and therefore to a tagging condition. For the purpose of these guidelines, however, the assessment of the residual lateral capacity of the building in the DS_i damage state is of interest provided that at the local level every damaged structural member is still capable of carrying vertical loads. If there is loss of local member vertical capacity in the DS_i damage state the building will be assigned a structural limit state that corresponds to collapse (STEP 4).

Hence, STEP 2 consists of subjecting a model of the building in the ith damage state to the same NSP analysis described at STEP 1. This exercise is to be repeated for all the damage states identified at STEP 1 for which the local ability of sustaining gravity and live loads is not compromised. This process leads to a family of NSP curves, two (one per orthogonal direction and, possibly, one for positive and negative directions as well) for each of such damage states.

Figure 2 shows NSP curves for the intact structure and for the damaged structure in damage states from DS_2 to DS_5 in the E-W direction (see Figure 1). The NSP curve for DS_6 is missing because it is assumed here that at that damage state some members were so severely damaged that they could not reliably carry vertical loads. Note that the pushover curve for a structure at the onset-of-damage state (i.e., DS_1) coincides with that of the intact structure.
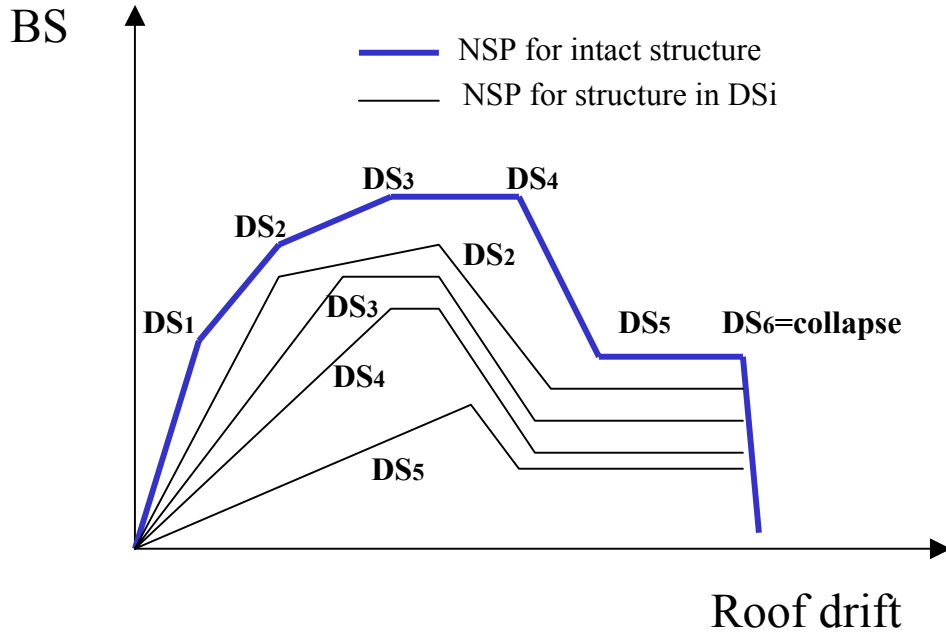
Figure 2: Hypothetical NSP curves for structure in the intact condition and at different levels of damage (i.e., DS_2 to DS_5).

Summary of STEP 2: apply NSP techniques to the damaged structure in all damage states DS_i for which vertical load carrying capacity is not compromised anywhere in the structure. Unless one of the two main orthogonal directions of the building is significantly weaker than the other, perform STEP 2 analyses for both directions.

Output of STEP 2: a family of NSP curves that are associated with different levels of initial building damage state DS_i for which local vertical capacity is preserved everywhere in the structure. Identify damage states DS_j, $j>i$, that show local loss of vertical load carrying capacity, if any.

> *C: In practice the NSP curves for the structure in the damaged state can be obtained by "re-loading" -- re-imposing an increasing deformation on -- the model of the structure after it has been quasi-statically unloaded from the ith damage state[5]. Obtaining these NSP curves by assuming parallel-to-elastic unloading/re-loading is a simple alternative that can result in comparable estimates of residual dynamic capacity (see STEP 3) (e.g., see the case studies). Another viable alternative for computing reloading stiffness values of damaged buildings presented in the PEER 508 study (Rutherford & Chekene, 2004).*

> *C: Unloading the structure from a damage state may create an initial offset in the damaged-structure NSP curve due to the residual permanent displacement in the*

---

[5] The use of an unloading procedure that cycles the structure to an equal displacement in the opposite direction has also been considered. It might be considered to better represent (statically) the behavior and damage of a structure during an earthquake. As of this date, the simpler unloading procedure has been found to give results that correlate better with dynamic analyses.

structure. The extent of this permanent displacement is somewhat an artifact of applying a static procedure to modeling the dynamic response of the structure subject to ground shaking. The residual displacement obtained from the NSP can be considered as an upper bound because the structure is not allowed to oscillate and therefore return to a residual offset closer to its original upright position. Hence, for the purpose of these guidelines the NSP curves for the structure in the damaged conditions are assumed to start from the origin of the axes (i.e., no permanent displacement). The effects of the expected (or measured) **dynamic** *residual offsets on the residual lateral capacities are accounted for in STEP 3.*

C: *As illustrated in Figure 2, the horizontal shift of the NSP curves for the damaged structures back to the origin does not shift the collapse (e.g., DS_6) displacement. In STEP 3, however, the collapse displacement will, in effect, be reduced by the residual offset.*

C: *The comment at STEP 1 on unsymmetrical structures applies to a greater degree to damaged buildings. This may sometimes apply to buildings that are symmetrical in their intact condition. Note also that certain of these states may be associated with local collapse and/or with important changes in stiffness or capacity in the transverse direction. In other words, in some cases (e.g., tilt-ups) a building characterized by a damage state associated with, say, lateral loads applied to the N-S direction may need to be "pushed" in the E-W direction as well.*

STEP 3: *Inferring dynamic response from static response*

The nonlinear *dynamic* behavior of the structure in both the intact and the damage states defined at STEP 2 is estimated here using the NSP from STEPS 1 and 2 and the provided (Microsoft Excel) spreadsheet SPO2IDA (Vamvatsikos and Cornell, 2001b; Vamvatsikos and Cornell, 2002). The suggested procedure is slightly different for the intact and the damaged cases and, therefore, they are treated separately below. The dynamic response of the *intact building* is evaluated for a full range of potential mainshock ground motion levels. The result of this operation, which is the dynamic counterpart of the static pushover curve, is called the Incremental Dynamic Analysis (IDA) curve (Vamvatsikos and Cornell, 2001a). The dynamic response of the *damaged building* is of interest here only at aftershock ground motion levels close to the ultimate capacity of the building and not for the full spectrum of ground motion intensity.

The use of the SPO2IDA tool requires that the NSP's used as input be normalized in both axes (i.e., base shear, BS, vs. roof drift, Δ) by the corresponding quantities at the onset of damage (or incipient yielding) of the structure. The engineer can use his/her judgement to identify an appropriate normalization point that can be associated with onset of damage or incipient yielding in the structure. Selecting an accurate yielding point is desirable but not crucial. It is, however, important that both the normalizing base shear, BS_y, and roof drift, Δ_y, values be consistent with the same selected point on the pushover curve.

However, the IDA's, which constitute the output of the SPO2IDA tool, have the Y axis expressed in terms of the ratio of a ground motion parameter rather than of base shear. The parameter selected here is the spectral acceleration, $S_a(T_1)$, at the fundamental oscillatory period of the intact structure, T_1, and the normalizing quantity is $S_{ay}(T_1)$, the spectral acceleration at incipient yielding. Of course, the two ratios in terms of base shear or of spectral accelerations are numerically equivalent. This change of variables on the Y axis for the IDA case is important in this procedure because the tagging strategy is based on exceedance of ground motion spectral acceleration (STEP 4) rather than base shear.

To facilitate the comparison of IDAs corresponding to different damage states, their ordinates should be "de-normalized" (namely, multiplied by $S_{ay}(T)$, where T is equal to T_1 for the intact structure IDA and to T_{DSi} for the IDA of structure in damage state DS_i). Under the assumption that the response of PG&E structures is dominated by the first mode, $S_a(T_1)$ for the intact structure (or $S_a(T_{DSi})$ for the structure in damage state DS_i) can be obtained simply by dividing BS by the building effective modal mass for the fundamental vibration mode, $M_1^* = \psi_1^2 \boldsymbol{\phi}_1^T \mathbf{M} \boldsymbol{\phi}_1$, where ψ_1 is the first-mode participation factor, $\boldsymbol{\phi}_1$ is the first modal shape, and $\mathbf{M}$ is the mass matrix. If the contribution to the response from higher modes is significant then more modal participation factors come into play. A detailed procedure on how to transform base shear into spectral acceleration can be found, for example, in the HAZUS manual (1999).

The procedure above applied to the structure in different states of damage yields, however, de-normalized IDAs that, in general, are expressed in terms of spectral accelerations at different oscillatory periods. The commentary provides approximate methods to convert $S_a(T_{DSi})$ into $S_a(T_1)$ for all damage states DSi. Note, however, that obtaining IDA's expressed in terms of spectral acceleration at the same period is convenient for graphical representation and visual comparison of IDA's but not strictly necessary for applying the procedure. More details follow in the commentary.

Numerical examples of base shear to spectral acceleration conversion and axes normalization are given in the case study section.

Intact structure

An IDA curve is generally considered a tool for predicting the dynamic *median* deformation (e.g., inter-story drift or roof displacement) of a structure for a given level of ground motion severity (here measured by $S_a(T_1)$[6]) (Vamvatsikos and Cornell, 2002). In these guidelines, however, the IDA curve is used in the opposite direction, namely to obtain the mainshock *median* ground motion level, S_a, that is expected to cause the intact structure to end up in each of the identified damage states, DS_i. Such S_a values can be read off the IDA curves at the roof drift values Δ_i associated with such states. Figure 3 shows a typical output of the SPO2IDA tool where the NSP curve (or, more precisely, its quadrilinear fit, as discussed in the commentary) is the input and the IDA curve is the output. Note that in Figure 3 the deformation measure on the X axis is the roof global

---

[6] The period T_1 is often dropped hereafter for simplicity.

ductility ratio, μ, which is the ratio of the roof drift to the roof drift at the onset of damage or incipient yielding. Further the IDA curve defines the global collapse capacity (indicated by a circle in Figure 3) of the intact structure. The basis for IDA curves is described in the commentary. It is important to emphasize that the IDA curves are to be considered as *median* curves. The record-to-record variability will be explicitly dealt with during the development of the fragility curves in STEPS 5 and 6.
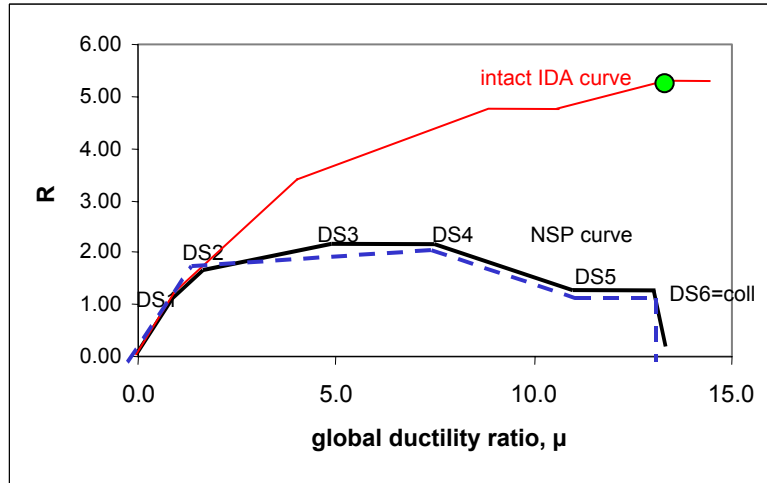
Figure 3: Hypothetical NSP and IDA curves for the building in the intact condition. In this case the abscissa represents the global ductility ratio, μ (namely, the roof drift divided by the roof drift at first yielding, i.e., at DS$_1$). The ordinate R is equal to BS/BS$_y$ for the NSP curve and to $S_a(T_1)/S_{ay}(T_1)$ for the IDA curve. Note: the dashed line is an example of quadrilinear fit of the pushover curve, as explained in the commentary to come.

Damaged structure

IDA curves are also part of the procedure applied to the damaged structure. In this case, however, IDA curves are not used for predicting the mainshock *median S_a* (given a roof drift value, Δ_i) that will cause the intact structure to end up in damage state DS$_i$, but rather for estimating the *median residual* dynamic lateral "capacity", $(\check{S}_{a,cap})_i$, of the damaged structure in each post-mainshock damage state DS$_i$ to resist aftershocks. $(\check{S}_{a,cap})_i$ is the (aftershock) ground motion level that is expected to cause subsequent collapse and, should the building still be occupied, life loss. The same SPO2IDA spreadsheet provides an estimate of $(\check{S}_{a,cap})_i$ as one of the points of the IDA for the damaged structure (Figure 4 shows an example for damage state DS$_3$). This capacity is defined either as the condition where small increases in "load" during aftershocks will cause arbitrarily large increases in deformation (i.e., where the IDA curve becomes effectively flat; this definition was also adopted by the SAC/FEMA 350-352 Guidelines (2000)[7]) or as the aftershock spectral acceleration that causes local collapse anywhere in the structure.

---

[7] The IDA curve could be also *nearly* flat close to collapse. *SAC used the point at which the local slope is 20% of the initial slope or less.*

Recall from the commentary of STEP 2 that the NSP curves for the damaged structures have been shifted to remove the *static* residual displacement offsets created by the NSP procedure. The IDA curves derived from those NSP curves, therefore, assume no residual offset. As one might expect, though, the residual offset after a mainshock influences the residual capacity to resist aftershocks, $(\check{S}_{a,cap})_i$ (e.g., Luco *et al.*, 2004; see Appendix C). In these guidelines, an IDA curve for each damaged structure that accounts for the residual offset is obtained by tracing the IDA curve that assumes no residual offset up to the point that has a displacement equal to the displacement capacity (defined in the preceding paragraph) minus the expected (or measured) *dynamic* residual offset (defined in the commentary). See the case studies for examples. Equivalently, the collapse displacement of the NSP curves found in STEP 2 (e.g., the displacement at DS_6 in Figure 2) can be reduced by an amount equal to the expected (or measured) *dynamic* residual offsets, and these NSP curves that account for the residual offset can be input into the SPO2IDA spreadsheet. An example of the resulting IDA curve is shown in Figure 4.

Even without considering a residual offset the IDA curves for the damaged structures will generally provide estimates of the residual capacities, $(\check{S}_{a,cap})_i$, that are not equal to that of the intact structure, namely $\check{S}_{a,cap}=(\check{S}_{a,cap})_1$.[8] (the estimates of the median capacity for the intact structure and for the damage state DS_1, which defines the Onset of Damage state, are the same). In contrast, dynamic analyses of damaged structures (e.g., Luco *et al.*, 2004) indicate that without a residual offset little or no reduction in the median lateral capacity relative to intact structures is expected, at least for the structures analyzed here. To reflect this observation, an adjustment to $(\check{S}_{a,cap})_i$ is made in these guidelines. As demonstrated in the case studies, the adjustment is achieved simply by multiplying $(\check{S}_{a,cap})_i$ by the ratio of the capacity of the intact structure to the residual capacity assuming no residual offset. Hence, if no residual offset is expected (or measured), the adjusted residual capacity will equal $(\check{S}_{a,cap})_1$. The NSP curve needs to be obtained for all the post-earthquake damage states (STEP 2) in which **none** of the structural elements has reached its ultimate vertical capacity to withstand gravity and live loads during the mainshock. All the damage states that do show loss of local vertical capacity will be automatically associated with collapse (STEP 4).

---

[8] This is a result of differences in the shapes of the NSP curves for the damaged versus intact structures, as illustrated in Figure 2.
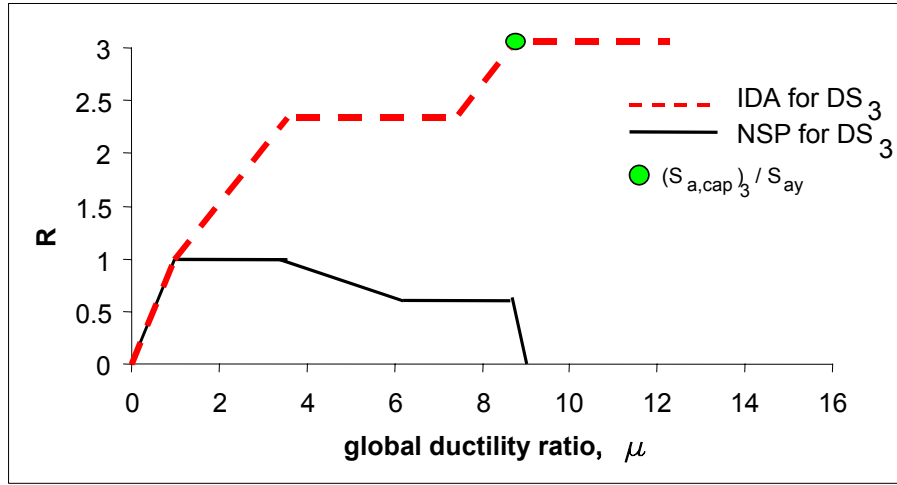
Figure 4: Estimate of the residual median capacity $(\check{S}_{a,cap})_3$ for damage state DS_3 (after accounting for the expected, or measured, residual offset after the mainshock). As in Figure 3, the ordinate R is equal to BS/BS_y for the NSP curve and to $S_a(T_{DS3})/S_{ay}(T_{DS3})$ for the IDA curve.
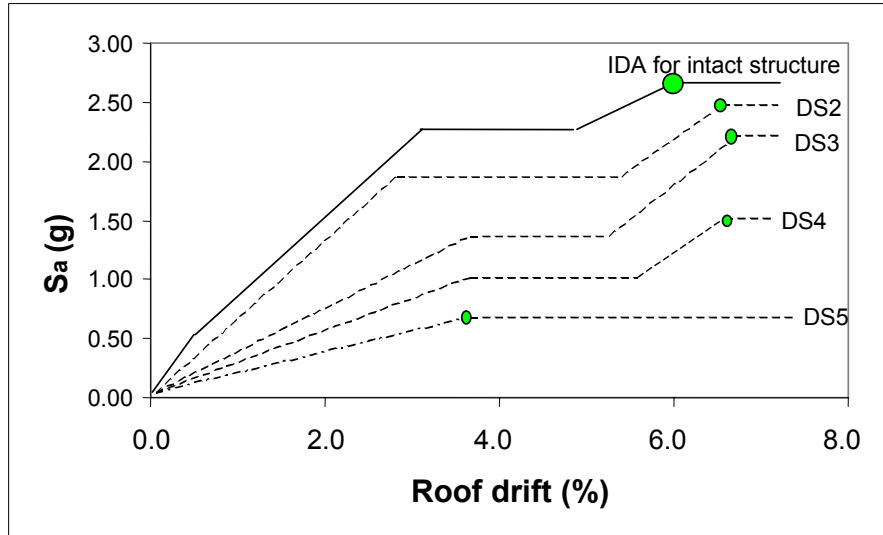
Figure 5: IDA curves for the intact structure and for the structure at different levels of damage (after accounting for the expected, or measured, residual offset after the mainshock *and* adjusting for the behavior observed in dynamic analyses of damaged structures). The circles represent the global collapse *residual* capacity of each case. All the IDA's have been de-normalized and scaled to the spectral acceleration at the same oscillatory period before including them in the same plot (see commentary).

16
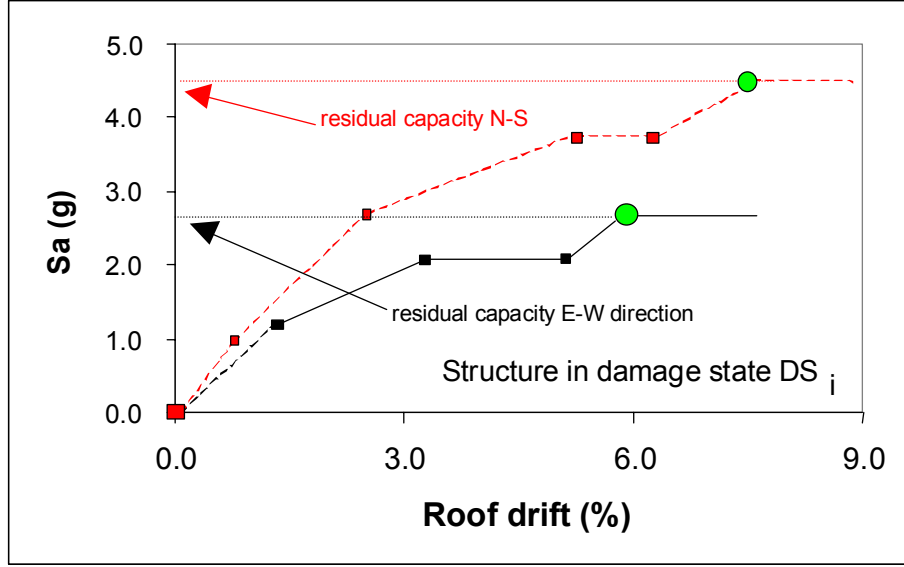
Figure 6: Residual global capacities for the building in damage state DS$_i$ estimated from IDA curves (dotted lines in the figure) for the two main orthogonal directions.

Summary of STEP 3: Using the SPO2IDA spreadsheet provided, estimate the dynamic response of the structure in its intact and damaged conditions from the corresponding NSP curves.

Output of STEP 3: the IDA curve for the structure in the intact condition (solid line in Figure 5) and estimates of the residual capacity $(\check{S}_{a,cap})_i$ for the damaged structure in each damage state DS$_i$ of different severity. The residual capacity is associated with a ground motion level that causes either global lateral instability (as the circles shown on the dotted IDA curves in Figure 5[9]) or local collapse of any element in the structure.

> *C: It is important to note that the spectral acceleration values corresponding to the median capacities $(\check{S}_{a,cap})_i$ obtained for damage state DS$_i$ (and the entire IDA curve as well) is in terms of an oscillatory period T_{DSi} which is in general longer than the initial period of vibration T_1 of the intact structure.[10] The lengthening of the fundamental period is due to the damage sustained by the structure. The value of T_{DSi} can be computed as follows:*

$$T_{DSi} = T_1 \sqrt{\frac{K_1}{K_{DSi}}}$$

---

[9] The damage state DS$_6$ is not included in the figure because in this illustrative example the local vertical capacity is assumed to be reached in at least one member at this damage state during the mainshock. Hence, DS$_6$ is automatically associated with collapse.

[10] Obviously this is not the case if, in STEP2, parallel-to-elastic unloading/re-loading is assumed for the NSP curves, which is another advantage of such an assumption. As demonstrated in the case studies, the resulting estimates of $(S_{a,cap})_i$ are comparable to those that make use of NSP curves computed by unloading and re-loading the structural model.

where K_1 and K_{Dsi} are the elastic stiffness values of the intact structure and of the damaged structure in damage state DS_i obtained directly from the respective pushover curves. Numerical examples can be found in the case studies.

*C: In order to display all the IDA curves for the intact and the damaged cases in the same plot (e.g., Figure 5), it is important that they be expressed in terms of the same reference spectral acceleration, which in this context is chosen to be the initial elastic fundamental period, T_1, of the intact structure. If T_{DSi} is different than T_1, an approximate method to derive $S_a(T_{DSi})$ from $S_a(T_1)$ consists of multiplying $S_a(T_1)$ by an average ratio of $S_a(T_{DSi})/S_a(T_1)$ computed from the ordinates of a few uniform hazard spectra at appropriate levels of hazard computed for the building site. Seismic hazard data are easily available from USGS at the USGS National Seismic Hazard Mapping Project website (*http://geohazards.cr.usgs.gov/eq/index.html*) or, at more levels of hazard for spectral acceleration at additional frequencies, from the CD released by USGS (2001). An alternative method consists of deriving an average ratio of $S_a(T_{DSi})/S_a(T_1)$ from an attenuation relationship suitable for the site using a few pairs of appropriate magnitude and distance values. If the attenuation relationship does not directly provide values for $S_a(T_{DSi})$, they can be obtained via interpolation. Finally, if the periods are in the moderate range, it may be sufficient to simply assume that the spectral acceleration ratio is proportional to the inverse of the ratio of the periods, as it would be if the spectrum displayed an equal spectral velocity in this range.*

C: As described above in the guidelines, an adjustment to $(\check{S}_{a,cap})_i$ is made to reflect the observation that the median residual capacity from dynamic analyses of damaged structures shows little or no reduction relative to intact structures if there is no residual offset. This adjustment is achieved by multiplying $(\check{S}_{a,cap})_i$ by the ratio of (i) the capacity of the intact structure, namely $(\check{S}_{a,cap})_1$, to (ii) the residual capacity of the damage structure assuming no residual offset. As will become clearer in the case studies, this adjustment will, in effect, convert $(\check{S}_{a,cap})_i$ from a value in terms of T_{DSi} to one in terms of T_1. Hence, other than for the purpose of including the IDA curves for the intact and damaged cases in the same plot, the conversion described in the preceding comment is not strictly necessary.[11]

C: The SPO2IDA spreadsheet requires also that the NSP curve be specified in a piecewise linear fashion. A quadrilinear fit to the computed NSP curve (see dotted line in Figure 3) may be necessary before the SPO2IDA tool can be used (Vamvatsikos and Cornell, 2002). The four linear lines represent the elastic part, the hardening part, the softening part, and the residual plateau of the pushover

---

[11] In fact, since the effect of the adjustment to $(S_{a,cap})_i$ is equivalent to finding the residual capacity by multiplying the intact capacity $(S_{a,cap})_1$ by the ratio of the residual capacities with and without a residual offset (both in terms of T_{DSi}), the ordinates of the IDA curves for the damaged structures do not need to be de-normalized from R to spectral acceleration.

backbone curve. Some degree of engineering judgment to achieve the best quadrilinear fit may be needed.

C: The residual capacity of the damaged structure in state DS_i may need to be evaluated for both main orthogonal directions of the building. Figure 6 shows examples of residual global instability capacities (indicated by circles) estimated with the aid of IDA's for both N-S and E-W directions of a building. In this case the residual capacity for the state DS_i will coincide with the residual capacity in E-W direction, the smaller of the two values. Note that, as explained above, the IDA curves in Figure 6 are expressed in terms of spectral acceleration at the same initial period of vibration, T_1, of the intact structure in the E-W direction.

C: The <u>dynamic</u> response to ground motion of increasing severity can, <u>conceptually</u>, be evaluated in a similar manner to that done in the nonlinear static procedure. Increasingly scaled versions of the same ground motion time history could be applied to the model of the intact building and the roof drift (or other appropriate deformation parameter) could be recorded versus $S_a(T_1)$ (Vamvatsikos and Cornell, 2001a). Further repeating the process for a suite of earthquake records permits the estimation of the <u>median</u> displacement (at each S_a level) representing the variety of future records of the same intensity. The resulting curve, namely the Incremental Dynamic Analysis (IDA), is, in effect, the dynamic counterpart of the NSP curve. An IDA curve provides more accurate information on how the building will behave <u>dynamically</u> during ground shaking of different severity levels. Analyses of this kind have been done to validate the studies in this report. See examples below and the study by Maffei and Hamburger (2004).

C: Note that IDA and NSP curves can be shown on the same graph because they share the same quantities[12] in both axes. Figure 3 shows one such NSP-IDA pair for one of the two main orthogonal directions of the building. Of course, a second different NSP-IDA pair can be constructed for the other orthogonal direction.

C: The procedure of performing multiple structural response analyses using scaled ground motion records may, again in principle only, be repeated for the structure in each of the damage states identified in STEP 1 and analyzed statically in STEP 2. The damage is typically reflected in decreased stiffness/capacity of damaged elements in the structural model. Again, if any damaged element at any damage state is considered to have "failed" (i.e., vertical ultimate capacity exceeded) during the mainshock, then the NSP and the IDA curves need not be computed (as is damage state DS_6 in the illustrative example). The collapse limit state will be assigned to such a damage state without further analyses. In general, for each structural damage state the result will be one or more IDA curves (possibly, again, one for each main perpendicular

---

[12] T*he ordinate R, which is BS/BS_y for NSP curves and Sa/Say for IDA curves, is numerically, if not conceptually, the same.*

direction of the building, and in principle, one for each of the positive and negative directions). For example, see Figure 6. For comparison purposes, the severity of the ground shaking will be expressed in terms of the spectral acceleration at the fundamental period (in one of the main perpendicular directions), T_1, of the intact building for all damage states.

C: The task described above would require performing many nonlinear dynamic analyses of the building in both the intact and the several damaged conditions identified at STEP 2. This has been done for the case study buildings in Phase 2 of this project, and in at least one case in practice (Maffei and Hamburger, 2004), but it is not expected to be common in even the best engineering practice in the near future. Instead it is assumed here that the IDA curves of the building (intact or damaged) can be estimated by those of simple nonlinear oscillators with force-deformation backbone curves equal to the corresponding NSP curves derived at STEPS 1 and 2 (coupled with an assumed force-deformation hysteretic behavior). The spreadsheet provides estimates of the peak dynamic roof drifts using the same basic assumption of FEMA 273 (1997) and ATC-40 (1996), namely that they can be adequately predicted by the response of an appropriate nonlinear SDOF oscillator. The spreadsheet, however, is not limited to bilinear elasto-plastic oscillators.

C: IDA studies on nonlinear oscillators defined by many different force-deformation NSP backbone curves and associated hysteretic behavior have been conducted and synthesized, permitting now the estimation of IDA curves directly from NSP curves without further need for performing nonlinear dynamic analysis. The IDA representation can be derived directly from a NSP curve based on empirical rules tuned to thousands of analyses conducted with different oscillators and different ground motion. Again, a spreadsheet (Vamvatsikos and Cornell, 2001b and 2002) is provided along with these guidelines for this purpose. A version of the SPO2IDA tool for SDOF oscillator of moderate periods can be found at http://tremble.stanford.edu/cgi-bin/spo2ida-mt.pl.

C: The SPO2IDA spreadsheet does not consider oscillators that have an initial displacement offset. Hence, the manner in which SPO2IDA is used in these guidelines to estimate the residual collapse capacity of a damaged structure with a residual offset is an approximation that may not agree well with the results of nonlinear dynamic analyses. To some extent, the adjustment to the estimate of $(S_{a,cap})_i$ produced by SPO2IDA that is made in these guidelines corrects for this discrepancy.

C: The "expected" residual displacement offset referred to in these guidelines can be based on residual-given-peak displacement data from nonlinear dynamic analyses (of intact structures). Some such data is presented in the case studies, but a more extensive source of information on the subject can be found in Ruiz-Garcia, 2004). Alternatively (or as an update), the residual offset after a mainshock can be measured directly in the field. In this latter case, portions of

STEPS 3-6 will need to be completed after a mainshock has occurred, or else they can be completed a priori for a range of potential residual offset values. Fortunately these steps are not very time-consuming, particularly in comparison to the steps that can be completed before knowing the value of the residual offset (i.e., STEPS 1-2 and most of STEP 3).

*C: It is worth emphasizing again that for the purpose of these guidelines, it is only the **residual** collapse capacities (either global or local) of the damaged structures that are of major interest. These are defined, as for the intact structure, as the ground motion that causes either global lateral instability or local collapse anywhere in the structure. Figure 5 shows the former case where global instability is reached. The **residual** capacity values measured in terms of spectral acceleration will be used in STEP 4 to evaluate the post-earthquake tagging condition designation. The spreadsheet provided, however, estimates the entire IDA and not only the residual capacity.*

STEP 4: *Occupancy Status for Damaged Building*

The criteria that follow are used to recommend the tagging condition (i.e., the *limit state*) to the structure in any specific *damage state*, DS_i, for which **no loss** of local or global vertical capacity is observed during the mainshock. If loss of vertical capacity is observed, then that damage state is associated with collapse[13].

The proposed criteria for tagging damaged buildings, in whichever damage states they may be, are expressed in terms of:

- P_0, the building-site-specific mean annual frequency (MAF) of exceedance of the ground motion corresponding to the median capacity, $(\check{S}_{a,cap})_1$, of the building in its intact conditions. P_0, which refers to the pre-earthquake conditions, can be obtained using conventional Probabilistic Seismic Hazard Analysis (PSHA) codes or directly from the *USGS website* (http://eqhazmaps.usgs.gov/) for a selected set of oscillator periods and firm-soil to soft-rock conditions.
- P, is the building-site-specific MAF[14] of the aftershock ground motion corresponding to the median capacity, $(\check{S}_{a,cap})_i$, of the building in the damage state DS_i. P is, strictly speaking, a time-varying quantity that decreases with time elapsed from the mainshock and, therefore, it is better computed using an aftershock PSHA (APSHA) approach, such as that presented in Wiemer (2000)

---

[13] Local collapse potentially represents a life-threatening condition. A damaged building that was made unstable by the mainshock may in fact become progressively unsafe or may (partially or globally) collapse under its own weight and live loads without the occurrence of any aftershock (e.g., ATC TechBrief2, 1999).

[14] The primary criteria proposed first in fact implicitly assume that one can use the pre-mainshock hazard or MAF, which is more familiar and more readily available, as a proxy for the post-mainshock or "aftershock hazard". The alternative criteria discussed later in the commentary are based more explicitly on the aftershock hazard as is more consistent with the intent of the procedure. In that case a new concept, equivalent constant rate, ECR, analogous to MAF is introduced.

and Yeo, 2004. (For an application of APSHA, see also Yeo and Cornell, 2004, which is attached for convenience in Appendix C.) However, although it requires only minor modifications to conventional PSHA codes, software for performing aftershock hazard is not yet widely used. For this reason, the primary criteria proposed here implicitly assume that one can use the pre-mainshock hazard or MAF, which is more familiar and more readily available, as a proxy for evaluating the post-mainshock or "aftershock hazard". The alternative criteria, discussed later in the commentary, are based more explicitly on the aftershock hazard as is more consistent with the intent of the procedure. The alternative tagging criteria account for the increased probability of collapse from pre- to post-earthquake conditions due both to decreased capacity and to increased (aftershock) seismicity

- Estimates of $\check{S}_{a,cap}$ for the intact building and of $(\check{S}_{a,cap})_i$ for all the damage states DS_i's.

The proposed primary tagging criteria are displayed in graphical form in Figure 7. The figure has two scales for the ordinates, the percentage of loss in $\check{S}_{a,cap}$ and the ratio of P/P_0 that measures the increase in frequency of exceeding the median residual capacity of the building damaged by the mainshock[15].

Capacity Loss (%)	P/P0
2	1.1
5	1.2
10	1.4
20	2.0
30	2.9
40	4.6
50	8.0

(a)   (b)
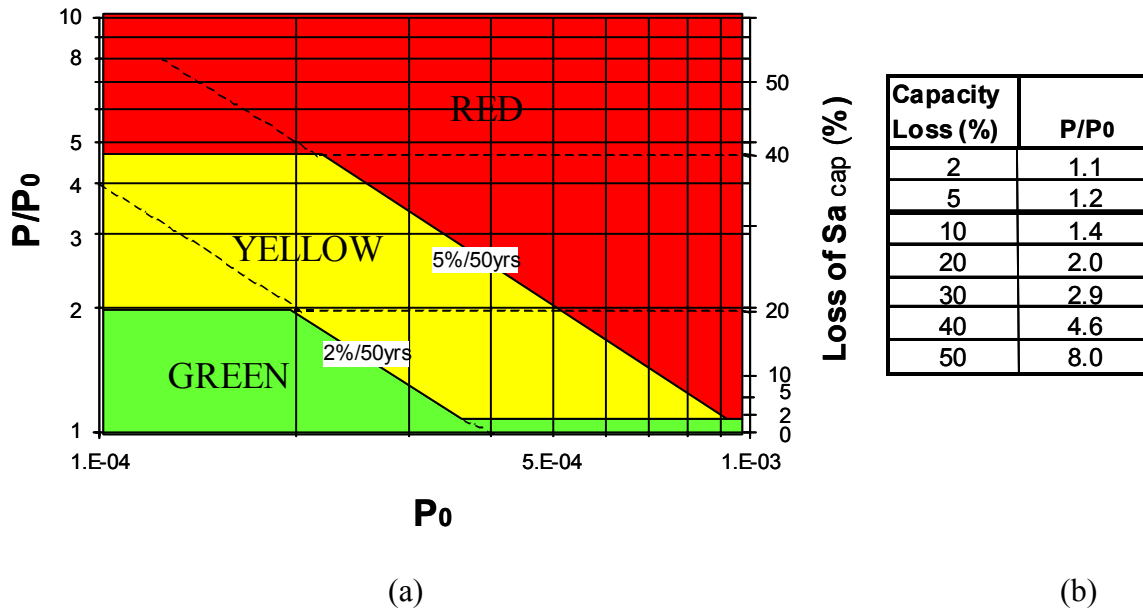
Figure 7: (a) Graphical representation of the recommended tagging criteria. (b) Average relationship for loss of ground motion capacity and rate of increase in mean annual frequency of exceedance of ground motion for coastal California sites for which the absolute value of the (log-log) slope of an average ground motion hazard curve in the surroundings of 10^{-3} annual frequency of exceedance is about three[16].

---

[15] The values of the quantities in Figure 7 and in the text are proposed by the authors and should be re-evaluated and customized by PG&E to fit their specific needs. Note that these values can also be tailored differently for structures of different importance.

[16] The hazard curve slope, which depends on the magnitude distribution and on the rate of decay of seismic waves with distance, is lower in Eastern United States, for example. Hence, in principle caution should be exercised when using this same chart in other areas of the world. The abscissa refers to the pre-earthquake

22

The criteria can be summarized as follows. Any building is identified by a particular value of P_0 that can be computed during "peace" time before any earthquake has occurred. A larger value of P_0 implies that the building is either relatively "weak", or that it is located in an area of higher seismic hazard compared to that considered in the original design, or a combination of both. The opposite is true for lower values of P_0. How the color of the tag changes with capacity loss can be found by searching on a vertical line at that specific value of P_0. Therefore a building whose P_0 is equal, for example, to 3×10^{-4} needs to be damaged severely enough to loose about 5% of its initial capacity before it is tagged Y and about 30% before it is tagged R. If the intact building had been much weaker or in a harsher seismic environment such that its value of P_0 were equal, for example, to 1×10^{-3}, then a nominal loss of lateral capacity of only 2% or larger would cause the building to be red-tagged. No yellow tag could be assigned in this case, the tag would be either green or red. Conversely a much stronger building with P_0 smaller than 2×10^{-4} would need to lose 20% of its original capacity before being tagged Yellow and 40% to be tagged Red. An explanation of the genesis of such values is provided in the commentary.

The illustrative example shown in Figure 8 refers to a structure located at a site for which $P_0 \approx 2.2 \times 10^{-4}$. For this pre-mainshock hazard level the structure is yellow-tagged if it looses about 15% of the original capacity and it is red tagged if it looses about 35% of the original capacity. In this case the damage state DS_2, which shows a residual capacity, $(S_{a,cap})_2$, greater than 85% of the capacity of the intact structure, $(\check{S}_{a,cap})_1$, is green-tagged. Similarly, the damage states DS_3 and DS_4 are tagged Yellow and Red, respectively, because $0.65 \times (\check{S}_{a,cap})_1 < (\check{S}_{a,cap})_3 < 0.85 \times (\check{S}_{a,cap})_1$ and $(\check{S}_{a,cap})_4 < 0.65 \times (\check{S}_{a,cap})_1$. The damage state DS_1 can be associated with the onset of damage (OD) limit state, which is within the green tag state boundaries regardless of the value of P_0. Similarly, the damage state DS_6, which corresponds to incipient (local and global) collapse limit state is always red-tagged.

---

conditions only; it is simply the long-term MAF of exceedance of the intact building ground motion capacity

[17] The values of the quantities in Figure 7 and in the text are proposed by the authors and should be re-evaluated and customized by PG&E to fit their specific needs. Note that these values can also be tailored differently for structures of different importance.

[18] For California sites, it is assumed here that the absolute value of the (log-log) slope of an average ground motion hazard curve in the neighborhood of 10^{-3} annual probability of exceedance is equal to 3.
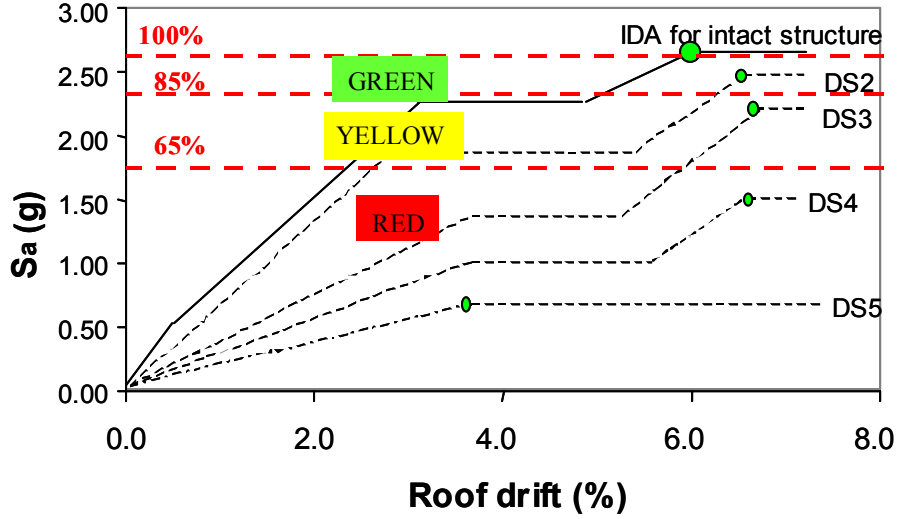
Figure 8: Tagging of different damage states within the illustrative example. The yellow tagging given to DS_3 assumes that the P_0 of exceeding the spectral capacity $(\check{S}_{a,cap})_1$ at the building site is about $\approx 2.2 \times 10^{-4}$.

Summary of STEP 4: apply criteria based on global residual capacity reduction and site-specific aftershock[19] ground motion hazard for mapping damage states into structural limit states.

Output of STEP 4: a one-to-one map of each damage state DS_i into one of the following four limit states: Onset of Damage (OD), Yellow tag (Y), Red tag (R), and Collapse (C).

> *C: The objective of this step is to determine whether a building that has sustained damage as defined by one of the damage states DS_i identified in the previous subsections can be safely occupied or whether access should be limited or forbidden. More formally, this step assigns structural limit states to the damage states identified in STEP 2.*

> *C: The post-earthquake occupancy status of the building is historically defined in terms of color tags posted to the building (e.g., ATC-20, 1989; ATC TechBrief 2, 1999; FEMA 352, 2000). In these guidelines the tagging definitions customized to PG&E buildings are as follows (PG&E, 2001b):*

> - *Green tag ("<u>inspected and safe</u>") implies that the building may require some repairs but is safe for immediate occupancy by PG&E personnel, pending completion of detailed evaluations.*
> - *Yellow tag ("<u>restricted occupancy</u>") implies that access to PG&E personnel in any hazardous area of the building should be restricted until repairs or stabilization can be implemented The building is open only for structural repairs, emergency operations, and retrieval of equipment. For buildings of critical importance, these operations may require emergency*

---

[19] See Footnote 3.

24

personnel access inside the buildings (or parts thereof) for essentially the duration of the emergency (i.e., 72 hours as per PG&E, 2001b).

- *Red tag ("<u>unsafe</u>") implies that the building is unsafe and it should not be occupied for at least the entire emergency period of 72 hours. After 72 hours, entry would be permitted for emergency stabilization of structural elements (after a structural review). In extreme cases, stabilization of a red-tagged building may not be possible or economical and the building may need to be demolished.*

*C: If needed, these designations could be further subdivided into more specific categories based on whether the damage is non-structural only or structural as well and on whether the building can pose a threat to occupants. FEMA 352, Section 3.3, suggests the following color tag definitions: **Green 1** if the damage is only non-structural and the structure is safe **Green 2** if the structure has suffered non-structural and structural damage and the structure is safe, **Yellow 1** if the structure has sustained non-structural damage to a level that could be unsafe for occupancy, **Yellow 2** if the structure has suffered non-structural as well as structural damage that pose a limited safety hazard, **Red 1** if the structure is severely damaged but repairable, and, finally, **Red 2** if the structure has sustained a great deal of damage to be a potential collapse hazard and should be demolished. This refinement, however, is not currently included in these guidelines.*

C: Historically, trained engineers have assigned the tagging categories only on the basis of visual inspection of the building. A number of different analytical approaches have been proposed, for use when time permits, to supplement the tagging procedure based on building inspection. Whereas the implied time-consuming engineering analyses are not feasible in the immediate post-earthquake period in which PG&E facility decisions are urgently needed, these previous proposals do give guidance as to how to make tagging decisions in the new context defined by the present guidelines. In these guidelines such analyses (STEPS 1 through 3) can be made <u>prior</u> to the earthquake during the assessment of the power system reliability. These same assessments can be made available to the inspectors of PG&E buildings in order for them to be able to make more informed decisions immediately after the event. For example, the FEMA 352 Guidelines for post-earthquake evaluation of steel moment-resisting frames suggest three different analysis-based procedures:

- *Determine the capacity of the damaged building relative to current code requirements*
- *Determine the capacity of the damaged building relative to pre-earthquake conditions*
- *Determine the probability of earthquake-induced collapse of the damaged building in a specified exposure period*

C: The first method has the clear drawback that some of the old buildings may not be fulfilling the requirements of the modern codes even in their intact state. This procedure may in principle lead to yellow- and red-tagging buildings even before the occurrence of damage caused by any earthquake. This option does have the benefit, however, of being associated with an absolute life safety criterion. This first option is considered here only in the alternative criteria below.

*C: The second method, despite some obvious caveats (e.g., the same capacity reduction from an originally "strong" and an originally "weak" building should **not** necessarily lead to the same tagging color), is appealing for its simplicity.*

C: A combination of the second and third method has been adopted as the "primary" criteria of these guidelines. The likelihood of building collapse is considered here to prevent the possibility that the second method alone awards a green tag to relatively lightly or moderately damaged, older, originally relatively weak buildings despite unsafe occupancy conditions. A tagging strategy based simply on reduction of lateral capacity with respect to that of the building in its pristine condition (i.e., the second method alone) may also fail to differentiate between initially "strong" and initially "weak" structures and, therefore, only partially promote seismic retrofit of buildings.

C: As stated above, the primary tagging criteria explicitly consider the likelihood, P, that the damaged-building capacity is exceeded but the computation of P is performed for simplicity using pre-mainshock PSHA. For these guidelines for the boundaries between green and yellow tags and between yellow and red tags, respectively, we selected P values to be equal to 2% in 50 years (mean return period, MRP, of 2,475 years) and 5% in 50 years (MRP of 975 years). These values may appear too restrictive when compared to building code requirements for new buildings that prescribe life safety as performance objective for a 10% in 50 years (i.e., MRP of 475 years) ground motion level. We selected low values to implicitly and partially account for the increased aftershock hazard that the damaged building is subject to when the inspection may take place perhaps one or two days after the earthquake. These values, which represent quantitative measures of acceptable risk, should be modified according to the building importance and severity of failure consequences.

C: If the proposed tagging criteria were simply based on maximum acceptable collapse risk of the partially damaged building, however, the green, yellow, and red tag areas in Figure 7 would be oblique bands delimited by straight lines of constant P values. The diagonal bands in Figure 7, however, are delimited by horizontal lines drawn somewhat arbitrarily at constant values of capacity loss of 2%, 20%, and 40%. "Weak", under-designed buildings that are potentially unsafe (i.e., larger P_0) even in pre-earthquake condition would not be tagged Y or R and possibly, at a later stage, retrofitted unless some identifiable physical damage occurred in the building. Tagging Y or R an undamaged building would be difficult to accept by owner and occupants. A hardly detectable capacity loss of

only 2% encourages Y and R tagging and it is meant here to simply serve as a trigger for action for such buildings. The lines at 20% and 40%, that increase the Y and R tagging areas of "strong" (smaller P_0) buildings, have been dictated by a different concept. Results from dynamic analyses (see Luco et al., 2004 in Appendix C) have shown, in general, that a rather widespread damage in the building is needed before the capacity drops by these amounts. In cases of widespread damage the assessment of the true building capacity is more uncertain and it is conservative to force some restriction of occupancy until further more detailed analyses are performed.

C: Note that a collection of figures such as Figure 7 could be produced to account for the time-varying nature of aftershock hazard. Such tagging criteria could be applicable after the earthquake at different snapshots in time when more detailed inspections and/or improved capacity analyses may take place. To mimic the decreasing aftershock hazard with time one could devise criteria that are less stringent as time goes by. This would be reflected by a change in the constant-P lines that separate green, yellow, and red tagging areas. Criteria applicable, for example, one month after the mainshock may have constant P lines demarcating the G, Y, and R areas at higher values than those displayed in Figure 7, which is meant to be applicable immediately after the mainshock. The increased knowledge about building capacity deriving from more detailed inspection and further engineering analyses may also call for the removal of the conservative lines at 20% and 40% capacity drops in the criteria applicable at a later stage.

C: A final remark is in order. It is conceptually preferable to develop tagging criteria in terms of MAF of building collapse rather than MAF of median ground motion capacity. This entails considering the ground motion capacity as a random variable as opposed to a constant. Under certain tenable assumptions the former MAF can be computed by multiplying the latter by a "correction factor", CF, larger than one that accounts for the aleatory and epistemic uncertainties in the ground motion capacity (called β in the section to come) and the slope of the hazard curve in the neighborhood of that ground motion level. Figure 7 could still be used as is with this alternative interpretation. As a first approximation, CF can be considered to be the same for the capacities in both the intact and the damaged cases and therefore it does not have any impact on the values of the oblique lines of constant P/P_0 that divide green, yellow, and red tag regions. For a particular application, the only change would be in the value, $P_0^{'}$, of the abscissa to be used to enter the graph in Figure 7, which will be larger than the MAF of exceeding the median ground motion capacity currently used. This new interpretation is briefly discussed again in the alternate criteria below.

C: As anticipated in the text, a second set of alternate criteria is based on aftershock PSHA. Although these alternative criteria are more in tune with the spirit of these guidelines, at the time of this writing the use of aftershock PSHA is still not common. Hence, they have been proposed here only as a viable

alternative although we recommend that in the future its use is considered by PG&E.

C: STEP 4 Alternate: *Occupancy Status for Damaged Building*

C: In this alternate approach to determining the tagging state of the structure the criteria are based on an assessment of the aftershock ground motion hazard at the site, $H^A(S_a)$, which equals an "equivalent" MAF. Analogous to the discussion above we denote the MAF associated with the median aftershock capacity, $(\check{S}_{a,cap})_i$, of the building in damage state DS_i as P^A when it is based on this aftershock hazard assessment. In this case the tagging criteria are stated as:

- *If P^A is less than $\alpha_1 P'_0$ then the tagging condition for DS_i is green.*
- *If P^A is more than $\alpha_1 P'_0$ but less than $\alpha_2 P'_0$ then the tagging condition is yellow.*
- *If P^A is more than $\alpha_2 P'_0$ the tagging condition is red.*

C: The MAF level P'_0 is the presumed new building design ground motion MAF. Subject to further debate, it is suggested that this value be taken as 2% in 50 years or 0.0004 per annum even in near-fault zones where other, lower definitions of the design ground motion may apply. The proposed values for post-earthquake-recovery-critical PG&E facilities are:

- *$\alpha_1 = 3$*
- *$\alpha_2 = 10$*

Such values are selected arbitrarily and can be used as default values before PG&E defines its own ones. These criteria plot as oblique bands in Figure 7 at levels about a factor of three higher than those shown there. The additional marginal adjustments might be made as well. These criteria do not, however, depend on the P_0 of the existing intact structure, which may be substantially higher or lower than P'_0 for new buildings. See the comments below for further discussion.

C: The aftershock P^A is not, however, a simple constant. The rate of aftershocks depends on the mainshock magnitude and the rate decays as a function of the time lag, τ, after the mainshock. To a lesser degree it also depends on the duration of the interval in the future during which the building will remain in the post-mainshock damaged state.

C: For current purposes, before explicit aftershock ground motion hazard results are available, we suggest the following approximations. Consider a Base Case, in which the mainshock moment magnitude is 7.0, the tagging decision is made within one day of the mainshock, and the duration of interest is in the order of a

one year. In that base case the effective[20] P^A is approximately[21] equal to the pre-mainshock hazard (for any Sa capacity level). So, for example, if the pre-mainshock MAF of exceeding a particular Sa capacity value is 0.001 per annum, then so is the effective P^A. By the criteria above a building with this Sa capacity would by green tagged. The pre-mainshock value may be obtained from an existing site-specific study or from the previously cited USGS web site. However, the P^A is approximately 3 times higher for a magnitude 7.5 event and about 6 times higher for an 8. For these mainshock values the same Sa capacity would have effective aftershock hazard, P^A, of 0.003 and 0.006 respectively. By the criteria above this building would be yellow tagged in the first case and red tagged in the second. (For a magnitude 6 P^A is 1 to 2 orders of magnitude lower than for a 7 and may be safely ignored.)

C: If a tagging decision can be delayed to a later date after the mainshock or if a decision is to be made a second time at a later date, the value of P^A will go down by a factor of about 0.75 at 7 days, a factor of 0.6 at 30 days, and 0.3 at one year after the mainshock. So for example the building with the Sa capacity with a 0.001 pre-mainshock hazard would find its effective aftershock hazard reduced from 0.006 to 0.0036 some 7 days after the mainshock, and, according to the criteria above, its red tag changed to yellow. For the most common early decisions the P^A is quite insensitive to the duration of interest provided it is about 6 months or longer.[22]

C: The analysis here is designed to echo the primary criterion. So, for example, it too makes the tagging criteria dependent on simply P^A, the MAF associated with exceedance of the median S_a capacity, and not on the MAF of collapse. The paper underlying the recommendations here, Yeo and Cornell (2004) is, however, based on the MAF of collapse, comparing this via α_1 and α_2 to the pre-mainshock collapse MAF. As discussed there the MAF of collapse exceeds the MAF associated with exceedance of the median capacity by a factor $exp[k^2\beta^2/2]$. This factor depends on the slope of the hazard curve, k, and the β (uncertainty measure) of the capacity. The k values of the pre-mainshock and post-mainshock (aftershock) hazard curves are very nearly equal. If the β's for the intact and damage-state capacities were approximately the same then the MAF's for collapse would have the same ratio as the MAF's associated with median

---

[20] The analysis here follows Yeo and Cornell (2004), whose article is included in Appendix C. By "effective" we mean here what that reference calls the "Equivalent Constant Rate" associated with a social discount factor of about 3.5%.

[21] The simplified procedure here is based on numerical experience with aftershock PSHA (Yeo, 2004). It is valid for the typical San Francisco Bay Area case where a single nearby fault (segment) is the dominant source of a damaging mainshock ground motion. In other areas, such as the Los Angeles region where several faults may contribute to the pre-mainshock hazard, the aftershock hazard will be a smaller portion of the pre-mainshock hazard. In time it is anticipated that aftershock hazard maps will be provided by a USGS web site in real time after an event to facilitate tagging on an event and site-specific basis. A test site has been operating for some time. Prior to an event the aftershock PSHA can also be done site-specifically for anticipated scenario mainshocks by simple modifications to existing PSHA codes.

[22] Values for other magnitudes, time lags and durations can be found in Yeo (2004).

capacity exceedance, and the α_1 and α_2 values should be the same on either basis. While the aftershock capacity uncertainty β may well be larger than that for the intact structure, especially when the building has not yet been carefully inspected and/or analyzed, the approximation may be close enough for current purposes. If so it implies that decisions about the α values can be thought of in relative MAF of collapse terms, e.g., how much larger an MAF of collapse (and potential fatalities) can be tolerated in post-quake circumstances.

C: The cited paper discusses circumstances and conditions that should be considered for setting the α levels, such as the importance of the structure to post-quake recovery. The values above are the highest recommended there, but the subject deserves broader professional discussion and consensus. The paper also discusses ways in which tagging restrictions might be eased for volunteer workers whose exposure is limited.

C: To get a sense of the implications of the proposed α and P'_o levels consider the following examples. The criteria imply that if a critical PG&E building designed to just meet current IBC standards has a MAF of exceeding the median intact[23] Sa capacity of 2% in 50 years (0.0004 per annum), then it may can be green tagged immediately after a magnitude 7.5 or less if it is undamaged, and yellow tagged for such an event even if it has lost some significant fraction of its capacity. On the other hand, if it were designed for the "deterministic" near-fault MCE with an implicit higher MAF of, say, 6% in 50 years (0.0012 per annum), then if undamaged it would be green tagged after a magnitude 7 but yellow tagged after a 7.5. Damage to the structure would reduce the Sa capacity and increase P^A for all these cases, potentially changing the tagging to a more restrictive level. Older buildings with lesser Sa capacities before and/or after the main event are also more at risk. But an undamaged building with a pre-mainshock "MAF capacity" or a damaged building with a post-mainshock "MAF capacity" of as high as 0.004 (20% in 50 years) would still be accessible on a restricted basis after a magnitude 7. (These numbers are appropriate, recall, for cases when the site mainshock hazard is dominated by a single nearby fault.)

C: It should be clearly understood that these aftershock hazard rate are what is referred to as ECR's or "effective constant rates" (Yeo and Cornell, 2004). They are much smaller than the immediate post-mainshock aftershock hazard rates. For example, as discussed above after a magnitude 7 the "effective MAF" is about equal to the pre-mainshock MAF for any Sa level and any site. However, in the first year after the mainshock the actual total probability of an aftershock exceeding that Sa level is about 30 times the annual probability that a mainshock will do the same. In the following year the aftershock probability will have

---

[23] The median capacity may be higher than this; the SAC/FEMA study of steel moment-resisting frame buildings (FEMA 350) found that IBC implied high confidence failure probabilities of 2% in 50 years or less, implying that the median capacity has an MAF of considerably less than 2% in 50 years.

decayed significantly while the mainshock probability will be unchanged[24]. The process of translating this transient aftershock rate into an equivalent constant rate (for the purposes of comparing the ECR with conventional tolerable constant incident rates) is approximately equal to simply multiplying the total expected number of aftershock events (e.g., collapses or exceedances of the median Sa capacity) by a "social discount factor" which may have a value of about 3.5%. Hence the factor 30 (which equals about 1/0.035). The user is cautioned that this ECR approach is not a practice that has been peer-reviewed, much less widely used. There is in fact little previous decision theoretical literature or practical guidance for dealing with such transient hazards in any public safety policy arena.

STEP 5: *Ground motion level associated with a structural limit state*

The proposed tagging approach (STEP 4) coupled with the IDA curve for the intact structure (STEP 3) leads to the identification of the *median* spectral capacity values associated with the onset of post-earthquake tagging status, denoted $\check{S}_a^{LS}$ for *limit state* LS (e.g., LS equal to OD, onset of damage; Y, yellow; R, red; or Coll, collapse). Identifying the median spectral capacity value for the green tag state is not necessary for reasons that will become clear in STEP 6. The process is shown in Figure 9.

From Figure 8 it follows that for this illustrative example the damage state DS_1 correspond to incipient OD, DS_2 is in Green, DS_3 is in Yellow, DS_4 and DS_5 are in Red, and DS_6 refers to incipient Collapse. Figure 9 shows how this information can be used to determine the *median* spectral capacity value, $\check{S}_a^{LS}$, for any *limit state*, LS. The value of $\check{S}_a^{LS}$ can be found immediately for OD and C whose onset correspond to one of the damage states (here, DS_1 and DS_6, respectively) by reading them off the IDA for the intact structure in Figure 9 at the drift value of Δ_{OD} and Δ_C, respectively. The values of $\check{S}_a^Y$ and $\check{S}_a^R$, however, are not readily available because the damage states DS_i (and, therefore, Δ_i) from the NSP curve in general do not correspond to the inception of the Y and R limit states. The onset of R, for example, occurs for a damage state in between DS_3 and DS_4 (Figure 8). In this case either the procedure is repeated for one or more intermediate DS's until the computed spectral acceleration capacity is, for all practical purposes, reasonably close to the target threshold, or, alternatively but less accurately, an interpolation scheme is used instead[25]. Finally, the value of $\check{S}_a^G$ is zero; any level of ground motion will generate a G tag or worse.

As mentioned earlier, this IDA-based procedure has identified the *median* spectral acceleration value corresponding to the onset of a given structural limit state. The ground motion intensity (i.e., spectral acceleration) at which the limit state (and associated

---

[24] These discussions assume that the mainshocks are Poissonian, i.e., "memoryless" and hence future mainshock event probabilities are not affected by the occurrence of a mainshock.

[25] For any given P_0 the loss in capacity that corresponds to the target boundary between two limit states is known from Figure 7. Therefore, the interpolation procedure will provide the target drift that corresponds to the desired drop in capacity. This drift is that associated with the inception of the limit state that was sought.

tagging) will occur cannot, in fact, be predicted perfectly. The value just identified is a "best guess", and it is assumed therefore that there is a 50-50 chance that the limit/tagging state (or worse) will be observed if this ground motion occurs at the site. There is a smaller chance at lower ground motion levels and a larger chance at higher levels.
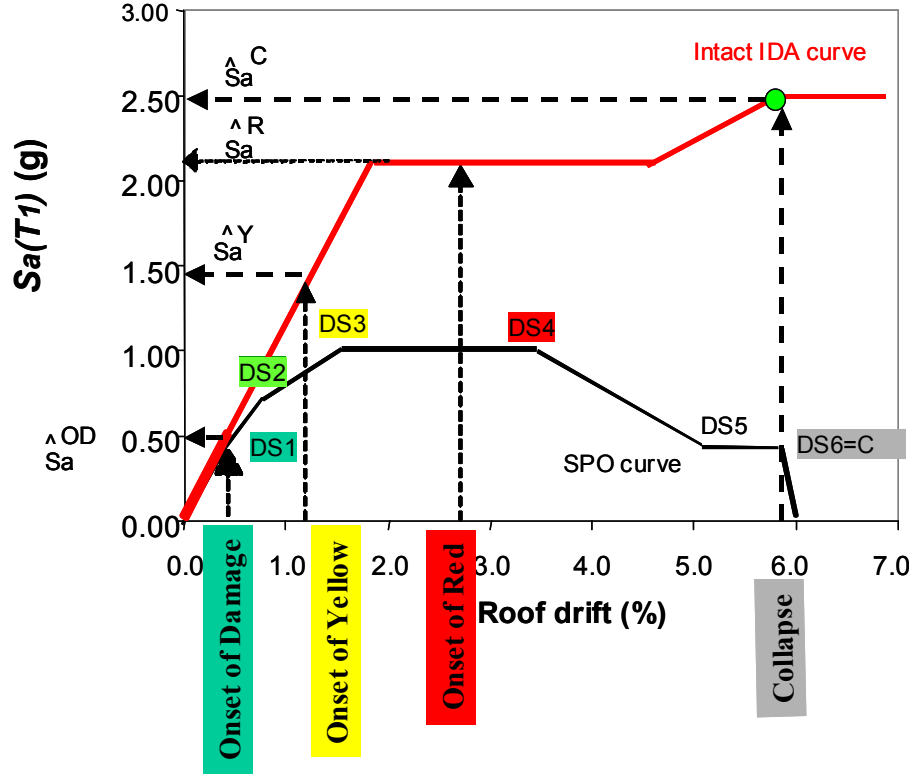
Figure 9: Median spectral acceleration capacity associated with all the structural limit states except the green tag state.

These chances are first quantified by estimating the dispersion, β, which is a combined measure of two basic kinds of uncertainty: *aleatory* uncertainty (or randomness) and *epistemic* uncertainty. The former kind manifests itself, for example, in the variability in the dynamic displacements produced by different ground motion records (even though they may have the same intensity value). Aleatory uncertainty is intrinsic in the random, unpredictable nature of earthquakes and cannot be reduced. The epistemic kind of uncertainty stems, for example, from both the limited accuracy of the selected response analysis approach and the imperfect knowledge of parameter values of the adopted mathematical model of the structure. Within the limits associated with current scientific knowledge, this second type of uncertainty can be reduced, at some expense, with more detailed investigation of the structure, more refined models, more testing of in-place material properties, etc.

Aleatory uncertainty (β_R)

Based on the results of many nonlinear dynamic analyses, it is known (e.g., Miranda; 2000) that the aleatory portion of the dispersion, β_R, depends on the initial period of

vibration of the structure. On average, the values of β_R follow the trend shown in Figure 10, namely short-period (high-frequency) structures show more record-to-record variability in their displacements (or correspondingly, in the spectral acceleration at which a given displacement or damage state is first observed). Further the response dispersion is larger for larger degrees of nonlinearity, especially when the ground motion is near the collapse capacity. This difference is captured in the three curves presented in Figure 10, one corresponding to collapse, one to the Red- and Yellow-tag conditions, and one to the less severe Onset-of-Damage limit state.

The curves in Figure 10 are based on average results of nonlinear dynamic analyses of many nonlinear oscillators with different NSP backbone curves and to somewhat arbitrary definitions of limit states based on average structural deformation levels. Hence, they are suitable as β_R default values. When applying the procedure in these guidelines, however, the provided SPO2IDA spreadsheet will provide structure-specific β_R, values for each limit state that should be used in place of those shown in Figure 10.
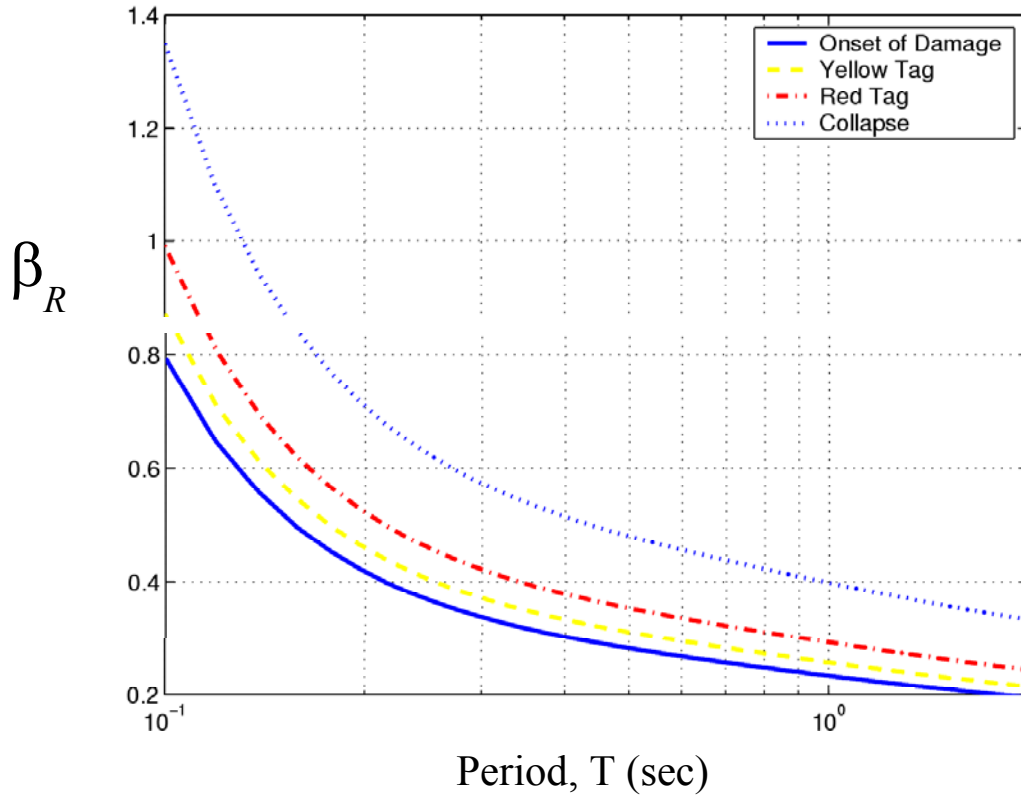
Figure 10: Recommended (default) values for β_R.

Epistemic uncertainty (β_U)

The epistemic part of the uncertainty, β_U, reflects the professional confidence that the selected model and the analysis procedure will predict accurate results. For example, the values for β_U will be larger (i.e., one will have lessor confidence) for complex, older structures (e.g., mill-type buildings) modeled using a simplified model and untested material properties than for a clean, modern steel moment-resisting frame whose

properties have been well determined and whose model has been developed with extreme care to details. Similarly the confidence in the results increases with the level of effort in the structural modeling (e.g., in a SMRF a center-line model yields less reliable results than a model with panel zones).

A review of the PG&E building stock (Table 1) justifies dividing the inventory into four categories of buildings for the purpose of estimating β_U values:

1. Tilt-up or concrete block buildings (retrofitted and un-retrofitted);
2. Mill-type buildings;
3. Prefabricated metal buildings
4. All other buildings

A detailed description of the type of buildings included in each category is provided in Appendix B.

Tables 2a through 2e provide two different sets of β_U values[26] to be applied to all buildings in the four categories. Each set is referred to here as either *Baseline* or *Improved*. The values for the *Baseline* case should always be used unless:

- the building is relatively simple (e.g., no structural irregularities), or
- the development of NSP curves accounts for specific characteristics of the building, such as structural irregularities or the effects of elements not typically considered part of the seismic-force-resisting system.

Appendix B gives conditions and requirements to change the evaluation uncertainty from *Baseline* to *Improved* for each building category. The conditions and requirements are intended to identify the characteristics that most significantly affect the uncertainty in a seismic evaluation for a given building type. The terms *Baseline* and *Improved* reflect a relative measure of uncertainty specific to the building category. They are not intended to have an identical meaning when applied to different building categories. The terms do not indicate an absolute measure of epistemic uncertainty.

Note that Table 2e is directly applicable to steel moment-resisting frames (SMRFs), which are included in the "all other buildings" category. For all the other types of buildings included in this category, the epistemic uncertainty is presumably higher. On a case-by-case basis, the engineer should exercise judgement to apply β_U values that are appropriate to the case under consideration. The values provided for other buildings in Tables 2a to 2d can be used as guidance, with β_U values in Table 2c (mill-type buildings) as an upper bound.

---

[26] The values of β_U were obtained by interviewing expert practicing engineers. The experts elicited in this study were Mr. William Holmes and Dr. Joe Maffei of Rutherford & Chekene, Oakland, CA, and Dr. Maryann Phipps of Estructure, El Cerrito, CA. These values were also compared with those provided by several Probabilistic Risk Assessment studies and by Dr. Robert Kennedy. A brief description of the β_U elicitation process can be found in Appendix B. Some of the values are quite large compared to others in the literature and may need revision with time.

Limit State	Evaluation Uncertainty	
	Baseline	Improved
Onset of Damage	0.6	0.35
Yellow Tag	0.6	0.4
Red Tag	0.6	0.4
Collapse	0.5	0.4

Table 2a: Recommended (default) β_U values for **tilt-up or concrete-block buildings (retrofitted)**.

Limit State	Evaluation Uncertainty	
	Baseline	Improved
Onset of Damage	0.7	0.4
Yellow Tag	0.85	0.65
Red Tag	0.85	0.65
Collapse	0.8	0.5

Table 2b: Recommended (default) β_U values for **tilt-up or concrete-block buildings (unretrofitted)**.

Limit State	Evaluation Uncertainty	
	Baseline	Improved
Onset of Damage	0.7	0.4
Yellow Tag	0.8	0.6
Red Tag	0.9	0.6
Collapse	1.0	0.6

Table 2c: Recommended (default) β_U values for **mill-type buildings**.

Limit State	Evaluation Uncertainty	
	Baseline	Improved
Onset of Damage	0.7	0.35
Yellow Tag	0.8	0.5
Red Tag	0.8	0.5
Collapse	0.9	0.4

Table 2d: Recommended (default) β_U values for **prefabricated metal buildings.**

Limit State	Evaluation Uncertainty	
	Baseline	Improved
Onset of Damage	0.3	0.25
Yellow Tag	0.6	0.5
Red Tag	0.6	0.5
Collapse	0.5	0.4

Table 2e: Recommended (default) β_U values for **SMRF buildings within the "all other buildings" category**.

Total uncertainty (β)

Finally the value of net dispersion, β, to be used in the determination of the fragility curve (STEP 6) is the SRSS value:

$$\beta = \sqrt{\beta_R^2 + \beta_U^2}$$

Given the values of β_R and β_U provided, the total dispersion ranges from $\sqrt{0.2^2 + 0.25^2} = 0.32$ when assessing the onset of damage of very simple, moderate-period SMRF structures that are carefully modeled and analyzed, to $\sqrt{1.35^2 + 1.0^2} = 1.68$ when estimating the collapse of older, fairly stiff complex mill-type buildings modeled and analyzed with limited effort.

Summary of STEP 5: Find the median and dispersion values for the ground motion levels corresponding to the onset of the OD, Y, R, and Coll limit states.

Output of STEP 5: One pair of values, $\check{S}_a^{LS}$ (median) and β (dispersion), for each of the four limit states corresponding to the onset of OD, Y, R, and Coll limit states.

C: In the literature several studies have dealt with the aleatory uncertainty in the median (nonlinear) response given a level of ground motion (or, alternatively, in the median ground motion necessary to induce a specified structural deformation level). Most of these studies considered either SDOF nonlinear oscillators or MDOF structures such as SMRFs or steel jacket-type offshore platforms. To our knowledge, no studies have investigated this issue for less "clean" structures, such as tilt-ups or steel frame buildings with concrete infill walls. The SAC project is one good example (e.g., FEMA 355F) where "hard" numbers of β_R based on multiple MDOF nonlinear dynamic analyses are available for several low-rise, mid-rise, and high-rise SMRF buildings. More recently uncertainty values have been obtained for a wide range of structural frame models by researchers such as Prof. H. Krawinkler and students (e.g., Medina, 2002) and Ibarra, 2003). Regarding β_R values of nonlinear SDOF oscillators, the most exhaustive effort in terms of breadth of structural periods and of hysteretic backbone and cyclic behavior analyzed is the work that forms the basis of the SPO2IDA spreadsheet (Vamvatsikos and Cornell, 2001b) provided here. Such values are, again, consistent with the assumption adopted both here and by FEMA 273 and ATC-40 that the nonlinear MDOF response of fairly stiff structures can be can be adequately predicted by the response of an appropriate nonlinear SDOF oscillator.

C: Very limited research has been devoted to date to a systematic estimation of the epistemic uncertainty in the structural nonlinear deformation caused by a given ground motion or, dually, in the ground motion necessary to induce a given structural deformation. Although limited to SMRF structures, the SAC project (e.g., FEMA 351 and FEMA 355F) is the most widely available reference for gathering information on β_U values. In the SAC reference β_U is intended to represent mainly the epistemic uncertainty in the estimation of demands and capacities. Although equations are provided to compute β_U values (e.g., see Appendix A in FEMA 351, Yun et al., 2000) from the

uncertainty in each separate component, the values of β_U for SMRF structures in Table A-1 of FEMA 351 range from 0.15 to 0.35 for the Immediate Occupancy Performance Level and from 0.25 to 0.60 for the Collapse Prevention Performance Level.

C: Except for the SAC project, the only available studies dealing with quantification of uncertainty can be found in the so-called "gray" literature pertinent to seismic fragility of structures common either in nuclear power plant Probabilistic Risk Assessment (PRA) and Seismic Margin Analysis (SMA) practice (e.g., containment structures and reinforced concrete shear-wall buildings), or in Department of Energy (DOE) hazardous facilities (e.g., waste storage tanks). Some examples are Kennedy et al., 1980; Kennedy and Ravindra, 1984; Kennedy et al. (1989); Bandyopadhyay et al. (1993); Reed and Kennedy (1994); Duffley et al. (1994); Klamerus and Cherry (2001); Kennedy (2001). We also had access to a PG&E document on the seismic evaluation of the Diablo Canyon Power Plant (PG&E, 2001a).

C: Regarding such nuclear PRA/SMA and DOE studies some comments are in order:

- *The buildings of interest to the nuclear industry and to DOE may not necessarily be very similar to those in the PG&E building stock. Hence, the β_U values provided in those studies are to be considered as illustrative but not necessarily strictly applicable to the PG&E buildings.*
- *Given the high-level consequences in case of structural failures of those facilities (e.g., release of radionuclides), often in such studies the limit state of interest is more related to crack-tightness in the concrete than to structural collapse. For example, the limit state considered for the Diablo Canyon turbine building (PG&E, 2001a) was defined as "onset of severe structural distress and significant structural degradation". Consequently, the β_U values provided there refer to levels of structural deformation that this current document would define as onset of damage (or somewhat beyond that). No information is available for more severe deformation levels associated here with Red-tag or Collapse limit states.*
- *In those studies the researchers use results from engineering analyses (e.g., Klamerus and Cherry, 2001) for obtaining β_U values but engineering judgement often plays an important role in the definition of those numbers.*
- *The values of β_U in different studies were not consistently intended to cover the same sources of epistemic uncertainty or were not found using the same techniques. Examples of sources of epistemic uncertainty considered there are "uncertainty in the dynamic modeling of the structure, lack of understanding of material capacity, and uncertainty due to the use of engineering judgment to supplement an inadequate amount of hard statistical data" (Kennedy, 2001).*

*C: Despite these shortcomings, the β_U values provided by the studies mentioned above consistently range between **0.3** and **0.4**. Such values are somewhat consistent with the β_U values for Improved evaluation provided in Tables 2a to 2e.*

C: Given the importance of the structure under consideration, in the PRA/SMA and DOE studies the amount of information about material strength and ductility capacities is often far superior to that for other civil structures. This factor has to be kept into consideration when setting the β_U values to be used in these guidelines.

C: In reality an additional source of uncertainty due to the "mis-tagging" of damaged buildings by engineers after inspection may have a potentially large impact on this procedure. The likelihood of "mis-tagging" a damaged building is expected to be lower if the engineer can have access to the results of studies based on these guidelines (which in turn are based on residual capacity associated with damaged states that can be observed during the inspection), rather than if he/she uses only engineering judgement based on experience. Mis-tagging in the conservative direction may be an engineer's tendency without the structure-specific guidance that analyses such as those proposed here provide. Mis-tagging in the unconservative direction may be more likely in buildings such as industrial steel frames or tilt-ups where the structural members are exposed to fast, easy inspection rather than in concrete frames where more intrusive and costly actions needed to expose members and joints are seldom taken. As per the advisory committee decision, the uncertainty due to mis-tagging is not accounted for in these guidelines.

STEP 6: *Computation of the fragility curves*

The fragility curve (Figure 11 to come) for a given structural limit state LS (LS equal to onset of damage, green, yellow, red-, or collapse state) provides the annual probability that the intact building will end up in the specified limit state (or *worse*) given the occurrence at the site of an earthquake ground motion of intensity S_a. The fragility curve, for the yellow-tag state, for example, is denoted as $F_Y(S_a)$.

Based on the common lognormal assumption, the curve's estimation for the generic structural limit state LS requires two parameter values, a median $\check{S}_a^{LS}$ value and a measure of dispersion, β. The former is the central value of the curve that correspond to an exceedance probability of 50%, the latter controls its slope (the larger the β value, the flatter the curve). Values of $\check{S}_a^{LS}$ and β are provided in STEP 5. The former parameter is referred to as the median spectral capacity value of that limit state.

The fragility curve, $F_{LS}(S_a)$, for the generic structural limit state LS is determined by plotting the values of probability $p = \{0.05, 0.25, 0.5, 0.75 \text{ and } 0.95\}$ versus the corresponding values, S_a:

$$S_a = \check{S}_a^{LS} e^{x\beta}$$

for the values of x equal to $\{-1.65, -0.67, 0.0, 0.67 \text{ and } 1.65\}$, respectively.[27]

---

[27] Additional values of p and x can be found in any table of the Gaussian distribution function (e.g., Benjamin and Cornell, 1970).
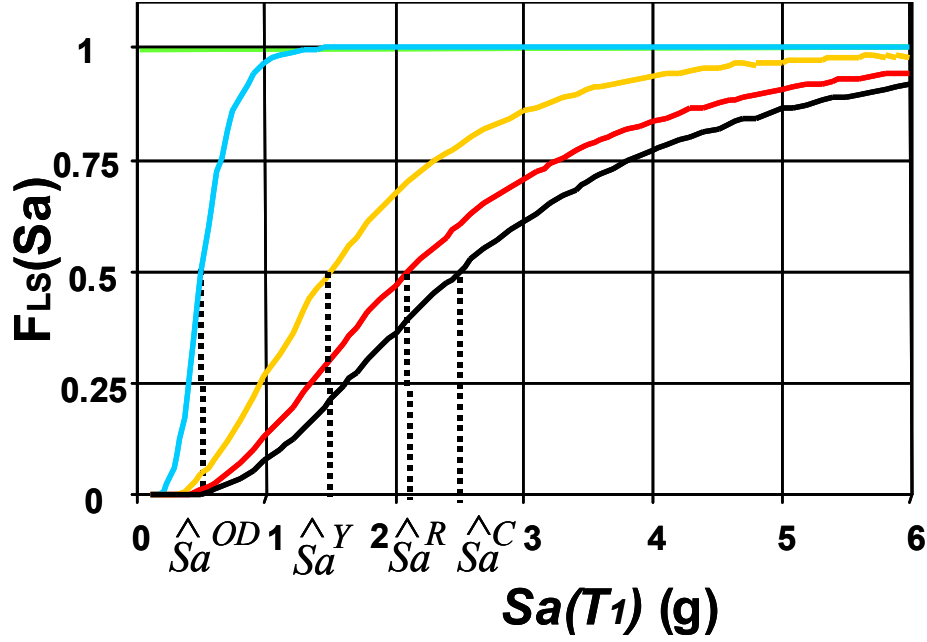
Figure 11: Fragility curves for onset of damage, green, yellow, and red tags, and for collapse of the building.

We assume that this illustrative example consists of a prefabricated metal building with fundamental period of one second analyzed according to the specifications of the *Baseline* evaluation (Appendix B). We used the $\check{S}_a^{LS}$ from Figure 9, the β_R values from Figure 10 for a structure of 1 sec fundamental period (i.e., 0.23 for OD, 0.25 for Y, 0.28 for R, and 0.40 for Coll), and the β_U values from Table 2d, Baseline case (i.e., 0.7 for OD, 0.8 for Y and R, and 0.9 for Coll). According to the SRSS operation defined above, the resulting β values are, therefore, 0.74 for OD, 0.84 for Y, 0.85 for R, and 0.98 for Coll. Figure 11 shows the resulting fragility curves for all the limit states.

Note that in Figure 11 the fragility curve for the green-tag state is equal to unity for all values of ground motions. This is because, by definition, the fragility curve provides the likelihood that the building will be in the given limit state or **worse** if a ground motion with specified S_a were to occur at the site. Because there are no structural limit states less severe than green, it follows that the building will have a green tag or worse with certainty for any level of ground motion. Note that fragility curve for onset of damage (OD) is the steepest of the four because the value of β is the smallest. The opposite is true for the fragility curve corresponding to the collapse state.

Summary of STEP 6: Compute and plot the fragility curves for the four limit states OD, Y, R, and Coll.

Output of STEP 6: fragility curves for the four limit states OD, Y, R, and Coll.

C: In some applications it may be convenient to keep the epistemic uncertainty, β_U, separated from the aleatory uncertainty, β_R when computing fragility curves. If this is done, a family of fragility curves rather than one (mean) fragility curve is associated with any structural limit state. The central point of each fragility curve in this family can be computed by applying again $S_{a,y}^{S} = \breve{S}_{a}^{LS} e^{y\beta_U}$. For example, the central value, $S_{a,y}^{S}$, of the median (50th), the 16th, and the 84th percentile fragility curves can be found by replacing y with the values of 0, -1, and +1 in the equation above. Each fragility curve in the family can be computed using $S_a = S_{a,y}^{S} e^{y\beta_U}$ where now, unlike before, β is replaced by β_U, and the slope is simply given by β_R. Figure 12 shows the mean fragility curve (β_U and β_R combined) along with the corresponding 16th, 50th, and 84th percentile fragility curves (β_U and β_R separated) obtained for the yellow tag condition in the illustrative example. The mean fragility curve in Figure 12 coincides with the fragility curve for the yellow-tag condition shown in Figure 11.

C: The interpretation of different fragility curves for the same limit state is straightforward. For example, the engineer is 84% confident that the true fragility curve for the yellow tag limit state does not exceed the 84th-percentile fragility curve shown in the figure. More precisely, this confidence applies at any one S_a value, and then the locus of such points is the 84th-percentile curve. To be above at one point does not necessarily insure that the entire curve is above. Figure 12 also shows the fragility curve one obtains from combining the two β's; this produces a <u>mean </u>estimate of $F_{LS}(S_a)$. This latter curve coincides with the fragility curve for the yellow-tag state in Figure 11.

C: The IDA for the intact structure is used in this procedure to assess the <u>median</u> ground motion, $\breve{S}_a^{LS}$, at which a certain tagging state LS (or worse) will be observed. As observed previously in the text, this assignment implies that the engineer should avoid using either a pessimistic – conservative – or optimistic assessments and judgments in STEPS 1 through 5.

C: The fragility curve, $F_{LS}(S_a)$, (or the family of fragility curves obtained if β_R and β_U are dealt with separately), in subsequent system reliability studies, may be multiplied by the likelihood of occurrence of ground motion level $S_a(T_1)$ at the fundamental period of vibration of the intact structure and then integrated over all values of $S_a(T_1)$. This operation can be described in discrete form, for example, for the Yellow limit state by the following equation:

$$P[LS \geq Y] \approx \sum_{i=1}^{N} P[LS \geq Y \mid S_a(T_1) = a_i] P[(T_1) = a_i] = \sum_{i=1}^{N} F_Y(a_i) P[S_a(T_1) = a_i]$$

The first term in the right hand side can be read off the fragility curve for the Yellow tag state for $S_a(T_1)=a_i$. The term $P[S_a(T_1) = a_i]$, which should be interpreted as the likelihood that $S_a(T_1)$ is in the neighborhood of a_i, can be found

by numerically differentiating the hazard curve for all the meaningful values of a_i. The result will be the annual probability of experiencing this tagging state or worse in the structure. Note that if the epistemic uncertainty is explicitly accounted for in the probabilistic seismic hazard analysis of the site, multiple hazard curves for $S_a(T_1)$ will be available besides the mean hazard curve. In this case the integration over all values of $S_a(T_1)$ will be repeated as many times as the number of hazard curves and the results of each integration will be weighted by the weight assigned to each hazard curve.
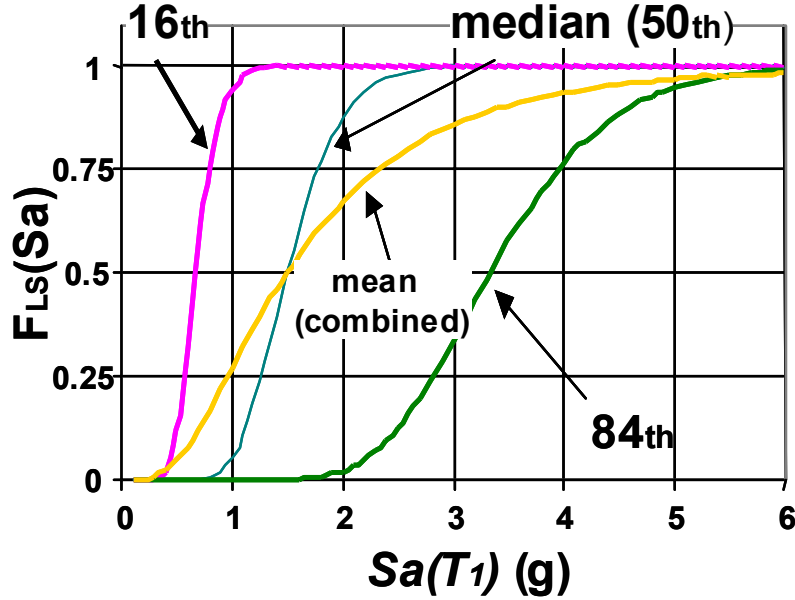

Figure 12: Fragility curves obtained both by keeping β_R and β_U separated (median (50th), 16th, and 84th) and by combining them (mean or combined estimate).

C: Note that the fragility curve of a particular state is, strictly, the probability that that state <u>or worse</u>, will be the outcome of experiencing a specified level of ground motion, as characterized by spectral acceleration, S_a. As implied by some of the terminology used above the fragility curve can also be interpreted as the (cumulative) probability distribution function, $F_{LS}(Sa)$, of a limit state "capacity" measured in ground motion intensity terms. In this interpretation the LS state will be observed if the ground motion input level (demand) exceeds this (random) capacity (measured in ground motion terms). To estimate the probability distribution of this random variable one can, in principle, run for a suite of ground motion records a series of incremental dynamic analyses (IDA's), observing for each record the first S_a level at which the limit state is observed. These represent observations of this "capacity". One then can refer to the median, $\check{S}_a^{LS}$, and dispersion[28], β, of this presumably lognormally distributed random variable.

---

[28] The dispersion is approximately equal to the coefficient of variation, but strictly it is defined here as the standard deviation of the natural log.

Application of the guidelines

Case Study No. 1: 3-story Steel Moment-Resisting Frame (SMRF) Building

The SMRF building analyzed here is the San Francisco Service Center Operations Building located at 2180 Harrison Street, San Francisco. The building is a 3-story structure built approximately in 1989 with a floor area of 62,600 square feet and outside dimensions of 98 feet by 217 feet.

The building is symmetric and has two sets of two EW frames and two sets of two NS frames. The application of these guidelines and the subsequent validation via nonlinear dynamic analyses of the IDA curve computed by the SPO2IDA spreadsheet was performed on only one of the E-W frames (Figure 13).
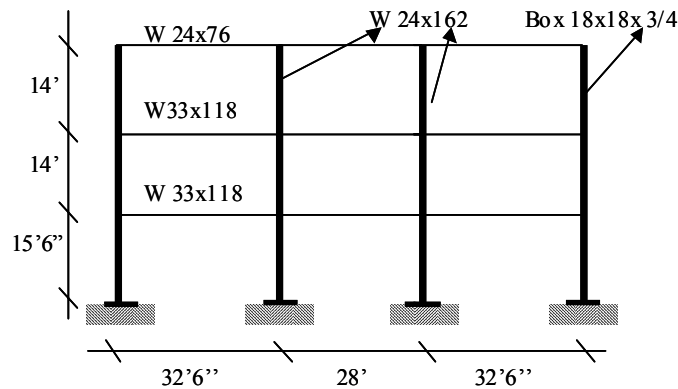
Figure 13: Schematic model of the frame

Structure Model:

The E-W moment-resisting frame of the structure is modeled with RAM-Perform V1.04, a commercially available structural analysis program. Beam-column connections are modeled as fracturing connections (described in next section), and the loading used is summarized in Table 3 below.

	1st Floor	2nd Floor	Roof
Dead Load (psf)	82	82	48 (53 for mass)
Perimeter Walls (lb/ft)	106	105	175
Live Load (psf)	50-150	50-150	40

Table 3: Values of dead loads and live loads used in the analysis

42

<u>Connection Model</u>:

Beam-column connections are modeled as point-hinge fracturing connections. Connection (flange) fracture is assumed to occur at 0.01 plastic hinge rotation, when the moment drops to 30% of its initial value. The connections are assumed to completely fail when the shear tab ruptures. This is expected to occur at 0.07 plastic hinge rotation resulting in the resisting moment and the vertical shear capacity dropping to effectively zero, as indicated by the dashed vertical line. These latter features, however, were not explicitly included in the model; due to software limitations the model continues horizontally indefinitely. This does not affect the conclusions, however, because, as discussed below, the occurrence of such an event will be considered as "collapse". A diagram of the connection moment-curvature curve is provided in Figure 14. Note: panel zone effects are not considered, and the yield strengths for the beams and columns are 36ksi and 50ksi, respectively.
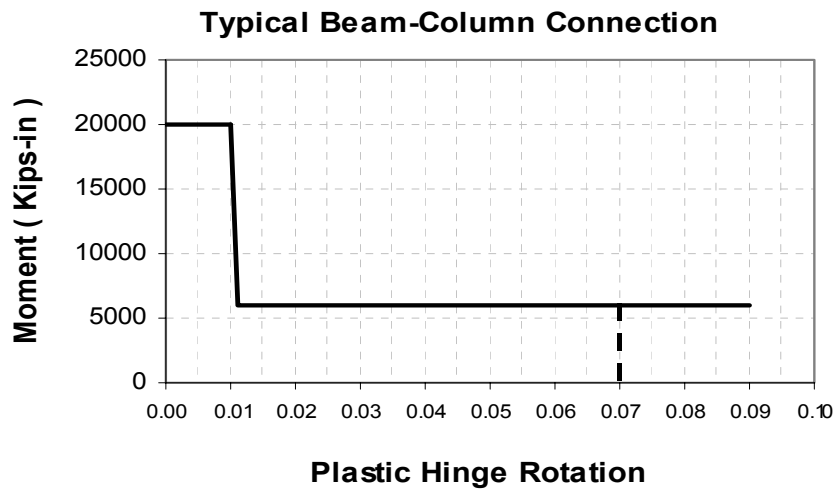
Figure 14: Beam-Column moment-rotation relationship.

<u>Application of the guidelines</u>:

STEP 1: NSP of the intact structure and identification of damage states

The bold line in Figure 15 shows the results of the NSP performed on the intact structure. The following damage states are identified and specified on this curve:

1. DS_1, or Onset of Damage. This state is defined where nonlinear behavior starts on the curve. The corresponding roof drift is $\Delta_1=0.9\%$

2. DS_2 is defined where the first considerable drop is noticed on the curve, related to the fracture of the exterior beam-column connections of the first floor. The corresponding roof drift is $\Delta_2=1.65\%$
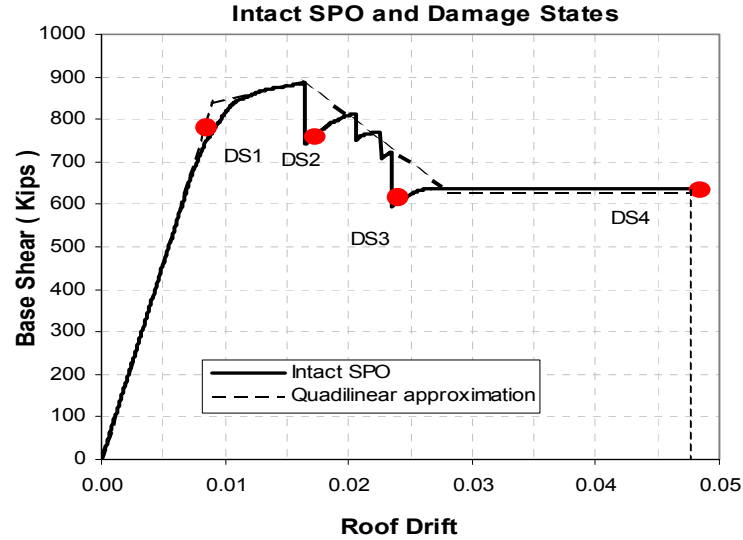
Figure 15: NSP curves for the intact structure. The NSP curve for DS_1 is identical to that for the intact structure. [See Figure 1]

3. DS_3 represents the second considerable drop on the curve, and is related to the fracture of interior connections. This is observed at a roof drift of $\Delta_3=2.4\%$

4. DS_4 is the drift where the <u>first</u> shear-tab failure is observed within the structure, i.e., a local plastic rotation of 0.07. The <u>roof</u> drift causing this damage state is $\Delta_4=4.8\%$. For reasons discussed above the NSP results are not valid beyond this point; we indicate this by the dashed vertical line at 4.8%.

Notice that these choices of damage states are not unique. Any other point relating to a change in any structure properties can be chosen as a damage state. Later, these damage states will be associated to different structural limit states.

Some of the values obtained from this Step 1 analysis are the initial stiffness of the intact structure and modal properties. The initial stiffness (K_1) is 93,300 Kips/rad, and the period of the intact structure is $T_1=0.73$ seconds.

STEP 2: NSP curves for the damaged structure

To obtain the NSP curves for each damage state DS_i, the intact structure is first "pushed" to that damage state (i.e., until the roof drifts specified in Step 1 are reached), then it is unloaded to zero base shear. After unloading, the structure, which in general experiences a certain level of static offset drift, is loaded again until failure, to be defined as the first local shear tab failure. The NSP curve obtained is the NSP curve for the damage state DS_i. The NSP curves for the damage states DS_2 and DS_3 are shown in Figures 16 and 17. Note that the model within the software used for the NSP analyses is such that the static pushover curves for DS_2 and DS_3 return to, and follow the original NSP curve for the

44

intact structure. (This, however, may not always be the case.) For this reason the first shear tab failure occurs again at a roof drift of 4.8%, beyond which the model is not valid, as implied by the dashed vertical lines.

From these curves the elastic stiffness of the damaged structure are estimated as K_{DS2}= 68500 Kips/rad, and K_{DS3}= 54500 Kips/rad, for damage states DS_2 and DS_3, respectively. These stiffness values and the fundamental period of the intact structure are used to find the fundamental period of vibration of the structure in these two damage states. Such periods of vibration will be used in Step 3.[29]
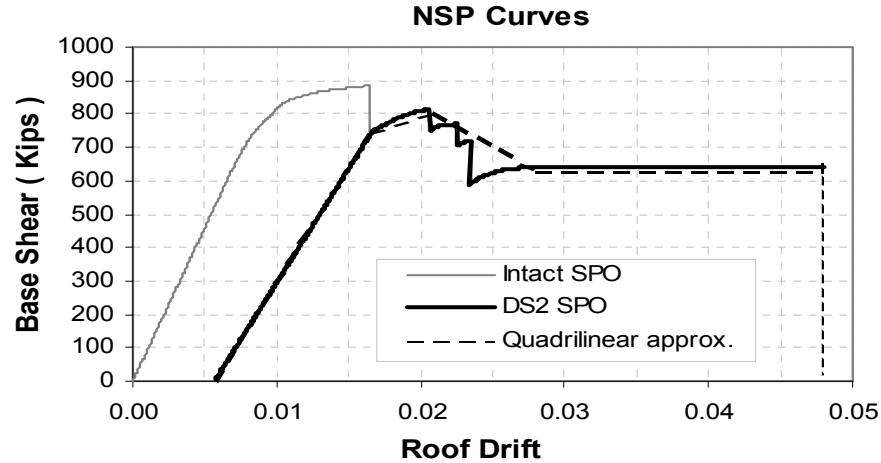
Figure 16: NSP curve for DS2 [See Figure 2]
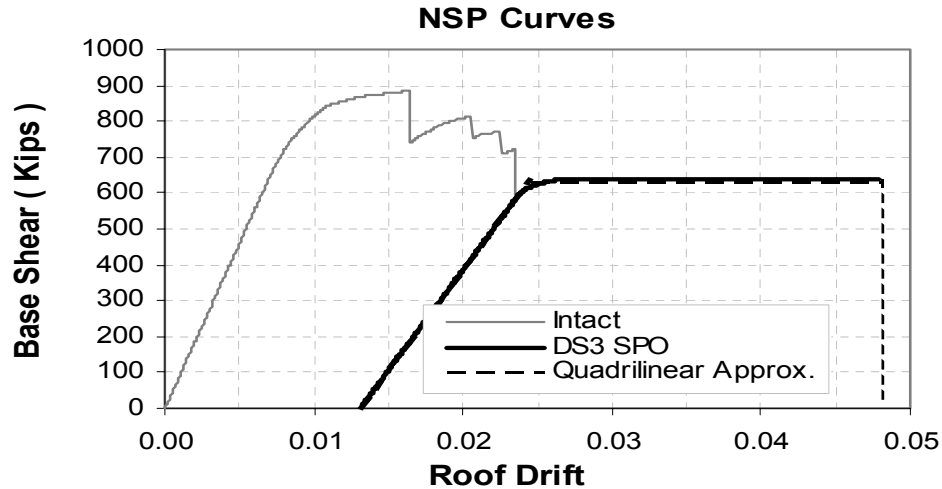
Figure 17: NSP curve for DS3 [See Figure 2]

---

[29] Note that the period of vibration of the structure in the two damage states is equal to that of the intact structure if, instead, parallel-to-elastic unloading/re-loading is assumed for the NSP curves of the damaged structure. In this case study, these "assumed" NSP curves are similar to those shown in Figures 16 and 17, and in STEP 3 we will demonstrate that the resulting estimates of the residual lateral capacity are almost identical.

STEP 3: From SPO to IDA

In this step we obtain the dynamic IDA estimates from the static NSP curves using the SPO2IDA software. To match the input requirements for this software we must conduct several simple steps of straight-line approximation of the NSP's and normalization of the axes. The normalized IDA that is output must then be "de-normalized" for proper interpretation. We go through these steps in detail in what follows.

In order to be used in the SPO2IDA spreadsheet, the NSP curves need be approximated by no more than four straight lines. The piecewise linear fit of the NSP curves is also shown in Figures 15 to 17 and in Table 4.

The damaged structure NSP's display a large initial residual static offset that is an artificial product of the static way in which the structure has been loaded and unloaded to reflect the mainshock response. For the same maximum displacement, on average a comparatively much smaller residual offset would be expected in a proper dynamic analysis. We have chosen therefore in these guidelines to remove that offset by shifting the damaged NSP's back to zero offset, as shown in Figure 18. Note that this shift does not reduce the roof drift at which collapse is predicted. To accomplish this shift, the value of the offset (given by the drift for point 1 in Table 4) is subtracted from all drifts in the other columns with the exception of the collapse point, as shown in Table 5. Later, in Step 3, the expected (or measured) dynamic residual offset is taken into account.
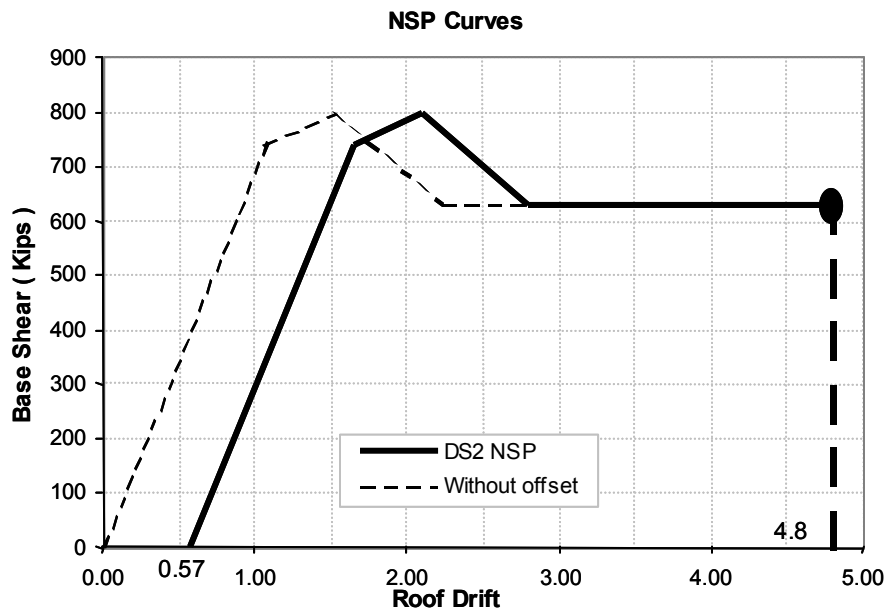

Figure 18: DS2 NSP with and without the offset. Note that local collapse state

46

	Point 1		Point 2		Point 3		Point 4		Point 5	
	Drift (%)	BS (K)	Drift (%)	BS (K)	Drift (%)	BS (K)	Drift (%)	BS (K)	Drift (%)	BS (K)
Intact	0	0	0.9	840	1.65	890	2.8	630	4.8	630
DS$_2$	0.57	0	1.65	740	2.10	800	2.8	630	4.8	630
DS$_3$	1.30	0	2.45	630	4.8	630				

Table 4: Quadrilinear approximation of the un-normalized NSP curves with static residual offsets (Figures 15-17).

	Point 1		Point 2		Point 3		Point 4		Point 5	
	Drift (%)	BS (K)	Drift (%)	BS (K)	Drift (%)	BS (K)	Drift (%)	BS (K)	Drift (%)	BS (K)
Intact	0	0	0.9	840	1.65	890	2.8	630	4.8	630
DS$_2$	0	0	1.08	740	1.53	800	2.23	630	4.8	630
DS$_3$	0	0	1.15	630	4.8	630				

Table 5: Quadrilinear approximation of the un-normalized NSP curves with the static residual offset removed. This offset is removed from the NSP curves of the damage states DS$_2$ and DS$_3$ by subtracting from the drift values in Table 4, excluding the collapse points (i.e., last value in each row), the values in the first column of each pertinent row.

	Point 1		Point 2		Point 3		Point 4		Point 5	
	μ	R	μ	R	μ	R	μ	R	μ	R
Intact	0	0	1	1	1.83	1.06	3.11	.75	5.33	.75
DS$_2$	0	0	1	1	1.42	1.08	2.07	.85	4.44	.85
DS$_3$	0	0	1	1	4.17	1				

Table 6: Quadrilinear approximation of the normalized NSP curves (without static residual offset). The normalization is obtained by dividing all the numbers under Points 3-5 in Table 5 by the corresponding numbers under Point 2 (i.e., the yielding point).

Furthermore, the NSP curves in Figures 15 to 18 are in terms of base shear and roof drift. As explained in the text, the SPO2IDA spreadsheet requires normalized NSP curves expressed in terms of global ductility ratio, μ, and the ratio, R, of the base shear, BS, to the base shear, BS$_{yi}$, at incipient yielding. Hence, the following normalization step is performed on NSP results from Step 2. Each NSP curve is considered separately, and the point corresponding to first yielding is selected on each of them (DS$_1$, DS$_2$, and DS$_3$ marks in Figure 15). The ordinates of these points are called BS$_{yi}$ and Δ_{yi}. These points are associated with column 2 in Table 5. Using R$_i$=BS$_i$/BS$_{yi}$, and $\mu_i = \Delta_i/\Delta_{yi}$, the input for SPO2IDA is as shown in Table 6.

Using the NSP curves in Table 6 as an input to the SPO2IDA spreadsheet produces the dynamic μ vs. R relationships (i.e., the IDA curves) for the intact structure and the damaged state structures (Table 7). The normalized NSP and IDA curve for the intact structure are shown in Figure 19. The SPO2IDA output is in terms of normalized drift ($\mu = \Delta/\Delta_y$) and normalized spectral acceleration, $R = Sa/Sa_y$, where Sa_y, is the yield acceleration to be discussed below.

	Point 1		Point 2		Point 3		Point 4		Point 5	
	μ	R	μ	R	μ	R	μ	R	μ	R
Intact	0	0	1	1	2	2.1	4	3.3	5.33	3.9
DS$_2$	0	0	1	1	2	2.05	4	3.2	4.44	3.6
DS$_3$	0	0	1	1	2	2.15	4	4.0	4.17	4.2

Table7: Normalized (median) IDA curves obtained via the SPO2IDA spreadsheet.

As stated, the IDA curves in Table 7 are in terms of μ and R, where R is now to be interpreted as Sa/Sa_y. A "de-normalization" process should be performed to produce more meaningful IDA curves directly in terms of roof drift vs. S_a. Tables 8 and Tables 9a and 9b demonstrate this procedure. Table 8 shows the results of de-normalizing the abscissa or displacement axis, by multiplying the μ's by the yield drifts from Point 2 of Table 5. Tables 9a and 9b show the ordinate transformation. For the intact structure, R is multiplied by Sa_y, which is estimated by BS_y (840 K) divided by the product of the mass of the structure (1380 K) and the first-mode participation factor (0.88). The result is Table 9a.

For the damaged structures, the R columns in Table 8 are also multiplied by their Sa_y values, i.e., by BS_y levels (740 and 630 for DS2 and DS3, respectively) divided by the same product of the mass and participation factor. The results are shown in Table 9b. (Note that these Sa_y values have the same _relative_ values as the BS_y values used to normalize the NSP abscissa.) The resulting spectral accelerations are associated with the periods of the damaged structures (T_{DS2} and T_{DS3}), which are 0.84 and 0.93 secs respectively. These were obtained by multiplying the intact structure's period by the square root of the inverse ratio of the initial stiffnesses discussed in Step 2.

To compare and plot all the IDA curves on the same figure it is necessary to use a common spectral acceleration, i.e., one associated with the _same_ _period_ for all cases, intact and damaged. We chose to transform the spectral acceleration at fundamental period of vibration, T_{DSi}, of the damaged structure in damage state DS$_i$ into $S_a(T_1)$ where T_1 is the fundamental period of vibration of the _intact_ structure. Hence, the ordinates (spectral accelerations) of the IDA curve associated with Table 9b for damage states DS$_2$ and DS$_3$ should be multiplied by $S_a(T_1)/S_a(T_{DSi})$. This value can be estimated from uniform hazard spectra at an appropriate level of hazard for the building site. In this example, we used the uniform hazard spectrum (UHS) with 10% probability of exceedance (PE) in 50 years for San Francisco provided by USGS. For these periods the

spectral acceleration ratios might also be estimated to close enough approximation by assuming the spectrum of future earthquakes will have the same spectral velocity in the period range of interest here, i.e., simply by the ratio of the periods. From the selected UHS, $S_a(0.73)/S_a(0.84)=1.12$, and $S_a(0.73)/S_a(0.93)=1.26$. Hence, the spectral accelerations in Table 9b are multiplied by 1.12 for DS_2, and by 1.26 for DS_3 (Table 10)[30].

	Point 1		Point 2		Point 3		Point 4		Point 5	
	Drift	R	Drift	R	Drift	R	Drift	R	Drift	R
Intact	0	0	0.9	1	1.8	2.1	3.6	3.3	4.8	3.9
DS_2	0	0	1.08	1	2.2	2.05	4.3	3.2	4.8	3.6
DS_3	0	0	1.15	1	2.3	2.15	4.6	4.0	4.8	4.2

Table 8: IDA curves in roof drift (in percent) versus R terms. The μ coordinate is transformed into drift by multiplying every μ cell in Table 7 by the yield drift corresponding to that state, i.e., the drifts in Table 5 for Point 2.

	Point 1		Point 2		Point 3		Point 4		Point 5	
	Drift	Sa(g)	Drift	Sa(g)	Drift	Sa(g)	Drift	Sa(g)	Drift	Sa(g)
Intact	0	0	0.9	0.69	1.8	1.45	3.6	2.28	4.8	2.7

Table 9a: Un-normalized IDA curve for the intact structure in terms of roof drift and S_a at the fundamental period of vibration of the intact structure.

	Point 1		Point 2		Point 3		Point 4		Point 5	
	Drift	$S_a(g)$	Drift	$S_a(g)$	Drift	$S_a(g)$	Drift	$S_a(g)$	Drift	$S_a(g)$
DS_2	0	0	1.08	0.61	2.2	1.25	4.3	1.95	4.8	2.20
DS_3	0	0	1.15	0.52	2.3	1.12	4.6	2.08	4.8	2.18

Table 9b: Un-normalized IDA curves for the structure in damage states DS_2 and DS_3. In this table S_a is the spectral acceleration at the fundamental periods of vibration of the structure in damage states DS_2 or DS_3.

	Point 1		Point 2		Point 3		Point 4		Point 5	
	Drift	$S_a(g)$	Drift	$S_a(g)$	Drift	$S_a(g)$	Drift	$S_a(g)$	Drift	$S_a(g)$
DS2	0	0	1.08	0.68	2.2	1.40	4.3	2.18	4.8	2.46
DS3	0	0	1.15	0.66	2.3	1.41	4.6	2.65	4.8	2.75

Table 10: Un-normalized IDA curves for structure in damage states DS_2 and DS_3. S_a is the spectral acceleration at the period of the intact structure for all cases.

---

[30] Note: the ratio of periods is 1.15 and 1.27 implying the equal spectral velocity approximation would have been adequate in this case.
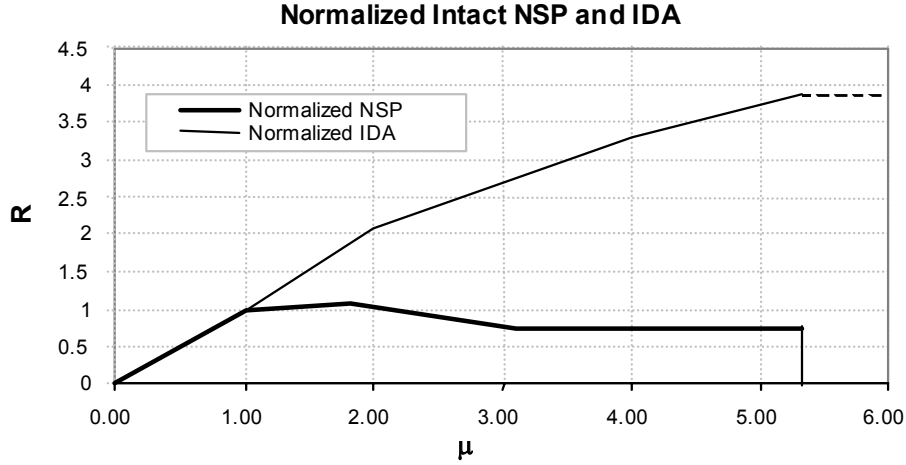
Figure 19: Normalized NSP and IDA for the intact structure. Here R is BS/Bsy for the NSP, and Sa/Say for the IDA [See Figure 3]

The IDA curves for the intact structure and for structure in different damage states expressed all in terms of the spectral acceleration at the fundamental period of the intact structure, are shown in Figure 20(a). Note that despite the somewhat more severe damage in DS_3, the IDA of DS_3 crosses the IDA curves for both the intact structure and DS_2. Like the NSP curves (e.g., Figure 18) they are derived from, however, these IDA curves assume no residual offset after the mainshock. Based on dynamic analyses of a similar structure carried out during Phase II of this project, the median residual offset (in terms of roof drift) for the structure in damage state DS_2 and DS_3 is 0.07% and 0.30%, respectively. (Note that these dynamic residual roof drifts are much smaller than those implied by the NSP curves.) As explained in the guidelines, IDA curves that account for this expected dynamic residual offset are obtained by tracing the IDA curves in Figure 20(a) to the point that has a roof drift equal to the roof drift capacity minus the residual offset – namely, 4.8%-0.07%=4.73% and 4.8%-0.30%=4.50% for DS_2 and DS_3, respectively. The resulting IDA curves are shown in Figure 20(b).

As seen in Figure 20(a), even without a residual offset the IDA curves for the structure in damage state DS_2 and DS_3 yield estimates of the residual capacities (2.46*g* and 2.75*g*, respectively) that are different than that of the intact structure (2.7*g*). In contrast, dynamic analyses of the structure in damage states DS_2 and DS_3 carried out during Phase 2 of this project indicate that without a residual offset little or no change in the median lateral capacity relative to the intact structure is expected. Hence, as explained in the guidelines, the residual capacity estimates from Figure 20(b) (i.e., *after* accounting for the residual offset), namely 2.45*g* for DS_2 and 2.58*g* for DS_3, are adjusted to reflect this observation. This is accomplished by multiplying these estimates by the ratio of the intact capacity to the residual capacity assuming no residual offset, namely 2.7*g* /2.46*g* and 2.7*g* /2.75*g* for DS_2 and DS_3, respectively. The final estimates of the residual capacities that will be used in STEP4 are, therefore, $(S_{a,cap})_2$=2.45*g**2.7*g* /2.46*g*=2.69*g* and $(S_{a,cap})_3$=2.58*g**2.7*g* /2.75*g*=2.53*g*. As noted in the commentary of the guidelines, these estimates are equivalent to multiplying the capacity of the intact structure (2.7*g*) by the ratio of the residual capacities with and without a residual offset (2.45*g*/2.46*g*=0.996

for DS$_2$ and 2.58g/2.75g=0.94 for DS$_3$). As alluded to in Step 2, the residual capacities estimated under the assumption of parallel-to-elastic unloading/re-loading for the damaged NSP curves are nearly identical to those estimated here (i.e., 2.68g instead of 2.69g for DS$_2$ and 2.56g instead of 2.53g for DS$_3$).
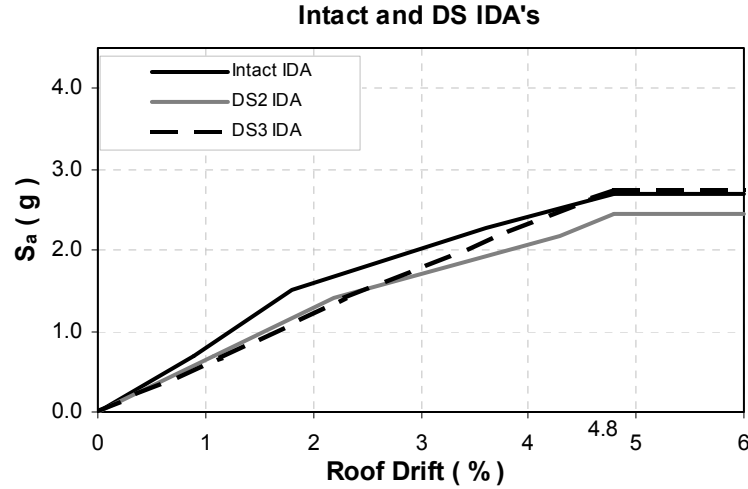
Intact and DS IDA's

Figure 20(a): IDA curves for the intact structure and for the damaged structure in damage states DS$_2$ and DS$_3$ *before* accounting for the expected dynamic residual offset. Again, the IDA curve for DS$_1$ is identical to that for the intact structure. The S_a's are all at the period of the intact structure.

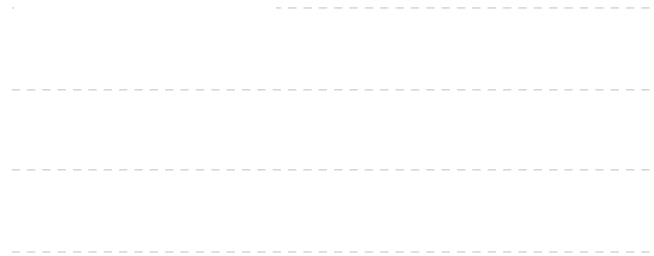**Figure 20(b):** IDA curves for the intact structure and for the damaged structure in damage states DS$_2$ and DS$_3$ *after* accounting for the expected dynamic residual offset, but *before* adjusting for the behavior observed in dynamic analyses of damaged structures. Again, the IDA curve for DS$_1$ is identical to that for the intact structure. The S_a's are all at the period of the intact structure.

Step 4: Occupancy Status for Damaged Building

In this step we determine what limit or tagging states to associate with each of the damage states. The simplest case, the onset of damage limit state, is predicted to occur at a drift of 0.9%.

Based on Figure 20a the intact structure will reach the 4.8% drift that implies collapse at a Sa value of 2.7g. From the results of STEP 3, the (median) S_a capacity estimates of the damaged structures are 2.69g and 2.53g. These are the aftershock ground motion intensities (as measured in terms of 0.73 sec period Sa) that are expected to cause (local) collapse of the damaged structures.

To determine the tagging states associated with DS_2 and DS_3 we must consider the loss in capacity and the probability (MAF) of an aftershock causing a collapse of the damaged structure. The spectral acceleration capacity reductions for DS_2 and DS_3 are 0.4% and 6.3% respectively. If the MAF of exceeding the median capacity of the intact building at the building location, P_0, were, for example, equal to 5×10^{-4}, then the damage state DS_2 is green-tagged whereas DS_3 is yellow-tagged. The damage state DS_4, which is associated with local collapse, is by default tagged red and it is used here as describing the incipient collapse for the purpose of developing fragility curves.

Step 5: Ground motion level at incipient structural limit state

In this step we identify the mainshock ground motion intensity that is expected to bring the intact structure to the verge of each relevant structural limit state. For the P_0 equal to 5×10^{-4} assumed above, the loss in capacity computed for damage sates DS_2 and DS_3 (0.4% and 6.3%, respectively) locates them well within the boundaries of Green and Yellow tags. Additional damage states should be considered in between DS_2 and DS_3 and in between DS_3 and DS_4 until the computed capacity of the building in these additional damage states has dropped by the quantity suggested by the tagging criteria (i.e., 2% and 20%) for the value of P_0. Luco et al. (2004) (see Appendix C) have considered a damage state in between DS_3 and DS_4 for this very same structure. Here, however, we estimated the values of the median roof drift, and from them, the values of the median spectral acceleration, $\check{S}_a^Y$ and $\check{S}_a^R$, corresponding to the incipient Yellow and Red tag states via interpolation. The resulting main shock ground motions causing the onset of all limit states, including Y and R whose values were estimated via interpolation, are shown in Table 11. These correspond to the median values of the limit state fragility curves.

Structural Limit State:	**OD**	**Y**	**R**	**C**
Median Roof drift:	0.9%	2.09%	3.4%	4.8%
Median ground motion:	0.65g	1.6g	2.25g	2.7g

Table 11: Median roof drifts and median $S_a(T_1)$ corresponding to incipient structural limit states (i.e, $\check{S}_a^{OD}$, $\check{S}_a^Y$, $\check{S}_a^R$, and $\check{S}_a^C$).

The values of β_R and β_U are taken from Figure 10 (for T=0.73 sec) and from Table 2e, for SMRFs, assuming the baseline analysis. The total dispersion, β, is the square root of sum of the squares of β_R and β_U. Values of β_R, β_U, and β for this example are shown in Table 12.

	Limit State			
	OD	Y	R	Collapse
β_U	0.3	0.6	0.6	0.5
β_R	0.25	0.28	0.32	0.45
β	0.39	0.66	0.68	0.67

Table 12: Values of β_U, β_R, and β used to obtain the fragility curves shown in Figure 22.
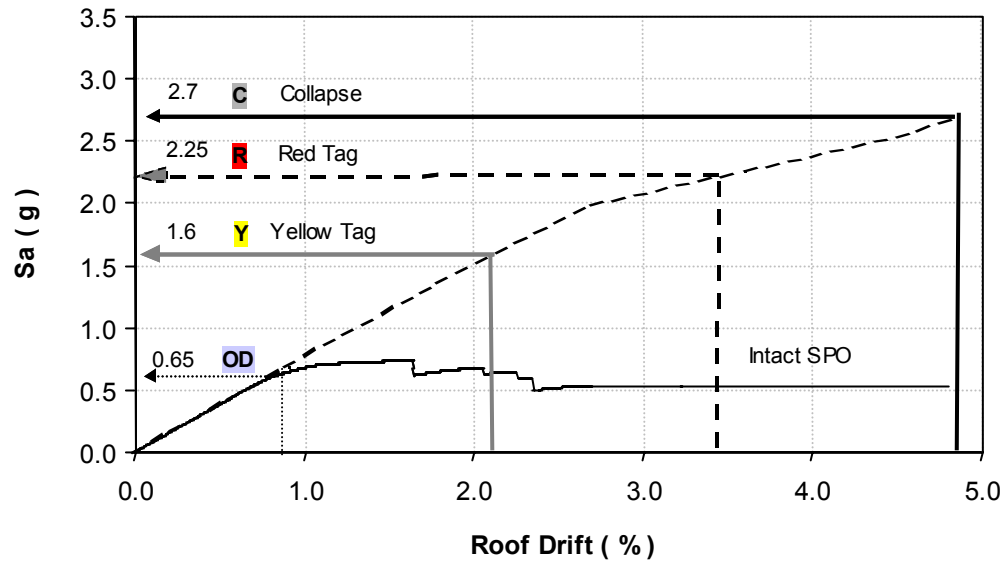

Figure 21: Median value of Sa causing the structure to enter or exceed Onset of Damage, Yellow Tag, or Collapse state. [See Figure 9]
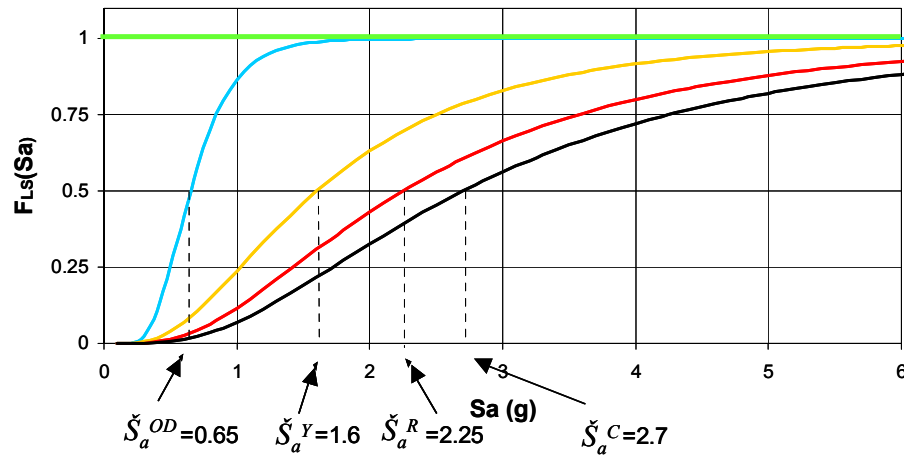

Figure 22: Fragility curves for the Onset of Damage state, the Yellow-tag state, and the Collapse state for this SMRF structure. [See Figure 11]

Step 6: Computation of the Fragility Curves

The fragility curves for each structural limit state (Figure 22) are found using the median spectral accelerations, $\check{S}_a^{LS}$, and the β values from STEP 5. Recall that the fragility curves are found using the equation $S_a = \check{S}_a^{LS} e^{x\beta}$, where the x values are reported in any table of the Gaussian distribution function.

Validation:

To confirm the accuracy of the SPO2IDA tool used in these guidelines, a suite of 30 ground motions (magnitude ranging from 6.5 to 6.9) was used to perform nonlinear dynamic analyses on the intact structure. The records are first scaled to have the same spectral acceleration, $S_a(T_1)$, at the first-mode period of the structure (T_1=0.73 sec) and then run through the structural model. This procedures was used to obtain so-called $S_a(T_1)$ versus maximum roof drift "stripes" at four different levels of $S_a(T_1)$. The stripes, together with the median IDA (solid black line) estimated from the nonlinear dynamic analyses, are drawn in Figure 23. The dashed line in the figure is the IDA produced from the NSP curves by the SPO2IDA spreadsheet. The agreement between the two IDA estimates is excellent. In particular, note that at a roof drift of 4.8% the median $S_a(T_1)$ from the nonlinear dynamic analyses is nearly equal to the (local) collapse capacity of the intact structure estimated (in STEP 3) via the nonlinear static procedure put forth in these guidelines.

To verify the validity of estimating the dynamic spectral acceleration capacities of the intact and damaged structures by the Guideline's nonlinear static procedure the following was done. Dynamic analyses such as those described above were conducted on the intact and on the damaged structures at spectral acceleration levels near the anticipated capacity values. The percentage of the 30 records in which local collapse (shear tab failure) is reached is plotted versus spectral acceleration level in Figure 24. The median (local) collapse capacity is obtained by interpolation from this curve. The dynamic capacities are 2.75, 2.4 and 2.05g for intact, DS2, and DS3 respectively. The agreement between these values and the Guideline's NSP procedure's estimates of capacities (2.7g for the intact structure, and 2.69g for both DS2 and 2.53g for DS3) is good for the intact structure but not satisfactory for the damage states DS2, and DS3. There is reason to believe that the damaged state dynamic capacities have been somewhat underestimated, because the model adopted to estimate them was based on the loaded and unloaded <u>static</u> pushover (NSP) which left a very asymmetrical fracture/damage state in the structure used for the dynamic analyses. This asymmetry has the tendency to cause larger nonlinear dynamic drifts (than would a more realistic model of the post-mainshock damaged structure); these larger drifts imply smaller S_a capacities.

In Phase 2 of this project (refer to Luco *et al.*, 2004 in Appendix C for more details), the residual capacities of a similar structure in damage states DS2 and DS3 were computed using back-to-back (mainshock-aftershock) dynamic analyses. First the intact structure was analyzed dynamically under the 30 earthquake records (considered as mainshocks) scaled to produce the roof drift associated with each damage state (i.e., 1.65% for DS2

and 2.4% for DS3). Then these 30 structures in each damage state were each analyzed dynamically under the same 30 earthquake records (now considered as aftershocks) scaled to produce the roof drift associated with collapse (i.e., 4.8%). The spectral acceleration of each scaled aftershock, which is the residual capacity of the structure in each damage state, was normalized by the spectral acceleration capacity of the intact structure under the same earthquake record. The median of this ratio across all 30 aftershocks by 30 damaged structures was found to be 0.98 and 0.92 for damage states DS2 and DS3, respectively. These ratios of dynamic capacities are within a few percent of those estimated using the nonlinear static procedure put forth in these guidelines.
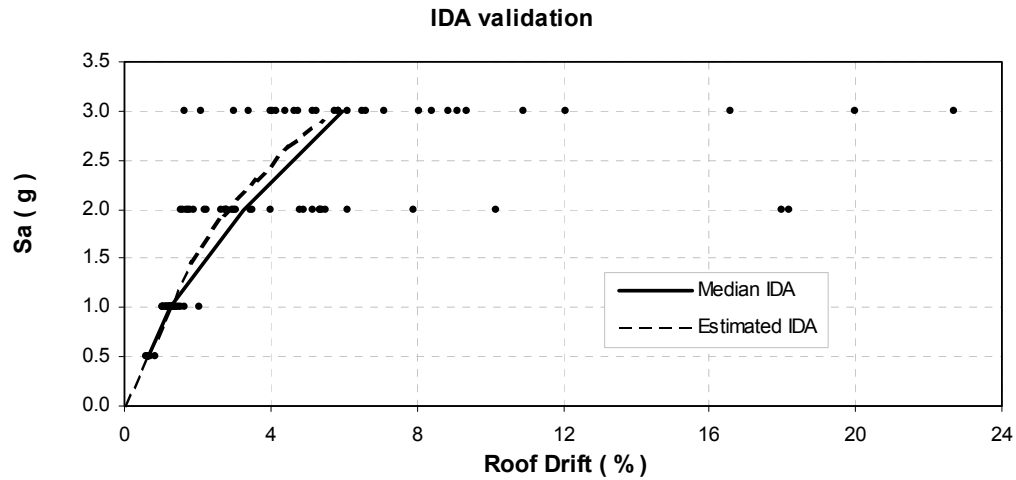

Figure 23: Validation of IDA for intact stucture. Comparison of the proposed NSP-based estimation procedure with the median of multiple nonlinear dynamic runs.
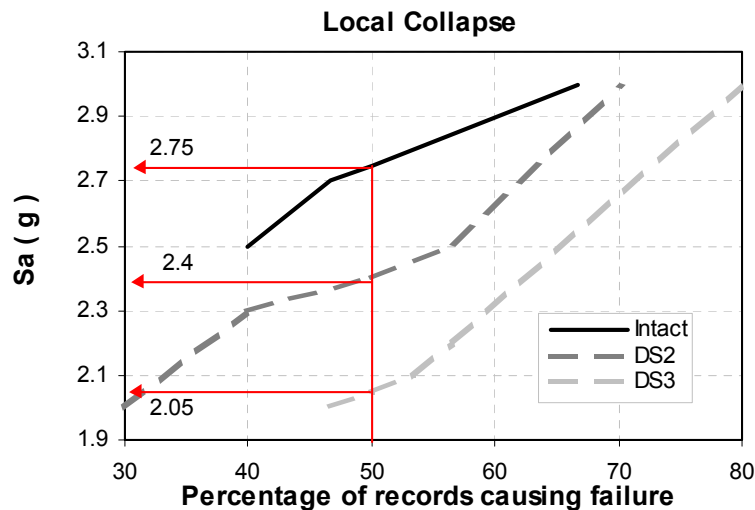

Figure 24: Validation of median spectral acceleration capacities based on multiple nonlinear dynamic.

Case Study No. 2: Tilt-up Building

To develop and validate the proposed procedure for use with tilt-up buildings, the response of a warehouse in Hollister CA, which has previously been studied by other researchers (Hamburger *et al*., 1996; Wallace *et al*. 1999), is considered. The warehouse is 300 feet by 98.5 feet in plan and 30 feet in height. The building was instrumented by the California Strong Motion Instrumentation Program (CSMIP) and has been subjected to ground shaking during the Morgan Hill (1984), Alum Rock (1986) and Loma Prieta (1989) earthquakes.

Based on the damage to tilt-up structures documented by the EERI reconnaissance team (1995) following the 1994 Northridge earthquake, our study focuses on predicting the ground motion intensity at which the roof diaphragm separates from the tilt-up panels on the perimeter of the building due to the failure of the roof-wall connections. Application of the proposed procedure for this purpose is described below followed by a validation of the results by means of a comprehensive series of IDAs performed with an ensemble of ten ground motions.

Structure Model

A plan view of the structure model used in the analyses described herein is shown in Figure 25. Currently, only ground motions acting parallel to the *x*-axis are considered. The model, which is in most respects similar to that used by Hamburger *et al*. (1996), consists of three key components: (1) the roof diaphragm, (2) the walls perpendicular to the ground motion (i.e., parallel to the *y*-axis in Figure 25) and (3) the connections between the roof diaphragm and these walls. The walls along gridlines 1 and 2 in Figure 25 are modeled as rigid supports, reflecting the fact that these elements are so stiff that they do not amplify the input ground motions at their bases. We assume that the shear capacity of the roof-wall connections along gridlines 1 and 3 is sufficient to transfer the shear forces from the roof diaphragm to the walls along these gridlines.

Roof diaphragm

The horizontal truss shown in Figure 25 is used to model the roof diaphragm. This truss model consists of linear-elastic and nonlinear bar elements. The chord elements along gridlines B and C and the web elements spaced at 18' 9" on center parallel to the *x*-axis are modeled as stiff linear-elastic elements so that all of the diaphragm deformation occurs in the nonlinear diagonal elements shown in Figure 25. With appropriate values assigned to the material properties of these nonlinear elements (i.e., those related to the size and spacing of the nails and the thickness of the plywood), the experimental results reported by Pardoen *et al*. (1999) can be reproduced, as shown in Figure 26. However, for the analyses reported herein, the material properties of these diagonal elements are selected to better represent the construction of the warehouse roof, including the presence of roofing material.

Walls perpendicular to ground motion

The walls perpendicular to the ground motion (along gridlines A and D) are modeled with standard linear-elastic beam elements. These elements are intended to represent the

30 ft high × 5.5 in thick reinforced concrete tilt-up panels at these locations. Hamburger *et al.* (1996) adopted a similar model. A truer representation of these walls would account for the fact that they are pinned at the base. However, preliminary tests with structure models that include a better representation of the wall indicate that the simplified wall model shown in Figure 25 is sufficiently accurate. As expected, modeling the walls with pinned bases stiffens the structure model slightly. This stiffening effect is accounted for in our simplified wall model by factoring the stiffness of the beam elements used to represent the wall.

Roof-wall connections

The roof-wall connections have been modeled in several ways in past studies. Hall (1999) and Wallace *et al.* (1999) represent the roof-wall connections with pairs of springs that produce a ductile response in tension and a nearly rigid response in compression. Hamburger *et al.* (1996) model the roof-wall connections with linear spring elements. A shortcoming of the connection models used in these previous studies is their inability to represent the brittle behavior of the roof-wall connections observed in past earthquakes. In particular, there are many documented instances from Northridge (1994) where the roof diaphragm separated from the wall, causing a portion of the roof to collapse that these models cannot properly represent.

In spite of recent experiments conducted to characterize the properties of the roof-wall connections used in tilt-up buildings (e.g., Pardoen *et al.*, 1999), there is still little data to support one model over another. Consequently, in this study, the roof-wall connections are modeled with nonlinear bar elements that are capable of reproducing two types of behavior, as shown in Figure 27. Note that in all cases the connection fractures when elongated beyond a prescribed value. The models shown in Figure 27 are intended to represent the behavior of roof-wall connections commonly used in practice, such as those shown in Figure 28.

Masses

The mass that drives the seismic response of the tilt-up building under consideration is associated with the roof diaphragm and the walls along gridlines A and D. The roof mass is based on a uniformly distributed roof load of 12 psf and is evenly distributed to the nodes on either side of the diaphragm along gridlines B and C (see Figure 25). The resulting seismic mass at each of these nodes is 0.029 k·s^2/in. The seismic mass associated with each wall is evenly distributed to the nodes along gridlines A and D in Figure 25 and is based on normal weight concrete (145 pcf) and a tributary wall height of 20 ft (two-thirds the total height of the wall). This tributary wall height is chosen to approximate the reaction at the top of the wall due to a triangular distribution of inertial forces over its height when it pivots about its base. The resulting seismic mass at each node along gridlines A and D due to the walls is 0.064 k·s^2/in. Note that the walls account for approximately 70% of the total seismic mass.

Modal properties

A modal analysis of the structure model described above yields the modal properties summarized in Table 13. The fundamental period of the model is 0.57s, which agrees

with the value computed by Hamburger *et al*. (1996) and measured by CSMIP accelerometers located at the center of the diaphragm. Note that only the "odd" modes of vibration have non-zero participation factors. This is because the even modes are anti-symmetric shapes that cannot be excited by a ground motion that acts through the center of rigidity of the model. Also note that the first four symmetric modes (1,3,5,7) account for 98.1% of the total effective seismic mass.

Application of the Proposed Procedure

Application of the proposed procedure is demonstrated here in detail for the Hollister tilt-up model shown in Figure 25 with ductile roof-wall connections shown in Figure 27a. It is assumed that the building has been retrofitted and that some of the conditions listed in Appendix B for the evaluation of tilt-up buildings have not been considered (in particular, the evaluation of foundation overturning and the evaluation of wall in-plane behavior). For brevity, the procedure is only presented for ground motions acting parallel to the x-axis shown in Figure 25; however, in practice, the analysis should also be conducted for ground motions acting parallel to the y-axis. Application of the procedure to a building with brittle connections is similar to that described below. Consequently, the details of the analysis of the brittle structure are not described; however, the resulting fragility curves for this case are presented in Step 6 in order to understand the how the assumed ductility of the roof-wall connections influence the fragility curves.

Step 1: Nonlinear static procedure (NSP) curve for the intact building

The NSP curve for the intact structure, which relates the base shear, *BS*, to a control displacement, Δ_C, is obtained by determining the required intensity of a prescribed load pattern, $\mathbf{F}$, for a series of monotonically increasing values of Δ_C. In this example, Δ_C is the displacement of the top of the wall at the intersection of gridlines 2 and D in Figure 25 and the load pattern is that associated with the first mode shape of the intact structure, i.e., $\mathbf{F} = \lambda \mathbf{M} \phi_1$, where $\mathbf{M}$ is the mass matrix, ϕ_1 is the mode shape associated with the first mode of vibration and λ is an intensity factor. The resulting NSP curve is plotted in Figure 29.

Referring to Figure 29, three inelastic events associated with the following damage states are identified.

1. *Onset of damage*. The onset of damage in the structure is identified in Figure 29 as DS$_1$, which corresponds to the wall displacement $\Delta_C = 0.9"$ at which the NSP curve first begins to depart from linearity. At wall displacements greater than $\Delta_C = 0.9"$, the roof diaphragm sustains damage. Observable structural damage associated with damage state DS$_1$ includes slight permanent deformation of some nails that fasten the plywood diaphragm to the framing members and possibly some minor damage to strain-sensitive roofing materials. All structural members are still able to support gravity and live loads.

2. *Significant roof diaphragm damage*. At damage state DS$_2$ in Figure 29, which manifests itself as a slight kink in the NSP curve at $\Delta_C = 7.5"$, the roof diaphragm

58

shows signs of permanent deformation including yielding and/or pull-out of nails, the enlargement of nail holes in the plywood diaphragm, the formation of gaps between adjacent sheets of plywood and noticeable damage to the roofing material. In addition, the roof-wall connections may show some signs of distress including enlargement of the nail holes in the framing members and/or metal connections, and yielding and/or pull-out of the nails. The building may also be leaning slightly. However, in this damage state, the roof-wall connections have not fractured and all structural members are still able to support gravity and live loads.

3. *Fracture of the roof-wall connections*. Damage state DS_3 in Figure 29, which coincides with the sharp and significant drop in the base shear at $\Delta_C = 11.9"$, is associated with the fracturing of a large number of roof-wall connections along one or both walls. For the structure considered in this example, where the strength of the roof-wall connections was considered deterministic, dynamic analyses at finely incremented S_a levels have shown that the initial failure of a small number of connections quickly leads to a total loss of lateral and gravity load carrying capacity. This is because the load carried by the fractured connections is transferred to adjacent connections (with same strength) that become overloaded as a result and also fail. Consequently, in this damage state, the structure has at least partially collapsed and many structural members are no longer capable of resisting gravity or lateral loads. At the end of this application section, a few results are included on the effects of explicitly considering the variability in the strength of roof-wall connections.

Step 2: NSP curves for the damaged building

To evaluate the post-earthquake residual capacity of the structure to withstand future seismic loads, a NSP curve is developed for each damage state identified in Step 1 that is capable of supporting gravity loads, i.e., damage states DS_1 and DS_2 in this case. DS_3 is in fact associated with incipient collapse. For damage state DS_1 (onset of damage), this NSP curve is identical to that of the intact structure; thus, only damage state DS_2 must be considered in this example.

Referring to Figure 30, the NSP curve for damage state DS_2 is obtained by (1) displacing the structure model to $\Delta_C = 7.5"$ (point 1), (2) quasi-statically unloading it to zero base shear (point 2) and (3) reloading it to failure (point 3). The sequence of points 2-3-4-5 defines the shape of the NSP curve for damage state DS_2. As discussed in the guidelines, the residual displacement associated with this pushover curve ($\Delta_C = 2.8"$) is ignored in this step and we horizontally shift the NSP curve for damage state DS_2 until its origin (point 2 in Figure 30) coincides with (0,0). As illustrated in Figure 31, we do not shift the failure displacement ($\Delta_C = 11.9"$); the resulting disconnect is bridged by simply extending the last segment of the pushover curve.[31] The expected (or measured) residual displacement will be accounted for in Step 3.

---

[31] The resulting disconnect is bridged by extending the last segment of the pushover rather than assuming perfectly-plastic behavior across the gap because the latter cannot easily be input into SPO2IDA. The effect on the final estimate of residual capacity is not expected to be significant.

The NSP curves for the intact structure and damage state DS_2 are plotted together in Figure 31. Note that the NSP curves are estimated to have the same initial slope; hence, $f_{DS_2} = f_1$, where f_1 and f_{DS_2} are the initial first mode frequencies of the intact and damaged structures, respectively[32]. Also note that the linear-elastic region of the NSP curve for damage state DS_2 is larger that that of the intact structure due to the strain hardening present in the roof diaphragm model (see Figure 26). The peak base shear is also larger for damage state DS_2 than it is for the intact structure, only because the last segment of the damaged pushover curve is extended in shifting the NSP back to zero residual displacement.

Step 3: Inferring dynamic response from static response

In order to use the SPO2IDA spreadsheet tool to predict the peak dynamic response of the intact and damaged structure, the NSP curves obtained in Steps 1 and 2 must be modified as follows.

1. *Piecewise linear idealization of the NSP curves.* The SPO2IDA spreadsheet requires that the NSP curves be defined in a piecewise linear fashion. Figure 32 shows plausible idealizations for the NSP curves obtained for the intact and damaged structures in steps 1 and 2 (assuming no residual displacement offset).

2. *Normalization of the base shear and displacement axes.* The SPO2IDA spreadsheet assumes that the base shear and displacement axes of the NSP curves are normalized by the corresponding quantities at the onset of damage. Thus, for the intact structure the displacement ordinates are expressed in terms of the global ductility ratio, $\mu = \Delta_C / \Delta_{Cy}$, where $\Delta_{Cy} = 1.4''$ is the yield displacement and the base shear ordinates are expressed as the ratio $R = BS / BS_y$, where $BS_y = 315$ kips is the base shear that corresponds to Δ_{Cy} in Figure 32a. Similar calculations are made for the damaged structure using the base shear and displacement values shown in Figure 32b. Plots of the normalized NSP curves for use with the SPO2IDA spreadsheet are shown in Figure 33.

Using the normalized NSP curves plotted in Figure 33 as input, the SPO2IDA spreadsheet predicts the dynamic response of the structure in its intact and damaged conditions. The resulting normalized median IDA curves associated with the intact and damaged structures (but assuming no residual displacement offset) are also plotted in Figure 33. Note that the IDA results are expressed in terms of $R = S_a(f_1) / S_{ay}(f_1)$ for the intact structure and $R = S_a(f_{DS_2}) / S_{ay,DS_2}(f_{DS_2})$ for the damaged structure, where $S_{ay}(f_1)$ and $S_{ay,DS_2}(f_{DS_2})$ are the first-mode pseudo-acceleration values that correspond to Δ_{Cy} in Figure 32. Based on the results summarized in Table 13, which suggest that the response of the tilt-up is dominated by its first mode, we assume $S_{ay}(f_1) = BS_y / M_1^*$ for the intact structure, where $M_1^* = \psi_1^2 \boldsymbol{\phi}_1^T \mathbf{M} \boldsymbol{\phi}_1$ is the effective modal mass of the first mode

---

[32] The same is true if parallel-to-elastic unloading/re-loading is assumed in order to approximate the NSP curve for damage state DS_2. The effect of this approximation on the NSP curve, and more importantly on the residual capacity estimated in Step 3, are small.

of vibration and ψ_1 is the first mode participation factor. M_1^* and ψ_1 are listed in Table 13. Similarly, $S_{ay,DS_2}(f_{DS_2}) = BS_{y,DS_2} / M_{1,DS_2}^*$ for the damaged structure. Figure 31 suggests that the initial elastic response of the damaged structure is identical to that of the intact structure; therefore, $M_{1,DS_2}^* = M_1^*$ for this building.

For the purposes of developing the fragility curves, it is beneficial to plot the IDA curves in terms of Δ_C and $S_a(f_1)$ for the intact structure or $S_a(f_{DS_2})$ for the damaged structure. These plots are shown in Figure 34. The displacement values in Figure 34 are obtained by multiplying the global ductility values shown in Figure 33 by $\Delta_{Cy} = 1.4''$ for the intact structure and by $\Delta_{Cy} = 2.0''$ for the damaged structure. The $S_a(f_1)$ ordinates shown in Figure 34a for the intact structure are obtained by multiplying the $R = S_a(f_1)/S_{ay}(f_1)$ ordinates in Figure 33a by $S_{ay}(f_1)$. Similarly, the $S_a(f_{DS_2})$ ordinates plotted in Figure 34b for the damaged structure are obtained by multiplying the $R = S_a(f_{DS_2})/S_{ay,DS_2}(f_{DS_2})$ ordinates in Figure 33b by $S_{ay,DS_2}(f_{DS_2})$.

Note that the spectral acceleration values shown in Figures 34a and 34b are those associated with the fundamental frequencies f_1 and f_{DS_2} of the intact and damaged structures, respectively. In general, $f_{DS_2} \neq f_1$.[33] However, for the purposes of determining the tagging condition in Step 4, the capacities for the intact and damaged structures must be expressed in terms of the same reference spectral acceleration, which is chosen to be that associated with the first mode of the intact structure, $S_a(f_1)$. Hence, the S_a axis for the damaged structure in Figure 34b is scaled by $S_a(f_1)/S_a(f_{DS_2})$.[34] However, because the first-mode frequencies of the intact and damaged buildings are identical in this example, $S_a(f_1)/S_a(f_{DS_2}) = 1.0$. We reiterate that this will not be the case in general. The resulting IDA curves for the intact and damaged structures are plotted in Figure 35. Also indicated in Figure 35 are the capacity of the intact structure and the residual capacity of the damaged structure (assuming no residual displacement offset).

An IDA curve for the damaged structure that accounts for the expected (or measured) residual displacement offset is also shown in Figure 35. In this example, the expected residual displacement is assumed to be equal to the static offset ($\Delta_C = 2.8''$). As explained in the guidelines and illustrated in Figure 35, the IDA curve that accounts for this residual displacement is obtained by tracing the IDA curve that assumes no residual offset up to the displacement equal to the collapse capacity minus the expected residual displacement, or 11.9"-2.8"=9.1". Accounting for the residual displacement offset reduces the residual capacity of the damaged structure, as one might intuitively expect.

---

[33] Unless, of course, parallel-to-elastic unloading/re-loading is assumed to approximate the NSP curve for the damaged structure.

[34] As explained in the commentary to the guidelines, this conversion is not strictly necessary because it is captured by the final adjustment that is made to the estimates of the residual capacity for the damaged structures.

Finally, the estimate of the residual capacity that accounts for the expected (or measured) residual displacement is adjusted to reflect the observation that, without a residual offset, little or no reduction in the residual capacity relative to that of the intact structure is expected. As explained in the guidelines, this is accomplished by multiplying the residual capacity estimate from Figure 35 (accounting for the expected residual displacement) by the ratio of the capacity of the intact structure to the residual capacity of the damaged structure assuming no residual displacement. The final estimate of the residual capacity for the structure in damage state DS$_2$, therefore, is $(\breve{S}_{a,cap})_2 = 2.12g *$ $2.63/2.36 = 2.36g$.[35] Note that it is only a coincidence that this final estimate of $(\breve{S}_{a,cap})_2$ happens to equal the residual capacity assuming no residual displacement offset.

Step 4: Occupancy status for the damaged building

As outlined in the text of the guidelines, the tag assigned to a structure in damage state DS$_2$ is based on

a) the reduction in the residual median lateral capacity relative to that of the intact structure, and

b) the MAF of exceeding the spectral capacity $(\breve{S}_{a,cap})_2$, which we denote P, and the MAF of exceeding the ground motion corresponding to the median capacity, $(\breve{S}_{a,cap})_1$, of the building in its intact conditions, which we call P_0.

Considering the capacities identified in Figure 35, we see that the reduction in the median capacity is approximately 10.2% and $(\breve{S}_{a,cap})_2 = 2.36g$. Referring to Figure 7, this reduction in capacity results in a green tag if $P_0 < 2.9 \times 10^{-4}$, a yellow tag if $2.9 \times 10^{-4} \leq P_0 < 7.3 \times 10^{-4}$, and a red tag if $P_0 \geq 7.3 \times 10^{-4}$. For the purposes of demonstrating the procedure, we assume that the MAF of exceeding $(\breve{S}_{a,cap})_2$ is about 2.9×10^{-4}. At this level of P_0 a drop of capacity of about 10% means onset of yellow tag[36]. In other words, if the tilt-up is deemed to be in damage state DS$_2$ following an earthquake, it should be yellow-tagged. Note that because damage state DS$_3$ is associated with at least a partial collapse of the structure, it is automatically red-tagged.

Step 5: Ground motion level associated with a structural limit state

The median mainshock ground motion intensities associated with the damage states identified in Step 1 are determined from the IDA curve associated with the intact structure plotted in Figure 35 (or Figure 34a). Referring to this figure, we see that $\breve{S}_a^{OD} = 0.22g$ for the onset of damage limit state, $\breve{S}_a^Y = 1.85g$ for damage state DS$_2$, which was assigned a yellow tag in Step 4, and $\breve{S}_a^C = 2.63g$ for the collapse limit state DS$_3$.

The dispersion of these capacities, β, is composed of an aleatory component, β_R, which is estimated from Figure 10, and an epistemic component, β_U, which is based on the

---

[35] Note that if parallel-to-elastic unloading/re-loading is assumed to approximate the NSP curve for the damaged structure, the residual capacity for damage state DS$_2$ is 2.31g, which is within about 2% of that computed in this example.

[36] If $2.9 \times 10^{-4} \leq P_0 < 7.3 \times 10^{-4}$, then DS$_2$ should still be yellow-tagged but an interpolation scheme should be used to find $\breve{S}_a^Y$ in STEP 5.

baseline values listed Table 2a. The net dispersion used in Step 6 is the square-root-sum-of-squares of these two components, i.e., $\beta = \sqrt{\beta_R^2 + \beta_U^2}$. The β values for the three damage states are summarized in Table 14.

Step 6: Computation of the fragility curves

Using the median mainshock ground motion intensities and dispersions obtained in Step 5 for the onset-of-damage, yellow-tag and collapse limit states, the fragility curves for these damage states are computed as described in the guidelines. The resulting fragility curves are plotted in Figure 36. Also shown in Figure 36 are the fragility curves computed for the tilt-up building assuming brittle roof-wall connections (the details of the calculations leading to the brittle-connection fragility curves have not been presented since they are similar in nature to those used to generate the fragility curves for the ductile connection case). Note that the onset-of-damage and yellow-tag fragility curves are identical for the two types of connections[16], but the fragility curves for the collapse limit state differ, reflecting the improved performance of the building when the roof-wall connections are ductile. As can be seen in Figure 36, the median collapse capacity of the building with ductile connections is approximately 10% greater than that of the building with brittle connections.

---

[16] At damage state DS_2, the roof-wall connections are in their linear-elastic range; hence, the behavior of the building is indistinguishable for the two connection types and the median mainshock ground motion intensities associated with DS_2, which depend only on the IDA results for the intact structure up to the displacement that defines this damage state, are identical. For the building with brittle connections, the reduction in the residual capacity for DS_2 (23%) is a little greater than that obtained for the building with ductile connections (19%); however, this difference is not enough to change the yellow-tag designation or the β-values for this damage state.

Validation of the Results

The median IDA curves predicted by SPO2IDA for the intact tilt-up building in the above example are validated by a comprehensive series of dynamic time-history analyses conducted with the ensemble of ground motions listed in Table 15. Each ground motion is scaled by the factor indicated in Table 15 so that the pseudo-acceleration at the fundamental period of the building ($T_1 = 0.57$ s) is $S_a(T_1) = 2.0g$.

For each of the ground motions listed in Table 15, nonlinear dynamic analyses of the tilt-up model were conducted for $0.4g \leq S_a(T_1) \leq 4.8g$ by scaling the record appropriately in accordance with the standard procedure for generating IDA curves. For each time-history analysis, the peak wall displacement at the intersection of gridlines 2 and D in Figure 25 (i.e., the control displacement, Δ_C, in the above example) was recorded. The peak wall displacements obtained for each accelerogram at the levels of ground motion intensity considered are plotted in Figure 37 for a tilt-up building with ductile roof-wall connections and a building with brittle roof-wall connections. Also plotted in Figure 37 is the median IDA curve based on the results of the time-history analyses and the 16th, 84th and 50th percentile (median) IDA curves predicted by SPO2IDA. Note that the axes in Figure 37 have been normalized as described earlier for use with SPO2IDA.

Figure 37 shows that for the building with ductile roof-wall connections, the median IDA curve predicted by SPO2IDA closely matches that based on the time-history results for all values of μ. The median collapse capacity predicted by SPO2IDA for this case ($\check{S}_a{}^C/S_{ay}$ =7.8) is approximately 8% less than that suggested by the median curve based on the time-history results ($\check{S}_a{}^C/S_{ay}$ =8.5). Thus, SPO2IDA appears to be an appropriate tool for predicting even the severe dynamic response of this building.

For the building with brittle connections, the agreement between the SPO2IDA results and the time-history results is excellent for $\mu < 5$, but weakens for larger ductility values with SPO2IDA consistently over-predicting the dynamic response of the system. One must recognize however that the time-history results are based on a relatively small sample size (ten recorded ground motions), so discrepancies should be expected in this region where the drift dispersion is large. Also, note that the median curve based on the time-history results falls well within the band defined by the 16th and 84th percentile curves predicted by SPO2IDA. Consequently, we conclude that for the building with brittle connections, the SPO2IDA results are reasonable and acceptable for the purposes of use with these guidelines.

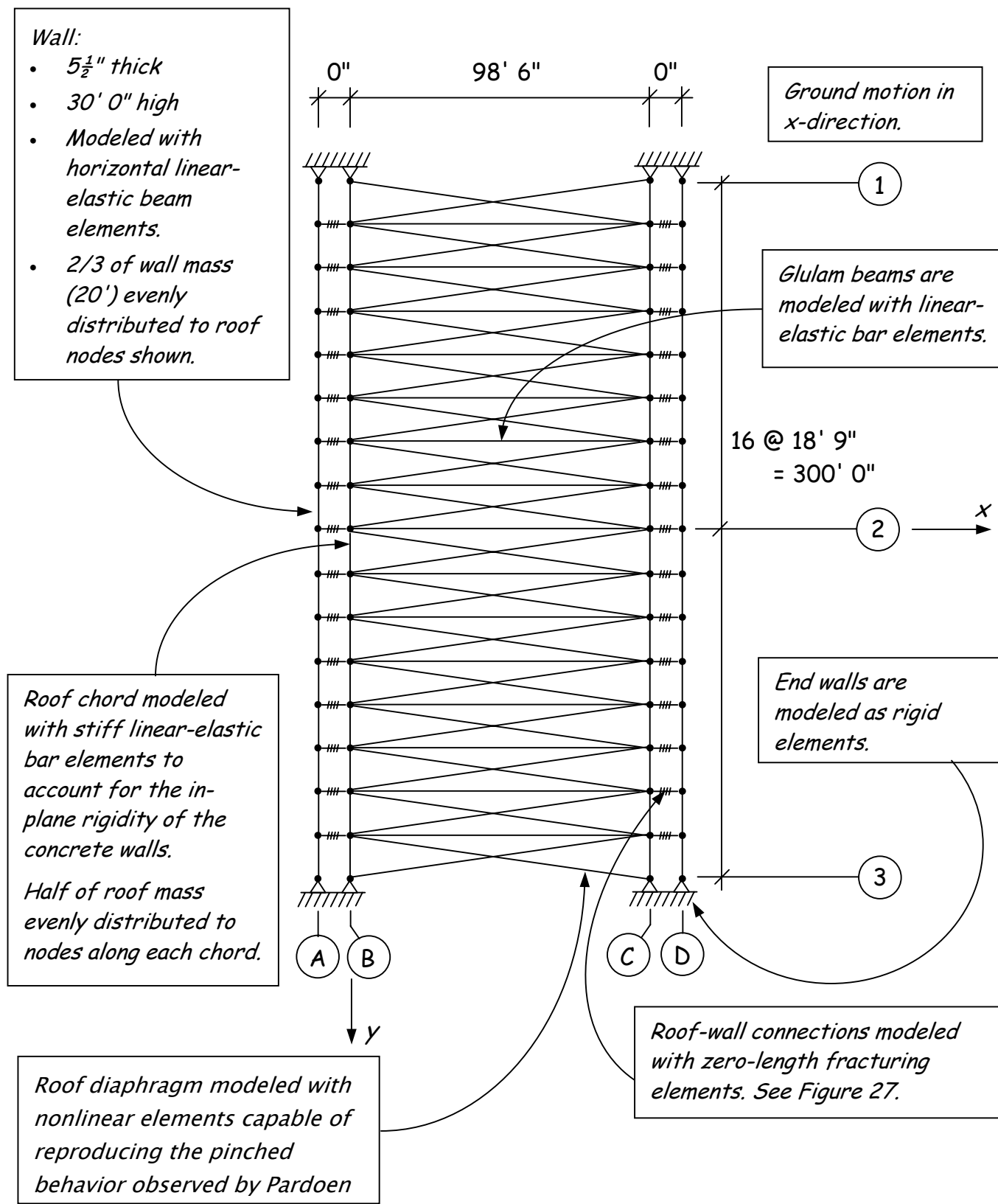**Figure 25.** Plan view of Hollister tilt-up.
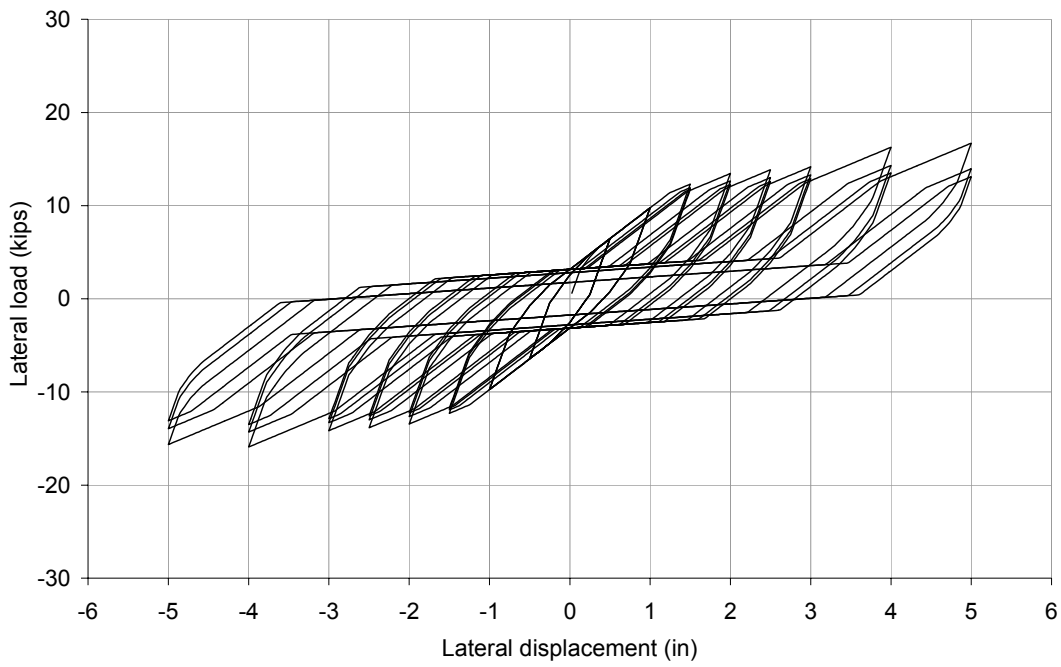
Figure 26. Load-displacement response of diaphragm element. Element calibrated to reproduce UC Irvine test results (NC Control – 16' x 20' specimen).

(a) Ductile

(b) Brittle
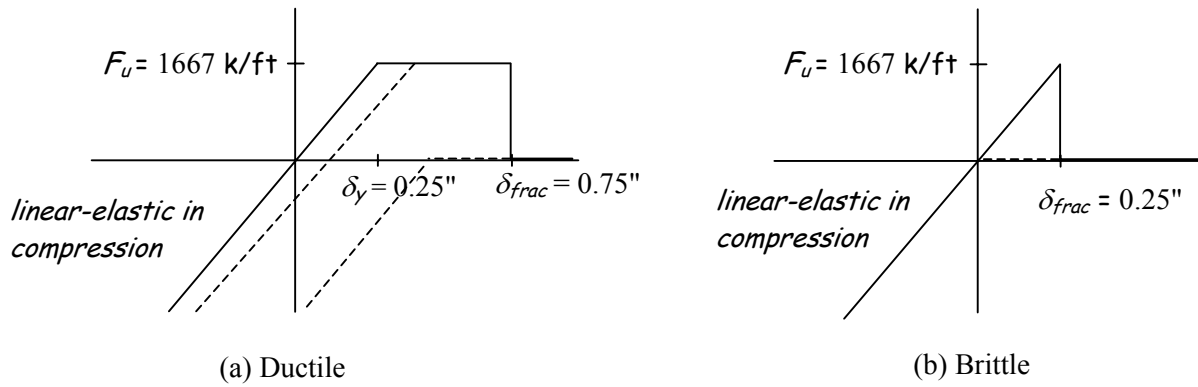
Figure 27. Roof-wall connection behaviors considered.
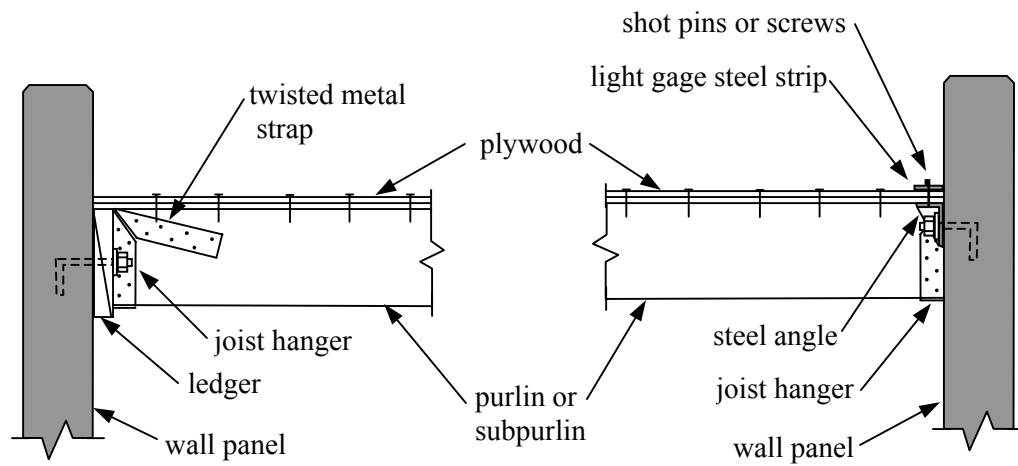
Figure 28. Roof-wall connections commonly used in current practice.
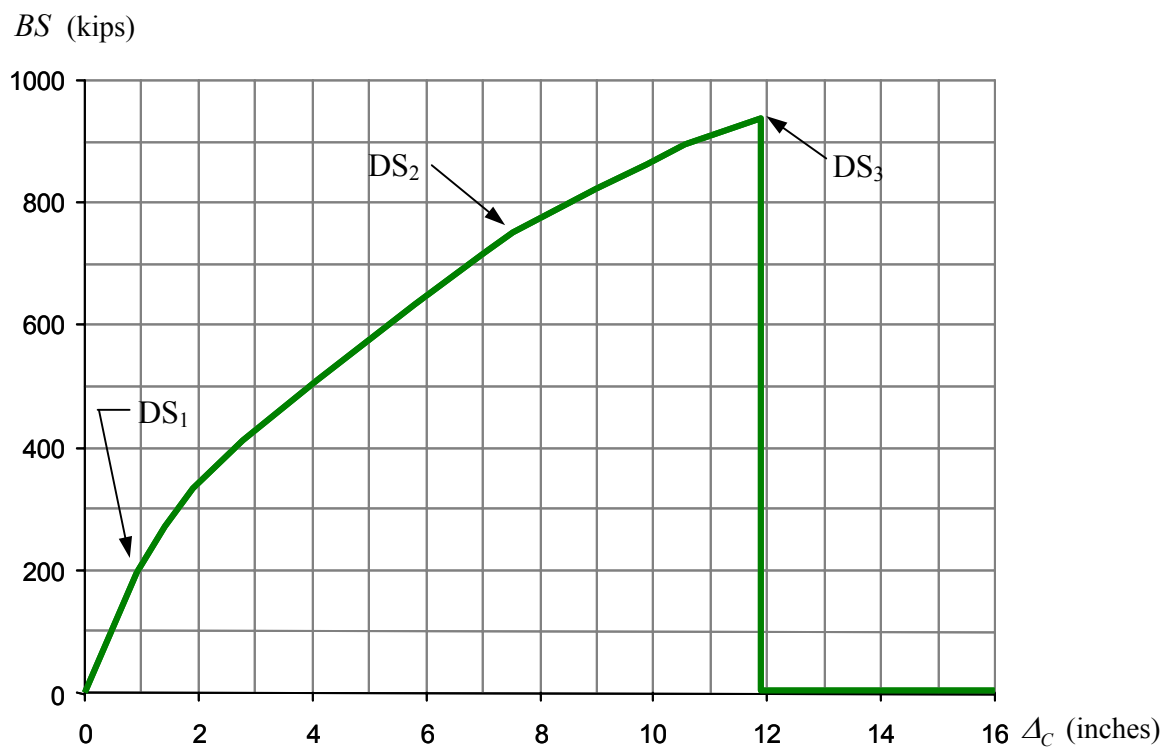
Figure 29. NSP curve for intact structure.

BS_{DS_2} (kips)
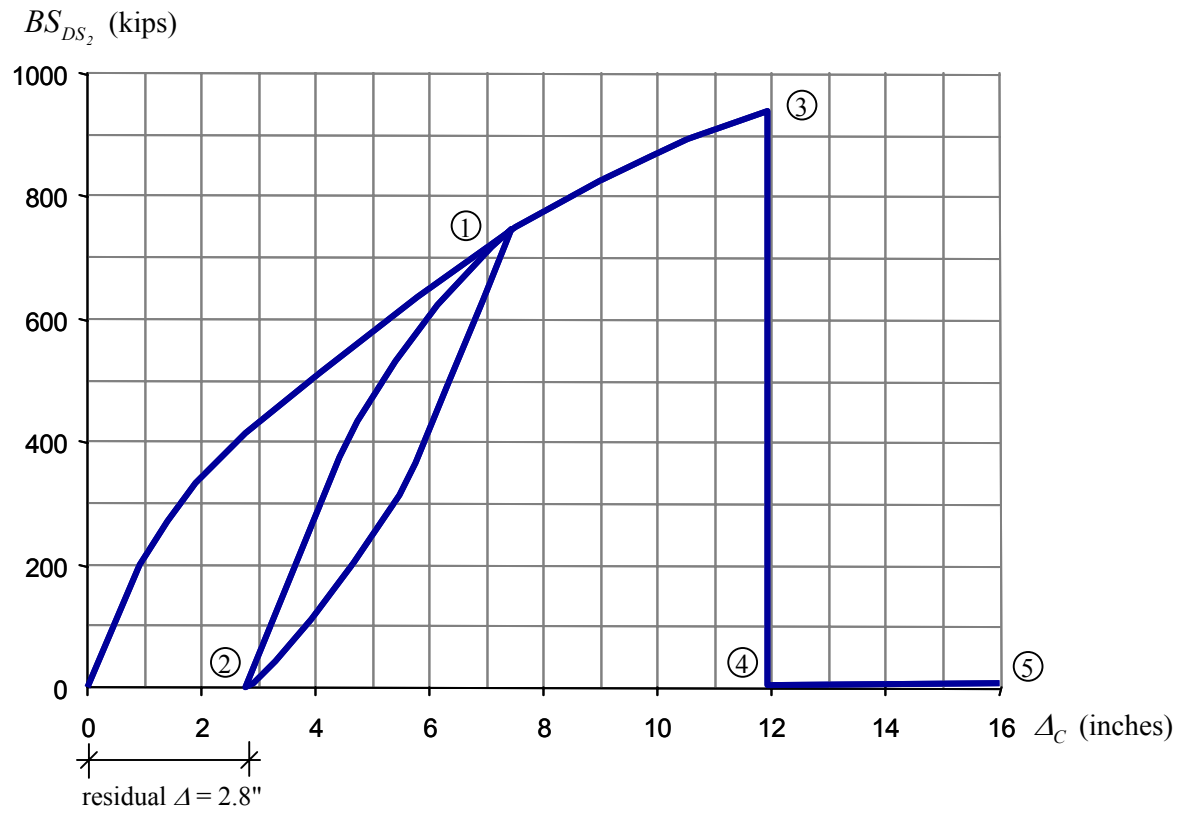
Figure 30. Development of the NSP curve for damage state DS_2.

BS or BS_{DS_2} (kips)
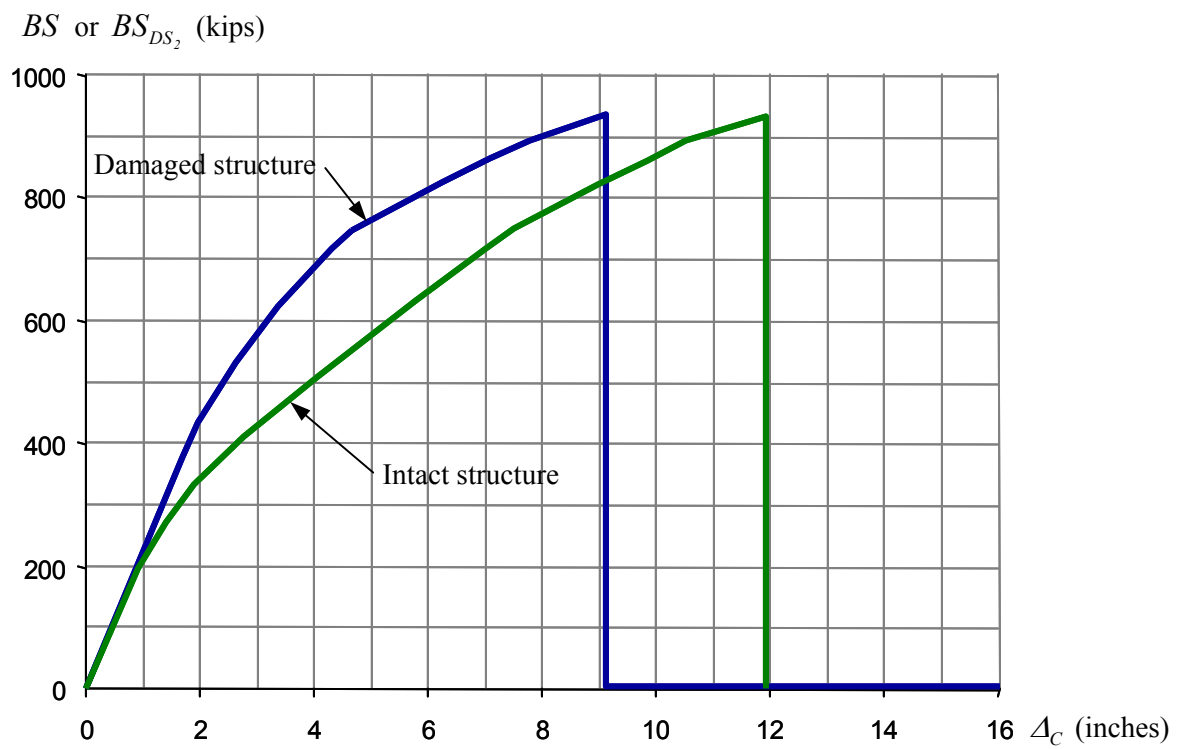
Figure 31. NSP curves for intact structure and damage state DS_2.

(a) Intact structure

BS_{frac} = 935 kips

Piecewise linear idealization

$0.16k_0$

$0.32k_0$

BS_y = 315 kips

Original NSP curve

k_0

Δ_{Cy} =1.4" $\Delta_{C,hard}$ = 8.1" $\Delta_{C,frac}$ = 11.9" Δ_C (inches)

(b) Damaged structure

BS_{frac,DS_2} = 935 kips

Original NSP curve

Piecewise linear idealization

$0.18k_0$

BS_{y,DS_2} = 450 kips

$0.50k_0$

k_0

Δ_{Cy} =2.0" $\Delta_{C,hard}$ = 4.8" $\Delta_{C,frac}$ = 9.1" Δ_C (inches)
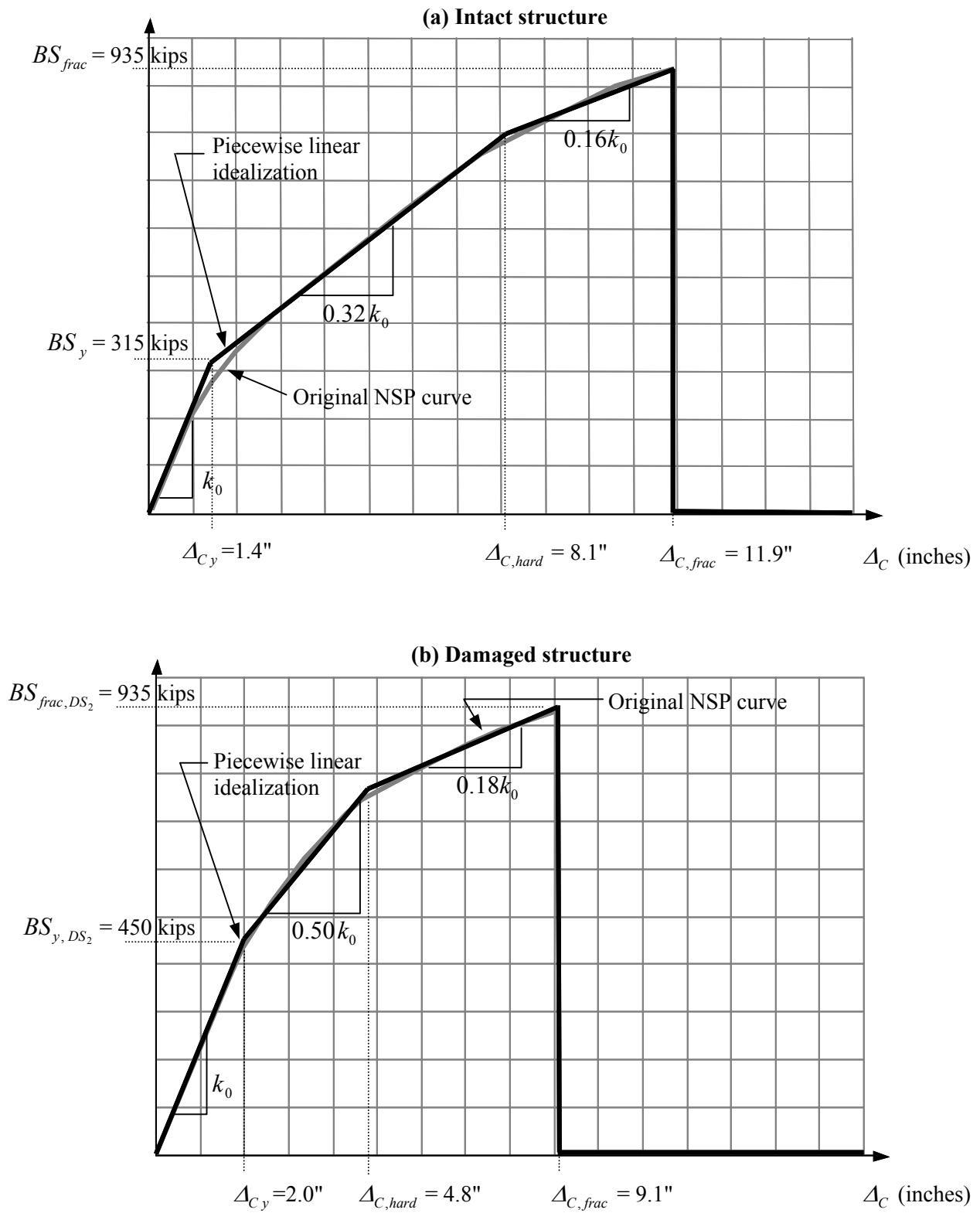
Figure 32. Idealized piece-wise linear NSP curves for intact and damaged structures.

(a) Intact structure

$$S_{a,cap}(f_1)/S_{ay}(f_1) = 7.8$$

Median IDA curve
predicted by SPO2IDA

Piecewise linear
NSP curve

$\mu = \Delta_C / \Delta_{Cy}$

(b) Damaged structure

Median IDA curve
predicted by SPO2IDA

$$S_{a,cap}(f_{DS_2})/S_{ay,DS_2}(f_{DS_2}) = 4.4$$

Piecewise linear
NSP curve

$\mu = \Delta_C / \Delta_{Cy}$
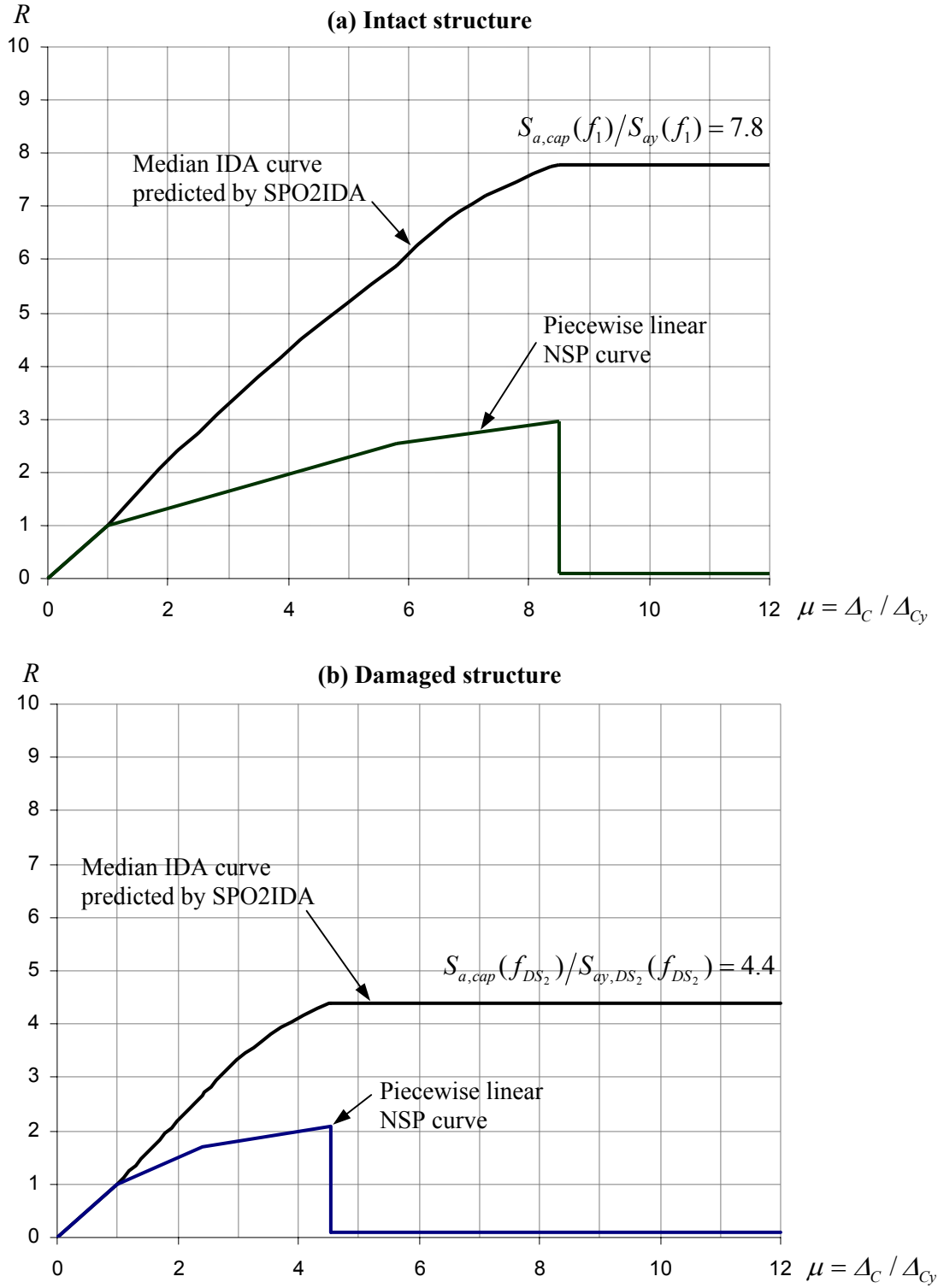
Figure 33. Normalized NSP curves and median IDA curves predicted by SPO2IDA for the intact and damaged structures. For the intact structure, $R = S_a(f_1)/S_{ay}(f_1)$ for the IDA curve and $R = BS/BS_y$ for the NSP curve. For the damaged structure, $R = S_a(f_{DS_2})/S_{ay,DS_2}(f_{DS_2})$ for the IDA curve and $R = BS_{DS_2}/BS_{y,DS_2}$ for the NSP curve.

70
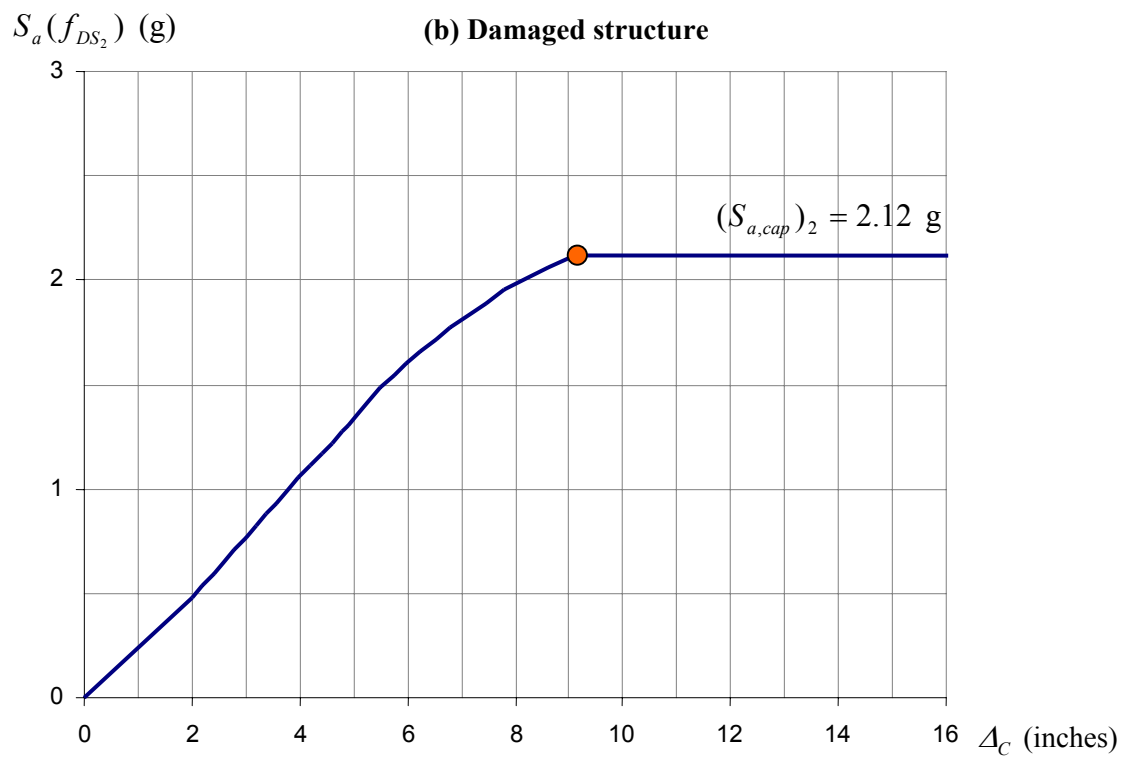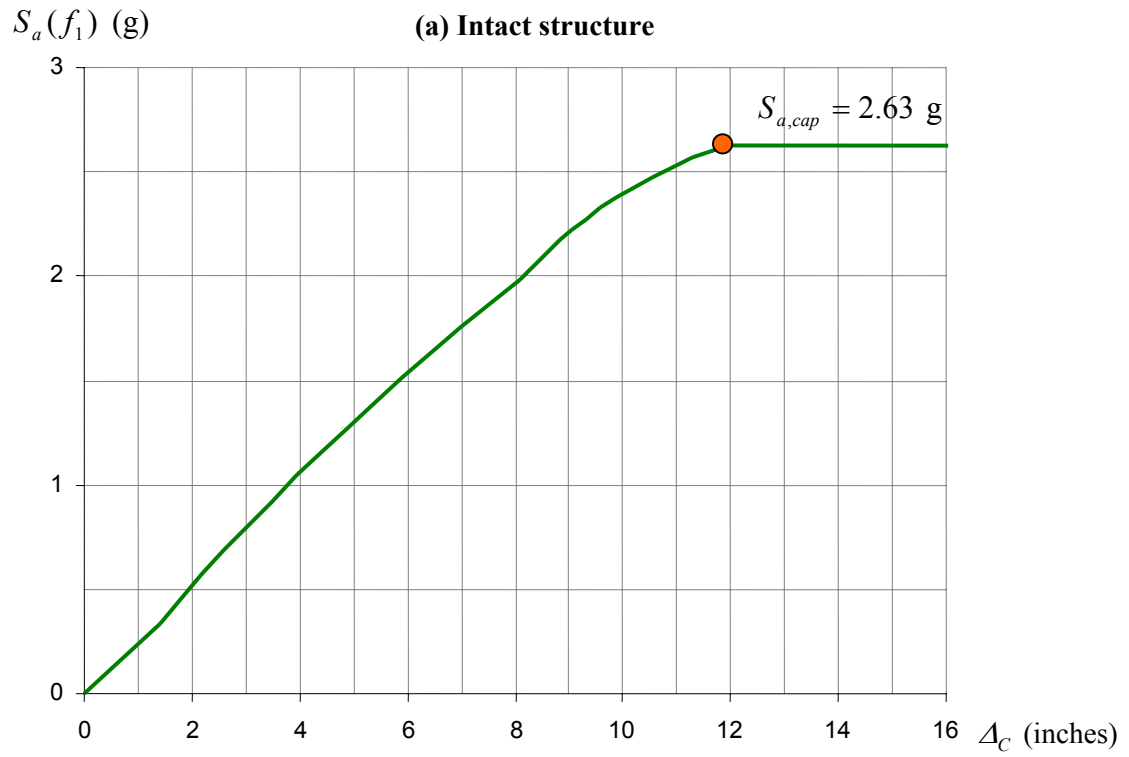
Figure 34. Median IDA curves for the intact and damaged structures.
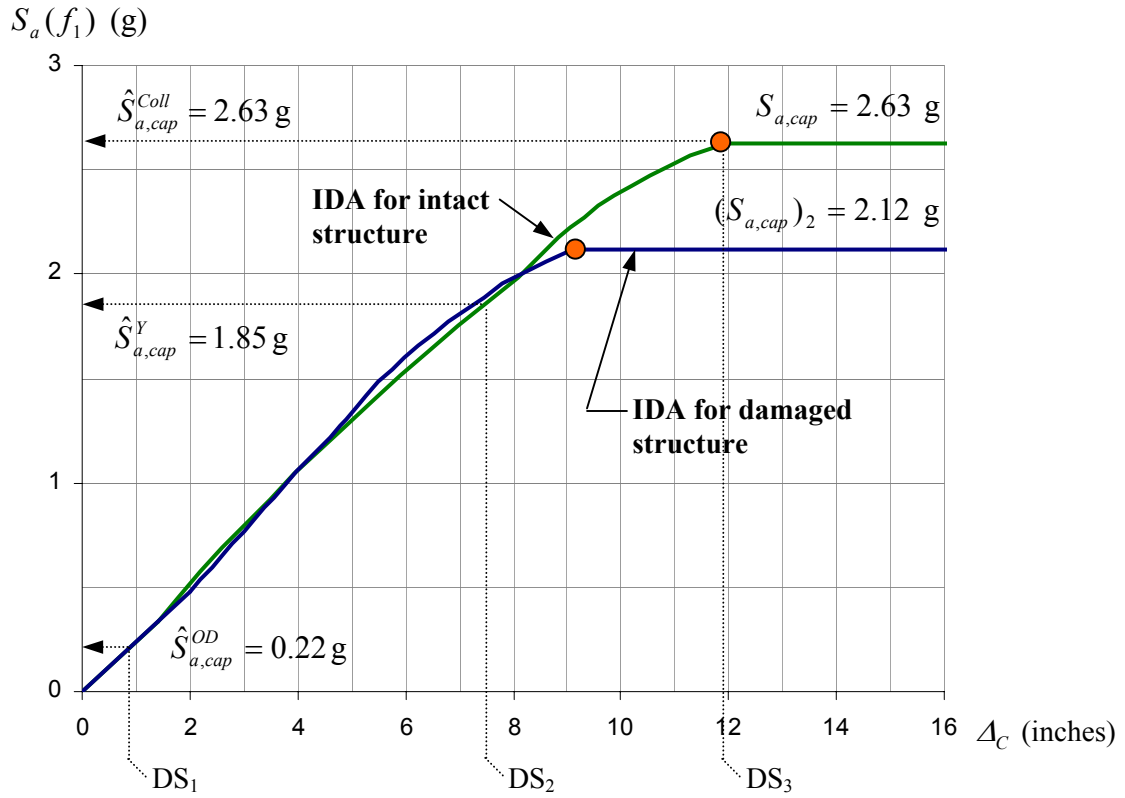
Figure 35. Median IDA curves for the intact and damaged structures in terms of $S_a(f_1)$. Note that for this example, $f_{DS_2} = f_1$ so $S_a(f_{DS_2}) = S_a(f_1)$.
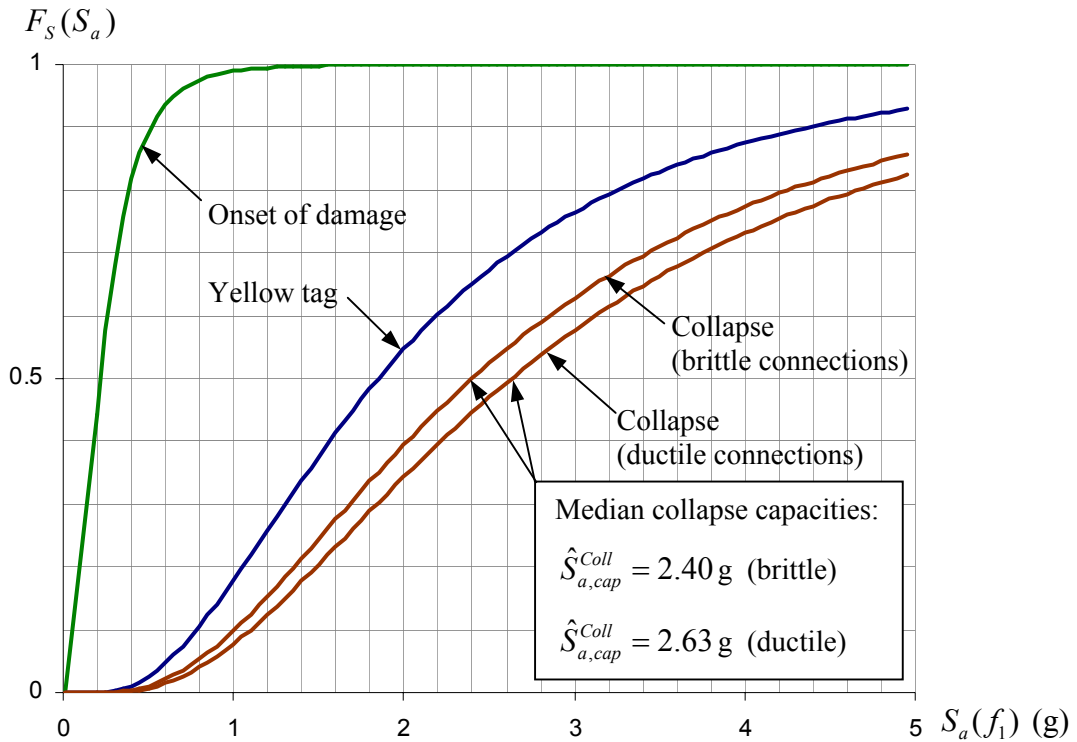
Figure 36. Fragility curves for the onset-of-damage, yellow-tag and collapse limit states. Note that for the onset-of-damage and yellow-tag limit states, the fragility curves for ductile and brittle connections are identical.

$S_a(f_1)/S_{ay}(f_1)$

Ductile roof-wall connections

Data points from dynamic analyses

16th percentile IDA curve predicted by SPO2IDA

Median IDA curve from dynamic analyses

Median IDA curve predicted by SPO2IDA

84th percentile curve predicted by SPO2IDA

$\mu = \Delta_C / \Delta_{Cy}$

$S_a(f_1)/S_{ay}(f_1)$

Brittle roof-wall connections

Data points from dynamic analyses

16th percentile IDA curve predicted by SPO2IDA

Median IDA curve predicted by SPO2IDA

Median IDA curve from dynamic analyses

84th percentile curve predicted by SPO2IDA

$\mu = \Delta_C / \Delta_{Cy}$

Figure 37. Comparison of median IDA curves obtained from dynamic analyses to that predicted by SPO2IDA.

73

Table 13. Modal properties of the intact tilt-up building model.

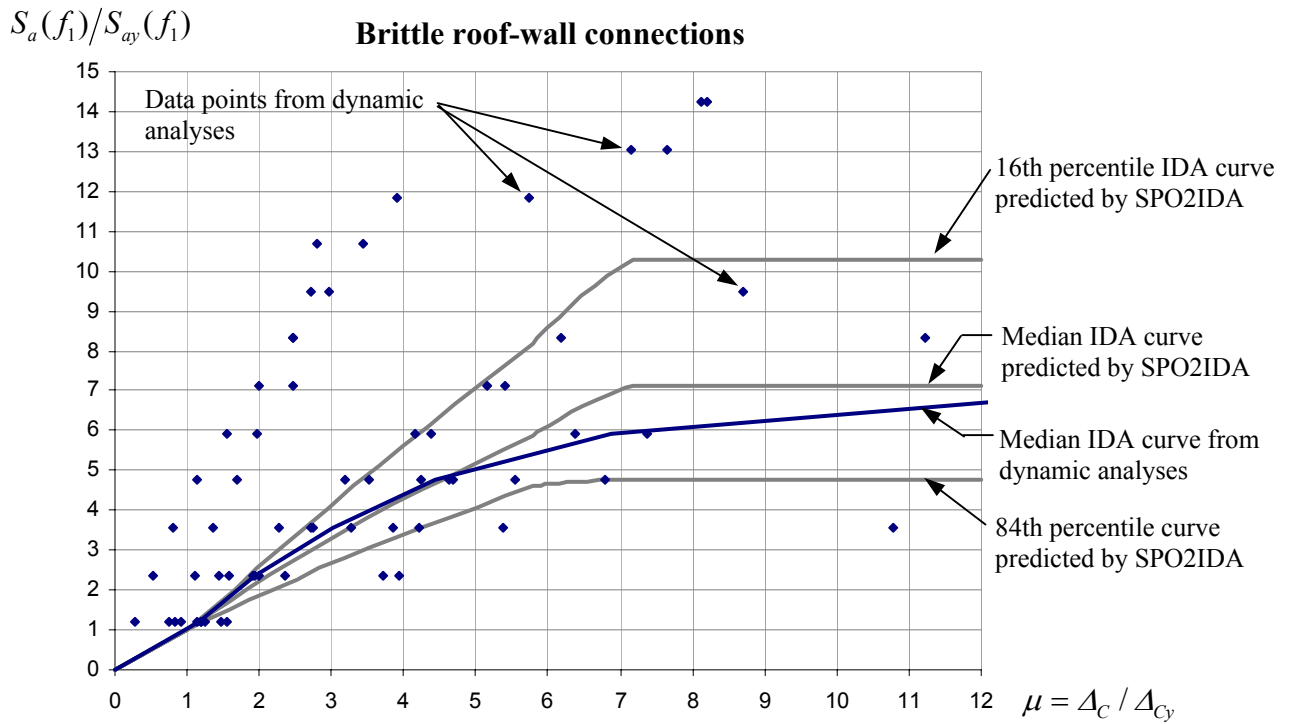| Mode n	Period, T_n (s)	Frequency, f_n (rad/s)	Damping ratio, ς_n	Participation factor, ψ_n	Effective modal mass M_n^*	Effective modal mass $\dfrac{M_n^*}{\sum_n M_n^*}$
1	0.573	11.0	0.046	1.56	2.418	0.858
2	0.307	20.5	0.037	0.00	0.000	0.000
3	0.227	27.7	0.039	0.49	0.240	0.087
4	0.193	32.6	0.041	0.00	0.000	0.000
5	0.175	35.9	0.043	0.27	0.073	0.026
6	0.163	38.5	0.044	0.00	0.000	0.000
7	0.155	40.5	0.045	0.17	0.029	0.010
					Total	0.981

Table 14. Aleatory (β_R) and epistemic (β_U) uncertainty associated with limit states.

Limit state	β_R	β_U	$\beta = \sqrt{\beta_R^2 + \beta_U^2}$
Onset of damage	0.27	0.6	0.66
Yellow tag	0.30	0.6	0.67
Collapse	0.46	0.5	0.68

Table 15. Recorded ground motions used for nonlinear dynamic analyses of the tilt-up building.

Ground motion	M_W	Distance (km)	$S_a(T_1)$ (g)	Scale factor $(2.0/S_a(T_1))$
1. Loma Prieta, Halls Valley (1989)	6.9	31.6	0.19	10.5
2. Landers, Palm Springs Airport (1992)	7.3	37.5	0.25	8.0
3. Northridge, Camarillo (1994)	6.7	36.5	0.44	4.5
4. Kobe, Tadoka (1995)	6.9	30.5	1.07	1.9
5. Kern Country, Taft Lincoln School (1952)	7.4	41.0	0.40	5.0
6. Coalinga, Gold Hill 2W (1983)	6.4	36.6	0.19	10.5
7. Imperial Valley, Niland F.S. (1979)	6.5	35.9	0.17	11.8
8. Morgan Hill, Hollister City Hall (1984)	6.2	32.5	0.14	14.3
9. Whittier Narrows, Saticoy St. (1987)	6.0	39.8	0.17	11.8
10. North Palm Springs, Indio (1986)	6.0	39.6	0.49	4.1

Effects of Random Connection Strengths

As mentioned in the description of damage state DS_3, when the roof-wall connections have the same strength and ductility, as assumed in the above analyses, the initial failure of a small number of connections usually leads to the total loss of lateral and gravity load carrying capacity as the load carried by the fractured connections is transferred to adjacent connections that become overloaded as a result and also fail. Consequently, the time-history analyses used to plot Figure 37 rarely fractured a fraction of the roof-wall connections. In particular, for those time-history analyses that used ground motions with intensities that were within ±30% of the intensity that caused all the roof-wall connections to fail, approximately 10% of the analyses performed on the structure modeled with ductile connections and 9% of the analyses performed on the structure modeled with brittle connections resulted in a damaged structure in which the percentage of fractured connections was less than 67% (but more than 0%). Furthermore, the intensity of those ground motions that produced a damaged structure in which a fraction of the roof-wall connections were fractured was usually close to the intensity required to cause all the connections to fail; i.e., for each ground motion there is only a small range of intensities in which a fraction of the roof-wall connections fail. Similar conclusions can be drawn from the nonlinear pushover analysis plotted in Figure 29, in which a sharp and significant drop in the base shear is observed at the roof displacement $\Delta_C = 11.9"$ due to all the roof-wall connections fracturing.

Unfortunately, the above observations do not agree well with what was observed following the 1994 Northridge earthquake, during which the roofs of tilt-up buildings partially collapsed as a result of localized roof-wall connection failures. It is speculated that the discrepancy between the results of the time-history analyses used to produce Figure 37 and the failures reported after Northridge may be due to the variability of the roof-wall connection strengths in the buildings that failed during the Northridge earthquake. For example, a connection that has a higher capacity than its neighbors may be able to arrest the progressive failure of all the roof-wall connections after one connection fails. In this section, we explore the plausibility of this explanation for the localized roof-wall connection failures observed in Northridge with a second, but no less important, objective of providing insight into how the analysis procedure for tilt-up buildings may be modified to include damage states characterized by the fraction of the roof-wall connections that failed during the mainshock.

Structure Model and Random Connection Strengths

In the following analyses, we consider the tilt-up building shown in Figure 25 with brittle roof-wall connections, whose behavior under load is as shown in Figure 27b. We assume that the tensile connection strength indicated in Figure 27b (F_u = 1667 k/ft) is the mean value of a Weibull random variable with a coefficient of variation (c.o.v.) of $\delta = 20\%$. Furthermore, we assume that the strength of each connection is independent of all other connections in the building.

Ground Motions

We are interested in the percentage of fractured roof-wall connections caused by an earthquake when the 30 roof-wall connections shown in Figure 25 are randomly assigned strengths drawn from the Weibull distribution described above. Due to the random assignment of the connection strengths, the percentage of fractured connections caused by an earthquake is also random. To quantify the variability in the percentage of fractured connections, 20 time-history analyses (each with a different realization of connection strengths) are performed for each ground motion listed in Table 15. Naturally, the intensity of the ground motions to use for the dynamic analyses is an important consideration. For example, if the applied ground motion is very weak, then none of the roof-wall connections will fail, while if the ground motion is very strong, then all the connections are likely to fail, regardless of the assumed distribution of their tensile strengths. This is because the common ground motion introduces a correlation between the collapses of different connections. Consequently, rather than scaling each ground motion to have the same $S_a(T_1)$ value, each ground motion is scaled relative to the spectral acceleration (denoted $S_a^*(T_1)$) at which all the connections fracture when their strengths are set to their mean value (F_u = 1667 k/ft). Table 16 lists $S_a^*(T_1)$ for each ground motion. In the following analyses, we let the ground motion intensity scale factor $\gamma = 1$ coincide with $S_a^*(T_1)$. Note that with this definition of γ, when the strengths of all the connections are assigned their mean values, they will all fail when $\gamma \geq 1$.

Results of the Time-History Analyses

The results of the time-history analyses described above are summarized for each ground motion in Figures 38a – 38j. Plotted in these figures for $\gamma = 0.7, 0.9, 1.0$ and 1.1 are (1) the empirical cumulative distribution functions (ECDFs) of the percentage of fractured connections and (2) the distribution of the damage along the length of the wall.

Empirical cumulative distribution functions

The ECDFs plotted on the left-hand side of Figures 38a – 38j quantify the probability that the percentage of fractured connections is less than or equal to some prescribed fraction $0 \leq \alpha \leq 1$ for each ground motion when it is scaled by $\gamma = 0.7, 0.9, 1.0$ and 1.1. The data points plotted in these figures correspond to the percentage of fractured connections recorded for each of the 20 realizations of connection strengths at the four levels of ground motion intensity considered. The lines are beta CDFs fitted using the method of moments to the 20 data points collected for each value of γ.

It is evident from the ECDF plots that as the intensity factor γ is decreased, a partial failure of the roof-wall connections is more likely to occur. In particular, we note that for $\gamma = 0.7$, the median of α lies between 15% and 90% for all ground motions considered; compare this result to those obtained from the time-history analyses performed with the roof-wall connection strengths set equal to their mean values, in which none of the connections fail when $\gamma = 0.7$, except for one ground motion (#4). Consequently, when

the roof-wall connection strengths are variable, the range of ground motion intensities that cause partial roof-wall connection failures is wider than that observed for the case in which all the connection strengths are set equal to their mean values. Furthermore, it is evident from the ECDFs plotted in Figures 38a – 38j that when $\gamma \geq 1$, which will cause all the connections to fail when their strengths are set equal to their mean values, there are many cases in which only a partial failure occurs. Therefore, we conclude from these plots that the variability of the roof-wall connection strengths is a plausible explanation for the partial failures observed after the Northridge earthquake.

Damage distribution plots

To gain additional insight into the performance of the tilt-up building shown in Figure 25 when the roof-wall connection strengths are variable, consider the damage distribution plots shown on the right-hand side of Figures 38a – 38j. The horizontal axis of these plots indicates the location along the length of the wall and the vertical axis measures the fraction of the simulations in which the connection at a particular location fails.

The damage distribution plots suggest that, in general, the connections near the middle of the wall are more susceptible to fracturing. This observation is reasonable when one assumes that the building responds in its fundamental mode of vibration, which is plotted in Figure 39 along with the third, fifth and seventh modes[37]. However, there are exceptions to this observation, notably ground motions 4 and 10 (Figures 38d and 38j, respectively), which appear to cause the connections near the ends of the wall to fail more often, and ground motion 9 (Figure 38i), which appears to create complex patterns of damage along the length of the wall. We remark that for each ground motion, the connection strengths are randomly selected for each simulation at each intensity level. Therefore, it is unlikely that the damage patterns observed for ground motions 4, 9 and 10 are due to "odd" combinations of connection strengths since the patterns can be seen at all four values of γ considered; instead, the unusual damage patterns seen in Figures 38d, 38i and 38j are likely due to unusual characteristics of these ground motions.

To verify this assertion consider Table 17, which summarizes the intensity of the response spectra at the fundamental mode of vibration, $S_a(T_1, \zeta_1)$, to that of the third, fifth and seventh modes ($S_a(T_n, \zeta_n)$, $n = 3,5,7$) for each ground motion plotted in Figure 38. Studying this table, we see that the three ground motions that exhibit the unusual damage patterns in Figure 38 (ground motions 4, 9 and 10) are also the "weakest" at the fundamental period of vibration of the structure relative to the higher modes of vibration. As indicated in Figure 39, unlike the case of the fundamental mode of vibration, the connection elongations near the ends of the wall for the higher modes of vibration are comparable to those near the midpoint of the wall; consequently, it is reasonable to expect damage patterns that are not concentrated near the midpoint of the wall when the ground motion has significant frequency content near the higher modes of vibration of the structure relative to the fundamental mode, as is the case for ground motions 4, 9 and

---

[37] Recall that only the "odd" modes of vibration have non-zero participation factors because the "even" modes are anti-symmetric shapes that cannot be excited by a ground motion that acts through the center of rigidity of the model.

10. We conclude therefore that the unusual damage patterns caused by ground motions 4, 9 and 10 are the result of the frequency content of these ground motions relative to the natural modes of vibration of the structure.

Figure 38. Empirical CDFs of the percentage of fractured connections and the distribution of the damage along the length of the wall for ground motions 1, 2 and 3.

(d)

(e)

(f)

Figure 38 (con't). Empirical CDFs of the percentage of fractured connections and the distribution of the damage along the length of the wall for ground motions 4, 5 and 6.
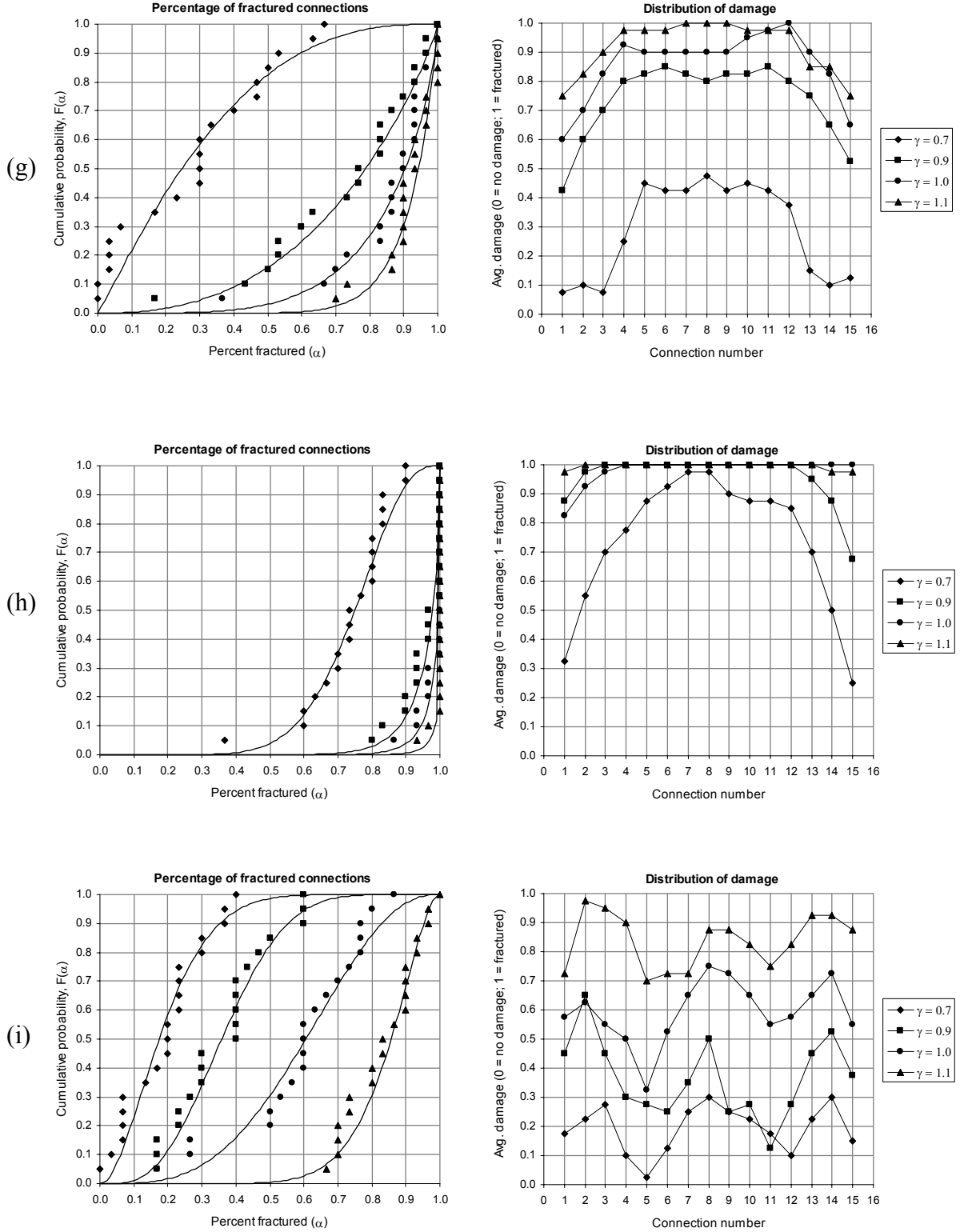
81

(g)

Percentage of fractured connections

Distribution of damage

(h)

Percentage of fractured connections

Distribution of damage

(i)

Percentage of fractured connections

Distribution of damage

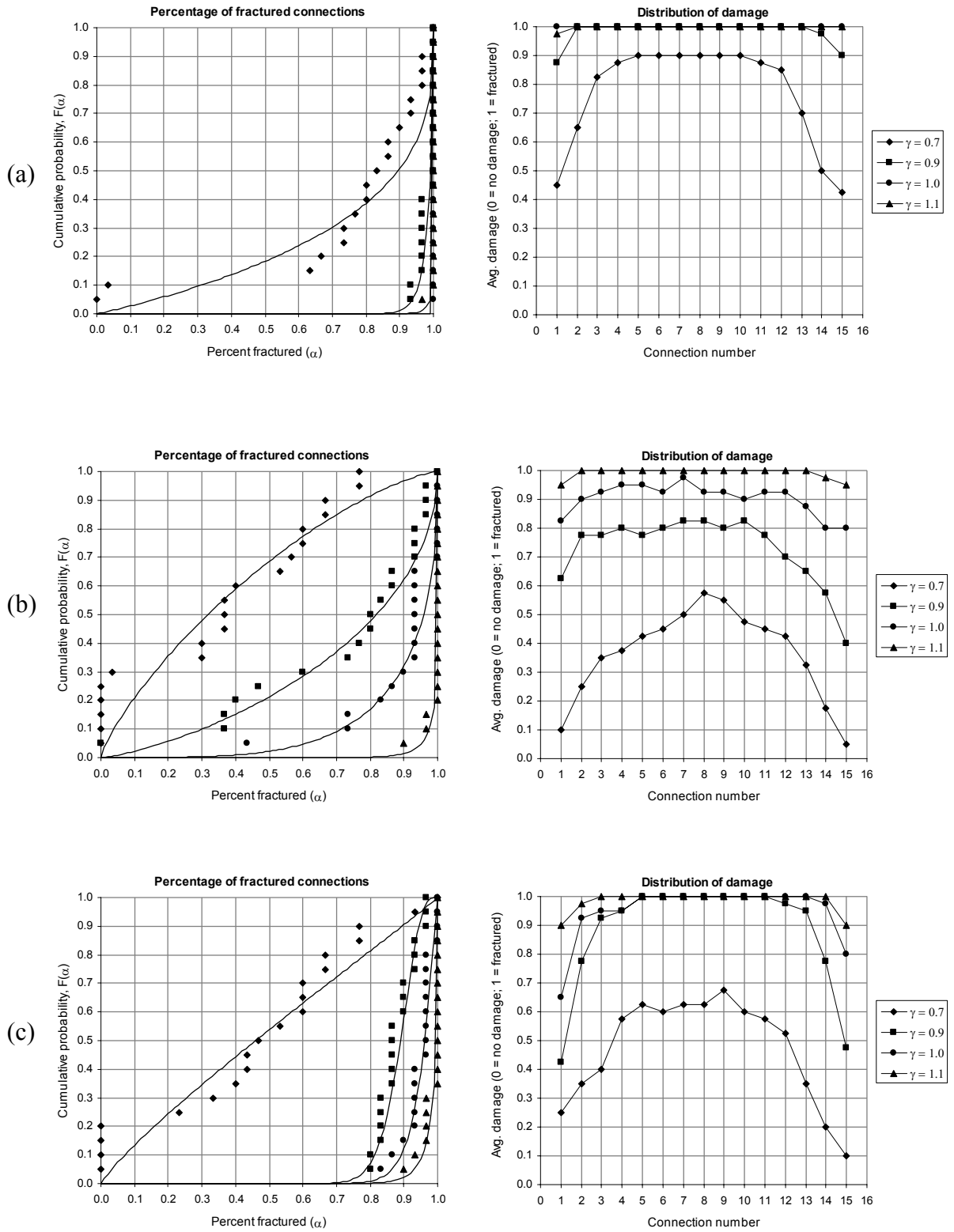**Figure 38 (con't).** Empirical CDFs of the percentage of fractured connections and the distribution of the damage along the length of the wall for ground motions 7, 8 and 9.
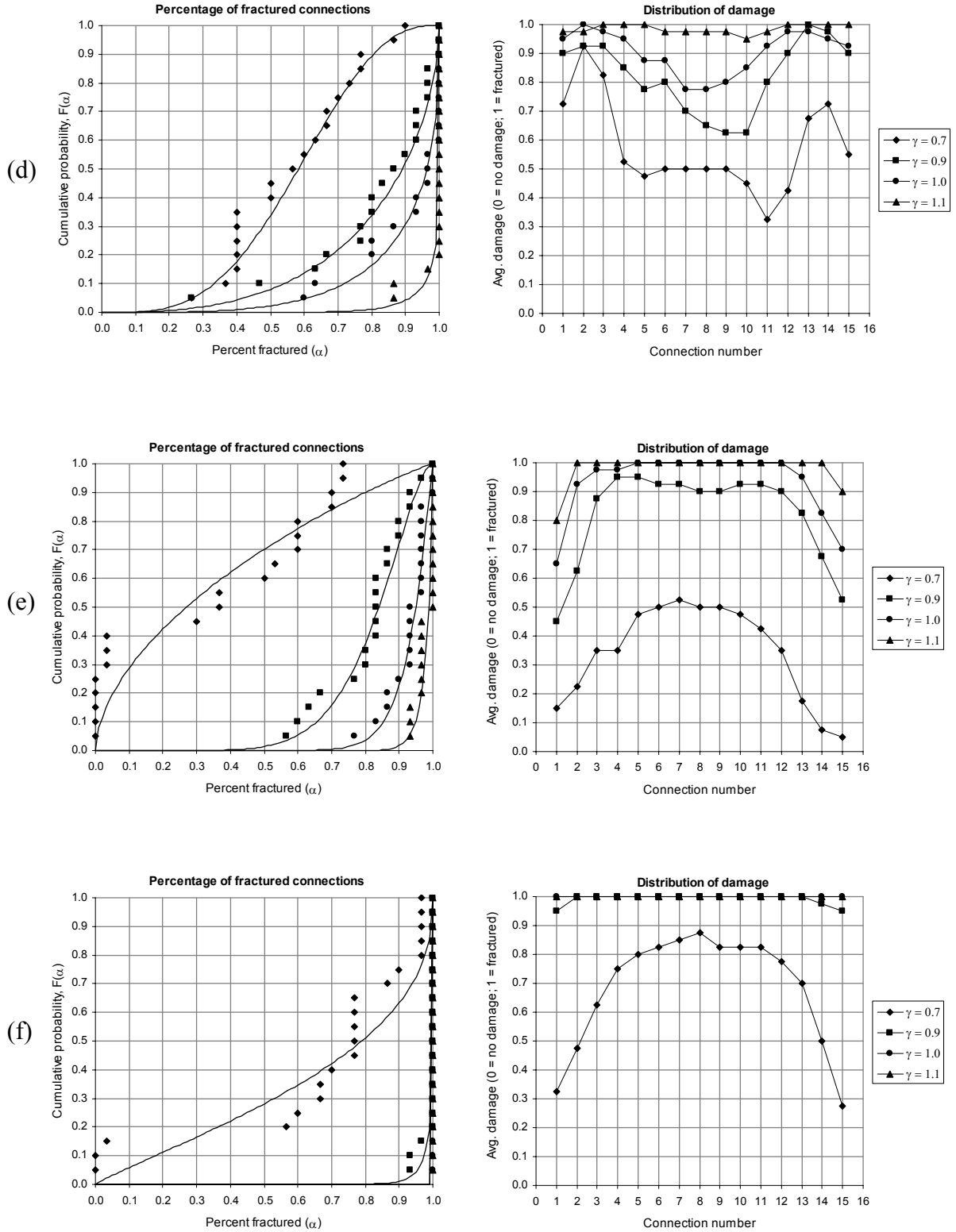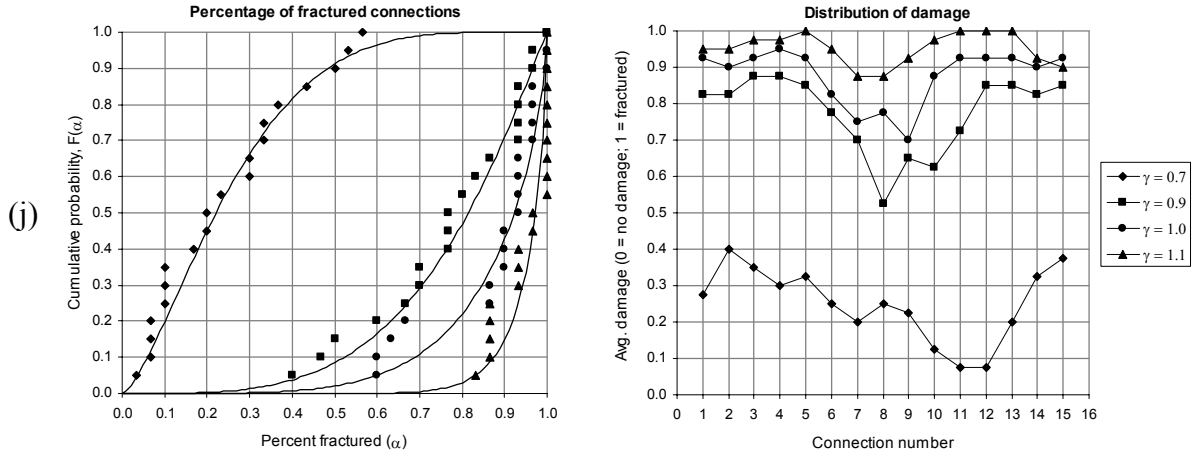
(j)

Figure 38 (con't). Empirical CDFs of the percentage of fractured connections and the distribution of the damage along the length of the wall for ground motion 10.

Mode 1 $T_1 = 0.573$ s
$\zeta_1 = 0.046$
$\psi_1 = 1.56$

Mode 3 $T_3 = 0.227$ s
$\zeta_3 = 0.039$
$\psi_3 = 0.49$

Mode 5 $T_5 = 0.175$ s
$\zeta_5 = 0.043$
$\psi_5 = 0.27$

Mode 7 $T_7 = 0.155$ s
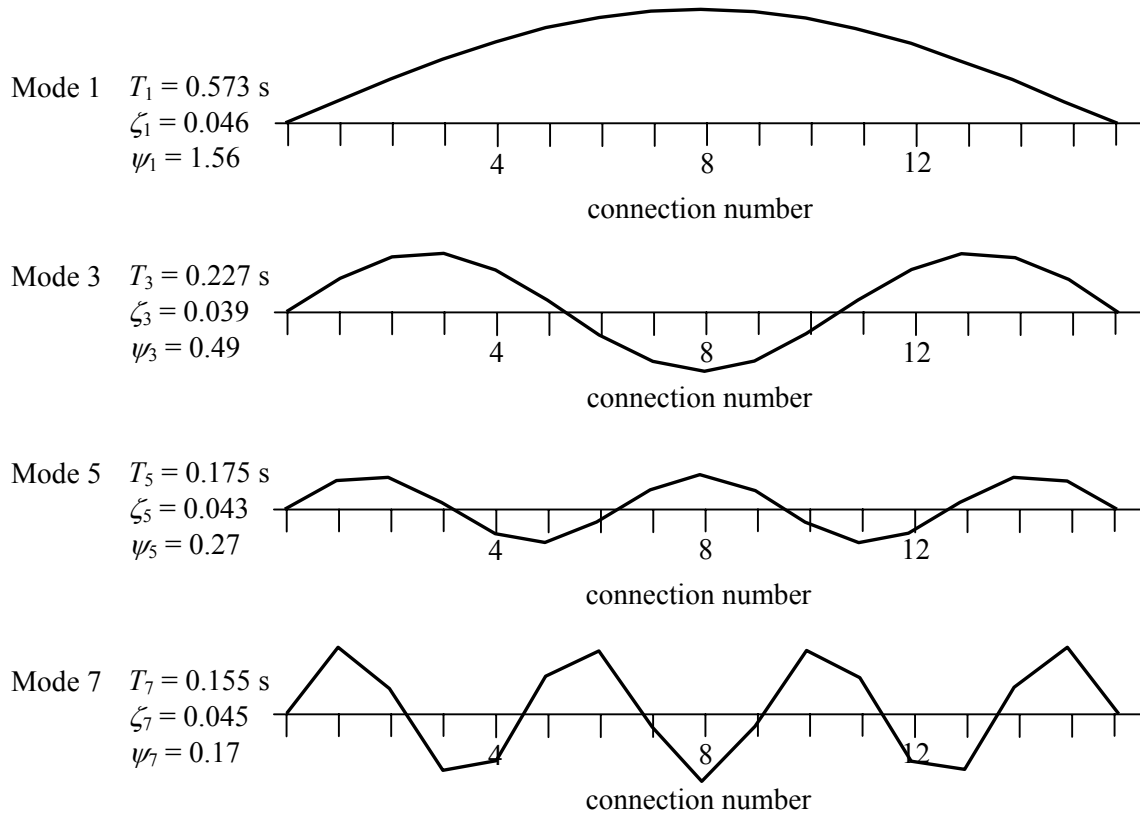$\zeta_7 = 0.045$
$\psi_7 = 0.17$

Figure 39. Modal connection elongations.

83

Table 16. Spectral acceleration, $S_a^*(T_1)$, at which all the connections fracture when their strengths are set to their mean value ($F_u = 1667$ k/ft).

Ground Motion (see Table 15)	$S_a^*(T_1)$ (g)
1	1.9
2	2.4
3	3.1
4	4.0
5	2.3
6	3.0
7	1.8
8	1.6
9	1.2
10	4.4

Table 17. Intensity of the response spectrum at the fundamental mode of vibration of the example tilt-up building relative to that corresponding to the third, fifth and seventh modes.

Ground Motion (see Table 15)	$S_a(T_1, \zeta_1)$ (g)	$\dfrac{S_a(T_1, \zeta_1)}{S_a(T_3, \zeta_3)}$	$\dfrac{S_a(T_1, \zeta_1)}{S_a(T_5, \zeta_5)}$	$\dfrac{S_a(T_1, \zeta_1)}{S_a(T_7, \zeta_7)}$
1	0.19	1.75	1.49	1.69
2	0.25	0.91	0.94	1.14
3	0.44	1.18	1.84	2.02
4	1.07	0.50	0.54	0.92
5	0.40	0.60	0.95	0.95
6	0.19	1.46	1.74	2.14
7	0.17	0.68	0.47	0.61
8	0.14	1.10	0.89	1.15
9	0.17	0.32	0.49	0.67
10	0.49	0.39	0.40	0.26

References

ATC-11, 1983. "*Seismic Resistance of Reinforced Concrete Shear Walls and Frame Joints: Implications of Recent Research for Design Engineers*", Applied Technology Council, 555 Twin Dolphin Drive, Suite 550, Redwood City, California 94065

ATC-20, 1989. "*Procedures for Postearthquake Safety Evaluation of Buildings*", Applied Technology Council, 555 Twin Dolphin Drive, Suite 550, Redwood City, California 94065

ATC-40, 1996. "*Seismic Evaluation and Retrofit of Concrete Buildings*", Vol. I-II, Applied Technology Council, 555 Twin Dolphin Drive, Suite 550, Redwood City, California 94065

ATC, 1999. *Earthquake Aftershocks - Entering Damaged Buildings*, TechBrief 2, Applied Technology Council, 555 Twin Dolphin Drive, Suite 550, Redwood City, California 94065

Bandyopadhyay, K., Cornell, C.A., Costantino, C., Kennedy, R.P., Miller, C., and A. Veletsos, 1993. "*Seismic Design and Evaluation Guidelines for the Department of Energy High-Level Waste Storage Tanks and Appurtenances*", Report BNL 52361 UC-406 UC-510, Department of Nuclear Energy Brookhaven National Laboratory, Upton, NY 11973

Bazzurro, P., Cornell, C.A., Menun, C., and M. Motahari, 2004. "Guidelines for Seismic Assessment of Damaged Buildings", *Proceedings of 13th WCEE*, Paper 1708, Vancouver, B.C., Canada, August 1-6.

Benjamin, J.R., and C.A. Cornell, 1970. "Probability, Statistics, and Decision for Civil Engineers", Mc-Graw Hill, Inc., New York.

Cornell, C.A., Vamvatsikos, D., Jalayer, F., and N. Luco, 2000. "Seismic Reliability of Steel Frames", Proc. IFIP WG 7.5, Working Conference on Reliability and Optimization of Structural Systems, Ann Arbor, MI, September.

Cornell, C.A., Jalayer, F, Hamburger, R.O. and Foutch, D.A., "The Probabilistic Basis for the 2000 SAC/FEMA Steel Moment Frame Guidelines," *Journal of Structural Engineering*, Vol. 128, No. 4, pp. 526-533, April 2002.

Degenkolb Engineers, 2004, "Application and Evaluation of Advanced Seismic Assessment Guidelines for Concrete Tilt-up Buildings", Report Prepared for PG&E/PEER Lifelines Program, Task 509, San Francisco, CA, December.

Duffley, T.A., Goldman, A., and C.R. Farrar, 1994. "*Shear Wall Ultimate Drift Limits*", Report NUREG/CR-6104 LA-12649-MS, Los Alamos National Laboratory, Los Alamos, NM 87545

Earthquake Engineering Research Institute (EERI), 1996, "Tilt-up-wall buildings", *Earthquake Spectra*, Supplement C to Vol. 11, pp 99-123.

HAZUS, 1999. "*Natural Hazard Estimation Methodology*", Federal Emergency Management Agency, FEMA (http://www.fema.gov/hazus/hazus6.htm)

FEMA 178, 1992. "*NEHRP Handbook for the Seismic Evaluation of Existing Buildings*", Building Seismic Safety Council, Washington, D.C., June.

FEMA 273, 1997. "*NEHRP Guidelines for the Seismic Rehabilitation of Buildings*", Building Seismic Safety Council, Washington, D.C., October.

FEMA 288, 1997. "*Background Reports: Metallurgy, Fracture Mechanics, Welding, Moment Connections and Frame System Behavior*", Report No. SAC-95-09, SAC Joint Venture, Sacramento, California, March.

FEMA 289, 1997. "Connection Test Summaries", Report No. SAC-96-02, SAC Joint Venture, Sacramento, California, June.

FEMA 306, 1999. "Evaluation of Earthquake Damaged Concrete and Masonry Wall Buildings', Basic Procedures Manual, prepared by ATC (ATC-43 Project), May.

FEMA 307, 1999. "Evaluation of Earthquake Damaged Concrete and Masonry Wall Buildings', Technical Resources, prepared by ATC (ATC-43 Project), May.

FEMA 350-352, 2000. "*Recommended Seismic Design Criteria for New Steel Moment-Frame Buildings (350); Recommended Seismic Evaluation and Upgrade Criteria for Existing Welded Steel Moment-Frame Buildings (351); Recommended Post-earthquake Evaluation and Repair Criteria for Welded Steel Moment-Frame Buildings (352)*", SAC Joint Venture, Sacramento, California, July.

FEMA 355D, 2000. "*State of the Art Report on Connection Performance*", SAC Joint Venture, Sacramento, California, September.

FEMA 355F, 2000. "*State of the Art Report on Performance Prediction and Evaluation of Steel Moment-Frame Buildings*", SAC Joint Venture, Sacramento, California, September.

FEMA 356, 2000. "*Prestandard and Commentary for the seismic rehabilitation of buildings*", Building Seismic Safety Council, Washington, D.C., November.

Gupta, B., and S. Kunnath, 2000, "Adaptive Spectra-based Pushover Procedure for Seismic Evaluation of Structures", *Earthquake Spectra*, Vol. 16, No. 2, pp 376-391

Hall, J.F., 1999. *"Seismic Response of Tilt-up Buildings"* Draft report to PG&E.

Hamburger, R.O., Harris, S.K., Martin, S.C., McCormick, D.L., and P.G. Somerville, 1996. *"Response of Tilt-up Buildings to Seismic Demands: Observations and Case Studies from the 1994 Northridge Earthquake"*, EQE International, Inc., San Francisco, CA.

Ibarra, L., 2003. "Global Collapse of Frame Structures Under Seismic Excitations", *Ph.D. Dissertation*, Dept. of Civil and Environmental Engineering, Stanford University, Stanford, California, September.

ICBO, 2000. "2000 International Building Code (IBC)*", International Conference of Building Officials* Publisher, Whittier, CA, 756 pp.

Kennedy, R. P., Cornell, C.A., Campbell, R.D., Kaplan, S. and H.F. Perla, 1980. "A Probabilistic Seismic Safety Study of an Existing Nuclear Power Plant", *Nuclear Engineering and Design*, Vol. 59, No. 2, pp. 315-338, , North Holland, Amsterdam, August.

Kennedy, R. P. and M.K. Ravindra, 1984. "Seismic Fragilities for Nuclear Power Plant Risk Studies", *Nuclear Engineering and Design*, V. 79, No. 1, pp. 47-68, North Holland, Amsterdam, May.

Kennedy, R.P., 2001. "*Seismic PRA Fragility Course*", Yucca Mountain Nuclear Waste Repository Project, Department of Energy, Course held in Las Vegas for AIC/BECHTEL engineers.

Kennedy, R.P., Short, S.A., McDonald, J.R., McCann, M.W., and R.C. Murray, 1989, "*Design and Evaluation Guidelines for Department of Energy Facilities Subjected to Natural Phenomena Hazards*", Interim Report DOE UCRL-15910, prepared for The Office of the Assistant Secretary for Environment, Safety & Health Office of Safety Appraisals United States Department of Energy, Lawrence Livermore National Laboratory, Livermore, CA 94550.

Klamerus, E.W., and J.L. Cherry, 2001. "*Structural Seismic Fragility Analysis of the Zion Containment*", Report NUREG/CR-6740 SABD2001-2504P, Sandia National Laboratories, Albuquerque, NM 87185.

Kunnath, S., and B. Gupta, 1999. "*Spectra-compatible Pushover Analysis of Structures*", U.S.-Japan Workshop on Performance-Based Earthquake Engineering Methodology for Reinforced Concrete Building Structures, Maui, Hawaii, 13 September.

Luco, N., Bazzurro, P., and C.A. Cornell, 2004. "Dynamic Versus Static Computation of the Residual Capacity of a Mainshock-Damaged Building to Withstand an Aftershock", *Proceedings of 13th WCEE*, Paper 2405, Vancouver, B.C., Canada, August 1-6.

Maffei, J., and R. Hamburger, 2004. "Seismic Assessment of the Building Located at 111 Almaden Street, San Jose, California", by Rutherford & Chekene and Simpson Gumpertz & Heger, Prepared for PG&E, August 6, 2004.

Medina, R. A., 2002. "Seismic demands for Non-Deteriorating Frame Structures and Their Dependence on Ground Motions", *Ph.D. Dissertation*, Dept. of Civil and Environmental Engineering, Stanford University, Stanford, California, November.

Miranda, E., 2000. "Inelastic displacement ratios for structures on firm sites", ASCE, Journal of Structural Engineering, Vol. 126, No. 10, pp. 1150-1159.

Moehle, J., and G.G. Deierlein, 2004. "A Framework Methodology for Performance-Based Earthquake Engineering", *Proceedings of 13th WCEE*, Paper 679, Vancouver, B.C., Canada, August 1-6.

Pardoen, G.C., Del Carlo, D. and R.P. Kazanjy, 1999. *"Stiffness of Timber Diaphragms and Strength of Timber Connections"* Report No. PEER-99/04, Pacific Earthquake Engineering Research Center, University of California, Berkeley.

Paulay, T., and M.J.N. Priestley, 1992. "Seismic Design of Reinforced Concrete and Masonry Buildings", John Wiley & Sons, Ltd., New York.

Paulay, T., 2000. "A Simple Displacement Compatibility-Based Seismic Design Strategy for Reinforced Concrete Buildings", *Proceedings of the 12th World Conference on Earthquake Engineering*, Paper No. 0062, Auckland, New Zealand, January 30-February 4.

Pacific Gas & Electric (PG&E), 2001a. "*Diablo Canyon Power Plant Long Term Seismic Program*", San Francisco, CA 94105.

Pacific Gas & Electric (PG&E), 2001b. Personal Communication, Electronic mail message from Kent Ferre dated December 4, 2001.

Pacific Gas & Electric (PG&E), 2001c. Personal Communication, Electronic mail message from Kent Ferre dated December 11, 2001

Reed, J.W., and R.P. Kennedy, 1994. "*Methodology for Developing Seismic Fragilities*", TR-103959 Research Project, prepared for Electric Power Research Institute (EPRI), 3412 Hillview Avenue, Palo Alto, CA 94304.

Ruiz-Garcia, J. (2004). "Performance-based assessment of existing structures accounting for residual displacements," *Ph.D. Dissertation (in preparation)*, Dept. of Civil and Environmental Engineering, Stanford University, Stanford, California.

Rutherford & Chekene Consulting Engineers, 2004. "Test Application of Advanced Seismic Assessment Guidelines 3-Story Steel Moment-Resisting Frame Building", Report Prepared for PG&E/PEER Lifelines Program, Task 508, Oakland, CA, October.

Structural Engineers Association of Northern California (SEAONC), 2001. "*Guidelines for Seismic Evaluation and Rehabilitation of Tilt-up Buildings and Other Rigid Wall/Flexible Diaphragm Structures*", SEAONC, San Francisco, CA.

Uniform Building Code (UBC), 1997. "Structural Engineering Design and Provisions", Vol. 2, International Conference of Building Officials (ICBO), Whittier, CA.

United States Geological Survey (USGS), 2001. "*Seismic Hazard Curves and Uniform Hazard Response Spectra for the United States*", Compact Disc, Version 3.10, by A.D. Frankel and E.V. Leyendecker, March.

Vamvatsikos, D. and C. A. Cornell, 2001a. "Incremental Dynamic Analysis", *Earthquake Engineering and Structural Dynamics*, Vol. 31, No. 3, John Wiley & Sons, Ltd., New York, April, URL: http://nausika.stanford.edu/docs/IDA-paper.pdf

Vamvatsikos, D. and C. A. Cornell, 2001b. *"SPO2IDA: Excel spreadsheet"*, Web implementation, URL: http://tremble.stanford.edu/cgi-bin/spo2ida-mt.pl

Vamvatsikos, D. and C. A. Cornell, 2002. "Practical Estimation of the Seismic Demand and Capacity of Oscillators with Multi-Linear Static Pushovers through Incremental Dynamic Analysis", *Proceedings of 7th U.S. National Conference on Earthquake Engineering*, Boston, July 21-25.

Wallace, J.W., Stewart, J.P. and A.S. Whittaker, (eds) 1999. "*Building Vulnerability Studies: Modeling and Evaluation of Tilt-up and Steel Reinforced Concrete Buildings*." PEER-PG&E Cooperative Research Program, University of California, Los Angeles, CA.

Wiemer, S., 2000. "Introducing probabilistic aftershock hazard mapping", *Geophysical Research Letters,* Vol. 27**,** pp. 3405-3408.
 URL: http://www.statsresearch.co.nz/statsei2/Abstracts/Wiemer/Wiemer.html

Yeo, G.-L., 2004. Stochastic Characterization and Decision Bases under Time-Dependent Aftershock Risk in Performance-Based Earthquake Engineering", *Ph.D. Dissertation*, Dept. of Civil and Environmental Engineering, Stanford University, Stanford, California, December.

Yeo, G.-L., and C.A. Cornell, 2004. "Building Tagging Criteria Based on Aftershock PSHA", *Proceedings of 13th WCEE*, Paper 3283, Vancouver, B.C., Canada, August 1-6.

Yun, S.-Y., Hamburger, R.O., Cornell, C.A. and D. Foutch (2002). "Seismic Performance Evaluation for Steel Moment Frames", *ASCE Journal of Structural Engineering*, Vol. 128, No. 4, pp. 534-545

Appendix A

Extension to include building-to-building uncertainty within same building class

These guidelines are directly applicable to specific buildings for which a detailed NSP curves are obtained according to the specifications provided here. The PG&E building inventory considered here consists of about 200 structures belonging to several buildings types (Table 1). It is likely that the cost of the engineering analyses necessary for the application of these guidelines may be so high that these detailed studies might be performed only for subset of such buildings. In this case, the procedure presented in this document needs to be expanded to incorporate an extra source of uncertainty due to the variability in response between buildings belonging to the same class (e.g., tilt-ups or mill types). This appendix will briefly outline the issues involved, should this source of uncertainty be included. No attempt, however, will be made to quantifying such uncertainty. PG&E may want to conduct a separate study with this specific scope.

Any building within a building class is characterized by a "true" (but unknown) fragility curve for each limit state, LS. This curve is fully characterized by a "central" (or median) point, $\check{S}_a^{LS}$, and by the slope of the curve, which is controlled by the aleatory uncertainty term, β_R. The central point of this curve, $\check{S}_a^{LS}$, however, is itself uncertain in an epistemic sense. The customary assumption is that $\check{S}_a^{LS}$ follows a lognormal distribution with a median value equal to $(\check{S}_a^{LS})_{med}$ and a dispersion measure given by the epistemic uncertainty term, β_U. As briefly described in the commentary of Step 6, this provides a first-order treatment of the uncertainty in the fragility curve and gives rise to a "family" of fragility curves (Figure 12). The central point of each fragility curve in this family can be computed by applying the equation $S_{a,y}^S = (\check{S}_a^{LS})_{med} e^{y\beta_U}$, where values of y are tabulated in any Gaussian distribution table. For example, the median (50th), the 16th-, and the 84th-percentile estimates of this central value, $S_{a,y}^S$, can be found by replacing y with the values of 0, -1, and +1, respectively, in the equation above. The slope of each fragility curve in this building-specific family is assumed to be equal to β_R. Therefore, one could define a "*median fragility curve*" for a limit state LS as being the median estimates of this family of fragility curves. The *median fragility curve* is characterized by the median estimate of the central (or median) point, $(\check{S}_a^{LS})_{med}$, and by the slope which is controlled by β_R.

All the buildings within a building class can be considered as a statistical population. Each building as a member of this population is characterized, as described above, by a "true" but unknown fragility curve for the same generic limit state, LS. As explained above, having done the proposed guidelines analysis, our available information about each building can be described in terms of a median estimate of the fragility curve with parameters, $(\check{S}_a^{LS})_{med}$ and β_R, and by an uncertainty measure of its central point given by β_U. In general the values of these three parameters vary from building to building within the same class. In particular, here we call β_{pop} the building-to-building variation of

90

$(\check{S}_a{}^{LS})_{\text{med}}$ across the buildings of the same class, and we call $(\check{S}_a{}^{LS})_{med}^{class}$ the median value of $(\check{S}_a{}^{LS})_{\text{med}}$ across the class of buildings. We also assume that we could compute $(\beta_R)_{avg}$ and $(\beta_U)_{avg}$, the average value of the β_R and β_U values for all the buildings in the class.

If we knew $(\check{S}_a{}^{LS})_{med}^{class}$, $(\beta_R)_{avg}$, $(\beta_U)_{avg}$, and β_{pop}, then we could represent the **mean** fragility curve for the entire class as the curve whose central (median) point is given by $(\check{S}_a{}^{LS})_{med}^{class}$ and whose slope, β_{class}, is obtained via an SRSS operation of three β's, namely $\beta_{class} = \sqrt{(\beta_R)_{avg}^2 + (\beta_U)_{avg}^2 + \beta_{pop}^2}$. This curve would be similar to one of those represented in Figure 11 but flatter to reflect the increased variability. If instead we prefer to keep aleatory uncertainty separated from epistemic uncertainty, then the generic building within a building class can be represented by a family of fragility curves whose *median fragility curve*, as defined above, whose central point is $(\check{S}_a{}^{LS})_{med}^{class}$ and its slope is controlled by $(\beta_R)_{avg}$. The building-to-building dispersion around $(\check{S}_a{}^{LS})_{med}^{class}$ of the median point of the fragility curves in this building-class-specific family is now $\beta_{Utot} = \sqrt{(\beta_U)_{avg}^2 + \beta_{pop}^2}$.

If the guidelines were to be applied to a specific building for which no engineering analyses are performed, then the mean fragility curve derived for its building class could be computed as explained above. However, we will not know the values of $(\check{S}_a{}^{LS})_{med}^{class}$, $(\beta_R)_{avg}$, $(\beta_U)_{avg}$, and β_{pop} unless we sample the population (i.e., consider different buildings in the class), compute the fragility curves (using these guidelines) of the sample structures, and then use the results to estimate the four parameters.

In practice because each class consists of many buildings, a brute-force random sample of the population may not be practical. Hence, it may be advisable to break each building class in sub-populations by identifying parameters (e.g., age, size, irregularities, etc.) that might affect the fragility curves of buildings within each sub-population, and then use more advance sampling techniques, such as stratified or latin-hypercube sampling. Such techniques may diminish the number of samples within a building class to a manageable number to be feasible in practice. A preliminary study should be conducted to identify the most effective parameters to be used to identify sub-population of buildings within each building class.

Appendix B

Evaluation of Epistemic Uncertainty for PG&E Buildings

Building categories

Category	Criteria for Inclusion	Approximate Number
Tilt-up or block	• Identified as *Tilt-Up* or *Concrete Block with Wood/Metal Deck Roof* in the PG&E inventory, <u>and</u> • 1 story or 1 story plus mezzanine, <u>and</u> • ≥3000 square feet in area, <u>and</u> • Structure does not have a diaphragm discontinuity or non-parallel systems (Table 16-M in UBC (1997))	18 tilt-up plus 15 block buildings in the prioritization inventory included in Table1.
Mill-type	Identified as *Mill-Type* in the PG&E inventory, consisting of older steel framing with concrete walls.	35 older urban substations.
Prefabricated metal	Identified as *Prefabricated Metal Building* in the PG&E inventory.	44 in the prioritization inventory of Table 1.
All other	Not meeting criteria for the above three categories.	99 in the prioritization inventory of Table 1.

Evaluation uncertainty

As described in the guidelines, the minimum level of seismic evaluation for all buildings includes a nonlinear static procedure analysis carried out according to the procedure described in the main body of this document. The seismic evaluation includes a performing nonlinear static procedure on the intact structure and additional nonlinear static procedures on the structure assuming it has been subjected to different identifiable damage states. Again, all seismic evaluations according to these guidelines should use expected strength values rather than nominal or lower-bound strengths.

The levels of epistemic uncertainty evaluation are defined as either *Baseline* or *Improved*. The *Baseline* case is expected to be used more often than the *Improved* case. Tables for each building category give conditions and required seismic evaluations to change the evaluation uncertainty level from *Baseline* to *Improved*. The conditions and required evaluations are intended to identify the characteristics that most significantly affect the uncertainty in a seismic evaluation for a given building type.

For all building categories, however, an *Improved* uncertainty evaluation always requires that:

- The structural drawings be available.
- Building inspection be carried out and consistency with drawings be checked and, in some cases, enforced[38].
- Testing of archaic materials be performed in cases where the material properties affect the seismic response.

If these requirements are not met, the epistemic uncertainty evaluation is *Baseline*.

Evaluation of uncertainty and β_U values

Tilt-up or block buildings

The evaluation uncertainty is *Improved* if **all** the required evaluations that the engineers deems important for estimating the structural response are carried out when the conditions identified below are present. Otherwise the evaluation uncertainty is *Baseline*. Note that some of the evaluations listed in the table may have to be considered in a *Baseline* evaluation as well to ensure reasonably accurate response estimates

The β_U values for this building category are reported in Table 2a for (recently) retrofitted buildings and in Table 2b for un-retrofitted buildings. . The β_U values given for Baseline assume that some but not all of the evaluations have been carried out. . In intermediate cases the engineer may use his/her judgment whether interpolation between *Baseline* and *Improved* β_U values are justified for the case considered.

Evaluations for TILT-UP OR BLOCK BUILDINGS

Condition	Required evaluation
All buildings in category	Evaluate the expected strength of the roof diaphragm in relation to the expected strength of the wall-to-roof tension connection.
All buildings in category	Evaluate the potential for foundation overturning or rocking to control the in-plane behavior of walls.
All buildings in category.	Evaluate the flexibility of the roof diaphragm in establishing the period of vibration of the building and in creating the NSP curve. The evaluation shall consider appropriate base conditions, such as pinned or flexible, for the out-of-plane walls.
Re-entrant corner per UBC (1997)	Evaluate collectors at re-entrant corners for the maximum force that can be delivered to them by the system, and include

---

[38] Note that if during inspection the engineer finds serious deficiencies in the lateral load resisting system due to missing or damaged elements (e.g., in prefabricated metal buildings, to allow equipment installation or door openings, rod braces are sometimes cut or removed, or baseplate bolts are missing) that were included in the design drawings, he/she should require these elements be installed or replaced before using Tables 2a to 2e to estimate epistemic uncertainty on the building response.

Table 16-M is present.	collector effects in the pushover analysis.
Metal-deck roof	Evaluate roof diaphragm behavior according to test data on metal deck diaphragms and an assessment of governing behavior modes.
In-plane wall behavior affects the pushover curve.	Evaluate wall in-plane behavior according to behavior modes identified in *FEMA 306* (Chapter 5 for Concrete and Chapter 6 for Block) and *FEMA 307* (Chapter 2 for Concrete and Chapter 3 for Block).

Mill-type buildings

The evaluation uncertainty is *Improved* if **all** the required evaluations that the engineers deems important for estimating the structural response are carried out when the conditions identified below are present. Otherwise the evaluation uncertainty is *Baseline*. Note that some of the evaluations listed in the table may have to be considered in a *Baseline* evaluation as well to ensure reasonably accurate response estimates.

The β_U values for this building category are reported in Table 2c. The β_U values given for Baseline assume that some but not all of the evaluations have been carried out. .   In intermediate cases the engineer may use his/her judgment whether interpolation between *Baseline* and *Improved* β_U values are justified for the case considered.

Evaluations for MILL-TYPE BUILDINGS

Condition	Required evaluation
All buildings in category	Evaluate the contribution of original steel braces, original concrete walls, and any added seismic elements according to their interaction in both the elastic and inelastic ranges of behavior.
All buildings in category	Evaluate in-plane composite action between steel framing and boundary members and concrete walls or diaphragms.
In-plane wall behavior affects the pushover curve.	Evaluate in-plane behavior of concrete walls according to behavior modes identified in *FEMA 306* Chapter 5 and *FEMA 307*, Chapter 2.
Concrete roof diaphragm behavior affects the pushover curve	Evaluate in-plane behavior of roof diaphragm according to behavior modes identified for walls in *FEMA 306*, Chapter 5 and *FEMA 307*, Chapter 2.

Prefabricated metal buildings

If the building contains any of the vertical structural irregularities of UBC (1997) Table 16-L or any of the horizontal structural irregularities of UBC (1997) Table 16-M, the evaluation uncertainty is *Baseline*.

If there are no structural irregularities, the evaluation uncertainty is *Improved* if **all** the required evaluations that the engineers deems important for estimating the structural response are carried out when the conditions identified below are present. Otherwise the evaluation uncertainty is *Baseline*. Note that some of the evaluations listed in the table may have to be considered in a *Baseline* evaluation as well to ensure reasonably accurate response estimates.

The β_U values for this building category are reported in Table 2d. The β_U values given for Baseline assume that some but not all of the evaluations have been carried out. . In intermediate cases the engineer may use his/her judgment whether interpolation between *Baseline* and *Improved* β_U values are justified for the case considered.

Evaluations for PREFABRICATED BUILDINGS

Condition	Required evaluation
All buildings in category	Field inspect the condition of lateral bracing and the bolting of column base plates, and include in the nonlinear static analysis the effects of any deficiencies observed.
All buildings in category	Include the contribution of cladding in the nonlinear static analysis, based on its behavior under in-plane lateral forces and deformations.

All other buildings

The evaluation uncertainty is *Baseline* if either horizontal irregularities 3 or 4 from UBC (1997) Table 16-M is present, or if horizontal irregularity 1 of UBC (1997) Table 16-M is present (torsional irregularity), or if system in classified as torsionally unrestrained according to Paulay (2000). The evaluation uncertainty is also *Baseline* if vertical irregularities 1, 2, or 3 of UBC (1997) Table 16-L are present (soft story, weight irregularity, or geometric irregularity). If none of these irregularities is present, the evaluation uncertainty is as determined below.

The evaluation uncertainty is *Improved* if **all** the required evaluations that the engineers deems important for estimating the structural response are carried out when the conditions identified below are present. Otherwise the evaluation uncertainty is *Baseline*. Note that some of the evaluations listed in the table may have to be considered in a *Baseline* evaluation as well to ensure reasonably accurate response estimates.

The β_U values for SMRF buildings are reported in Table 2e. The β_U values for other types of buildings belonging to this "all other"category can be estimated based on the β_U values for tilt-up, mill-type, and prefabricated metal buildings provided in Tables 2a to 2d. Interpolation may sometimes be in order. The β_U values for mill-type buildings could be considered as an upper bound for any structure in this category. Note that the β_U values given for Baseline assume that some but not all of the evaluations have been carried out. . In intermediate cases the engineer may use his/her judgment whether

interpolation between *Baseline* and *Improved* β_U values are justified for the case considered.

Evaluations for ALL OTHER BUILDINGS

Condition	Required evaluation
All buildings in category	Consider in the evaluation building elements such as partitions, infill walls, cladding, or gravity framing that affect the seismic response of the structure. Such elements are included in the evaluation whether their effect is beneficial or detrimental and irrespective of whether they have traditionally been identified as non-structural elements or elements not part of the seismic-force-resisting system.
Seismic-force-resisting elements are discontinuous, or vertical irregularity 4 of UBC (1997) Table 16-L is present (in-plane offset).	Explicitly consider the potential behavior modes, using laboratory test results, of the elements that support the discontinuous elements, in comparison to the maximum force and displacement demands that can be imposed on the elements by the system.
Vertical irregularity 5 of UBC (1997) Table 16-L is present (weak story).	Run the nonlinear static analyses with a range of vertical distributions of lateral force, or run nonlinear time-history analyses, to assess the potential for developing a story mechanism and to evaluate the expected story deformation as a function of global deformation.
Horizontal irregularity 2 of UBC (1997) Table 16-M is present (re-entrant corner).	Evaluate collectors at re-entrant corners for the maximum force that can be delivered to them by the system, and include collector effects in the pushover analysis.
Horizontal irregularity 5 of UBC (1997) Table 16-M is present (nonparallel systems).	Carry out a three-dimensional nonlinear static analysis of the structure considering a number of possible loading directions.

Elicitation of β_U values

The β_U values elicitation exercise was conducted for different cases that ranged from relatively simple buildings analyzed using considerable modeling effort (e.g., a prefabricated metal building at *Improved* level) to complicated buildings and limited modeling effort (e.g., a mill type building at *Baseline* level). Values were elicited for the Onset of Damage, Yellow, Red, and Collapse limit states.

To avoid any type of "anchoring" due to previous experience with quantification of epistemic uncertainty not consistent with these guidelines (e.g., in HAZUS), the experts were not asked directly for β_U values but rather for estimates of structural deformation values (e.g., roof drift) corresponding to incipient OD, Y, R, and Collapse limit states. In the case of tilt-up buildings the experts preferred to provide their estimates in terms of the

spectral acceleration at incipient limit state rather than in terms of drift. The experts were asked to provide estimates of median values and of 25% and 75% percentile values of such deformations or spectral accelerations The experts were told to assess the 25% and 75% percentile values in such a way that they felt that the "true" value of the parameter was equally likely to be inside or outside of that range. The experts provided their estimates with the understanding that they previously had conducted thorough analyses of the building as described by these guidelines. By design, the estimates did not include engineer-to-engineer tagging variability. As per PG&E request, such variability will be dealt with outside these guidelines by thoroughly training the PG&E building inspectors.

The β_U values for each expert were then computed assuming that such deformations followed a lognormal distribution. The β_U values included in Tables 2a to 2e consist of the weighted average values where each expert was given equal weight. The values included in the tables were obtained using the weighted average of the β_U values computed by considering the drift ratios (or spectral acceleration ratios in the case of tilt-ups) of the 25%-ile to the 50%-ile values, the 75%-ile to the 50%-ile values, and the 25%-ile to the 75%-ile values. The β_U values computed using the three ratios are somewhat different because the data elicited from the experts do not exactly follow a lognormal distribution as hypothesized during the calculation.

Appendix C

Copy of Most Relevant References

For convenience, a copy of the following papers is included:

- Bazzurro, P., Cornell, C.A., Menun, C., and M. Motahari, 2004. "Guidelines for Seismic Assessment of Damaged Buildings", *Proceedings of 13th WCEE*, Paper 1708, Vancouver, B.C., Canada, August 1-6.

- Luco, N., Bazzurro, P., and C.A. Cornell, 2004. "Dynamic Versus Static Computation of the Residual Capacity of a Mainshock-Damaged Building to Withstand an Aftershock", *Proceedings of 13th WCEE*, Paper 2405, Vancouver, B.C., Canada, August 1-6.

- Yeo, G.-L., and C.A. Cornell, 2004. "Building Tagging Criteria Based on Aftershock PSHA", *Proceedings of 13th WCEE*, Paper 3283, Vancouver, B.C., Canada, August 1-6.